

TIME RESOLVED SPECTROSCOPY OF LASER INDUCED AIR PLASMA

A THESIS SUBMITTED TO
THE GRADUATE SCHOOL OF NATURAL AND APPLIED SCIENCES
OF
MIDDLE EAST TECHNICAL UNIVERSITY

BY

MUSTAFA KURT

IN PARTIAL FULFILMENT OF THE REQUIREMENTS
FOR
THE DEGREE OF DOCTOR OF PHILOSOPHY
IN
PHYSICS

AUGUST 2007

Approval of the thesis:

TIME RESOLVED SPECTROSCOPY OF LASER INDUCED AIR PLASMA

submitted by **MUSTAFA KURT** in partial fulfillment of the requirements for the degree of **Doctor of Philosophy in Physics Department, Middle East Technical University** by,

Prof. Dr. Canan Özgen _____
Dean, Graduate School of **Natural and Applied Sciences**

Prof. Dr. Sinan Bilikmen _____
Head of Department, **Physics**

Assoc. Prof. Dr. Akif Esendemir _____
Supervisor, **Physics Dept., METU**

Examining Committee Members:

Prof. Dr. Ramazan AYDIN _____
Physics Dept., METU

Assoc. Prof. Dr. Akif Esendemir _____
Physics Dept., METU

Assoc. Prof. Dr. Enver BULUR _____
Physics Dept., METU

Assoc. Prof. Dr. Serhat Çakır _____
Physics Dept., METU

Assoc. Prof. Dr. Selim Osman Selam _____
Astronomy and Space Science Dept., Ankara University

Date:

“I hereby declare that all information in this document has been obtained and presented in accordance with academic rule and ethical conduct. I also declare that, as required by these rules and conduct, I have fully cited and referenced all material and results that are not original to this work.”

Name Surname: Mustafa KURT

Signature:

ABSTRACT

TIME RESOLVED SPECTROSCOPY OF LASER INDUCED AIR PLASMA

KURT, Mustafa

Ph.D., Department of Physics

Supervisor: Assoc. Prof. Dr. Akif ESENDEMİR

August 2007, 105 pages

The laser beam interaction with matter and the plasma generation have been studied for many years. In some applications what is really important is to understand the composition and the temporal evolution of the species in the interested medium. In this thesis, time resolved optical spectroscopy was employed to understand the evolution of the plasma which is produced by interaction of Infrared (1.064 μm) laser beam with air.

In this thesis, a new technique is suggested to analyze the time evolution of laser induced breakdown spectroscopy. The suggested method and the instrumentation of the setup are tested with a single gas (He). After the tests, we analyzed time sequence spectra of Laser Induced Air Breakdown. The suggested method is based on triggering the laser and the spectrometer at different time and applying the spectrometer trigger time by adding the time delay (Δt) between them by using the pulse generator.

The results show that the decay rates are slowing down microseconds after the excitation of the plasma. The results of the time-resolved measurements of the line spectra show that different component of the air has different decay rate, and lifetime. The lifetime of helium is 20 μs , and the decay start 5 μs after the initiation of plasma. Air has 12 μs lifetime, and the decay start 3 μs after the initiation of the

plasma. Also, the decay rate and the lifetime depend on the state. We also calculate Doppler velocity for different component and different emission states. Doppler velocities show that the component which has great mass has small velocity, the component which has small mass has high velocity.

KEY WORDS: Laser Induced Breakdown Spectroscopy (LIBS), Time Resolved Laser Induced Breakdown Spectroscopy (TRELIBS), Spectroscopy, Plasma, Air Plasma, Spectral Analysis, Doppler velocity.

ÖZ

LASER İLE OLUŞTURULMUŞ HAVA PLAZMASININ ZAMANSAL ANALİZİ

KURT, Mustafa

Doktora, Fizik Bölümü

Tez Danışmanı: Doç.Dr. Akif ESENDEMİR

Ağustos 2007, 105 sayfa

Madde ile laser demetinin etkileşimi ve oluşan plazmanın karakteristik özellikleri, bilim insanları tarafından uzun yıllardan beri çalışılmaktadır. Bazı plazma uygulamalarında, oluşan plazmanın özelliklerinin zamansal analizi önemli olabilmektedir. Bu tezde, havada IR laser ışın demeti kullanılarak oluşturulmuş plazmanın zamansal çözümleri çalışılmıştır.

Havada oluşturulmuş plazmanın zamansal analizini yapmak için, yeni bir metod önerilmiştir. Bu method ve düzenekteki bileşenlerin güvenilirliği, tek bileşenden oluşan helyum gazı kullanılarak test edilmiştir. Methodun temelinde, laser ve spektrometreyi farklı sinyaller kullanarak tetiklemek, her spektrum alımından sonra, spektrometreyi tetikleyen sinyale 1 μ s lik gecikmeler vererek, plazma sürecini taramak oluşturmaktadır.

Sonuçlar göstermiştir ki, laser ile oluşturulmuş plazma için sönümlenme süresi mikro saniyeler mertebesinde. Plazmanın zamansal analizi yapıldığında, farklı bileşenler için sönümlenme süresi ve plazma yaşam süresinin farklılıklar gösterdiği görülmüştür. Helyum için yaşam süresi 20 μ s olarak görülmüş ve plazma oluşumundan 5 μ s sonra sönümlenme sürecinin başladığı görülmüştür. Hava için yaşam süresi 12 μ s olarak ölçülmüş ve plazma oluşumundan 3 μ s sonra sönümlenme

sürecinin başladığı görülmüştür. Elde edilen spektrumdan, Doppler kaymaları belirlenerek değişik bileşenler için parçacık hızları hesaplanmıştır. Hesaplamalar göstermiştir ki; parçacık kütlesi arttıkça parçacık hızı düşmektedir.

Anahtar Sözcükler: Lazer Uyarımlı Plazma Spektroskopisi (LIBS), Zaman Çözümlemeli Lazer Uyarımlı Plazma Spektroskopisi (TRELIBS), Spektroskopy, Plazma, Hava Plazma, Spektral Analiz, Doppler hızı.

TO MY FAMILY
and
TO MY TEACHERS

ACKNOWLEDGEMENTS

I am grateful to my supervisor Assoc. Prof. Dr. Akif ESENDEMİR for her guidance and comprehension.

I would like to thank to Prof.Dr. Ramazan AYDIN and Dr. Ali ALAÇAKIR, for their special guidance and support throughout my research.

It is a very big pleasure for me to thank to Prof. Dr. Ramazan AYDIN since he shared his endless experiences and knowledge during my work. If I had never met him, this work wouldn't have been completed and meaningful.

I also thank to Assoc. Prof. Dr. Enver BULUR for his valuable criticisms during the committee meetings.

I would like to thank all the people in the physics department for their endless help during this work.

It is a great pleasure for me to thank to my parents, without their valuable support, all this work was not possible.

Special thanks go to my family who always shared my excitements and enthusiasms during my study.

TABLE OF CONTENTS

ABSTRACT.....	iv
ÖZ.....	vi
DEDICATION.....	viii
TABLE OF CONTENTS.....	x
LIST OF TABLES.....	xii
LIST OF FIGURES.....	xiii
CHAPTERS	
1 INTRODUCTION	1
2 LASER INDUCED BREAKDOWN SPECTROSCOPY	3
2.1 Laser Induced Breakdown Spectroscopy.....	3
2.2 Advantages of LIBS	4
2.3 General Application of LIBS.....	6
2.4 Aim of This Study.....	7
3 THEORY OF PLASMA SPECTROSCOPY AND LASER INDUCED PLASMA SPECTROSCOPY	8
3.1 General Properties of Plasma	8
3.2 Physics of Laser Produced Plasmas.....	11
3.2.1 General Properties.....	11
3.2.2 Atomic processes in plasmas.....	12
3.2.3 Breakdown Initiation and Growth	13
3.2.4 Equilibrium relations in plasmas	15
3.3 Parameters Constituting an Emission Signal	16
3.4 Evaluation of Plasma Parameters	18
3.4.1 Temperature Measurement.....	19
3.4.2 Stark Broadening of Atomic Lines.....	21
3.4.3 Doppler Width of Atomic Lines.....	21
3.5 Radial Distribution of Spark Parameters.....	24

3.6	Lifetime Measurements.....	25
3.6.1	Delay Methods.....	25
3.6.2	Beam Measurements.....	28
3.6.3	Hanle Effect.....	31
3.7	Developments of Laser Induced Plasma Spectroscopy.....	32
4	TIME RESOLVED LASER INDUCED BREAKDOWN SPECTROSCOPY ACQUISITION SYSTEM	39
4.1	Experimental Setup.....	39
4.1.1	Light source for plasma generation.....	41
4.1.2	Measurement of Laser Pulse energy.....	44
4.1.3	Acquisition of the plasma spectrum.....	45
4.1.3.1	Spectral Calibration of Spectrometer.....	47
4.1.4	Pulse Generation and Timing.....	50
4.2	Data Acquisition.....	51
5	OBSERVATIONS and DATA ANALYSES.....	54
5.1	Spectral Analysis by LIBS.....	54
5.2	Analysis Method of Spectral Lines.....	56
5.3	Helium Plasma Data Analysis.....	58
5.4	Air plasma Lines Analysis.....	69
6	CONCLUSION.....	88
	REFERENCES.....	93
	APPENDIX A.....	99
	APPENDIX B.....	103

LIST OF TABLES

Table 4.1	Specification of used Spectrometer.....	46
Table 4.2	He-Hg lines wavelength between 200-1100 nm.....	49
Table 5.1	Molecular weight and assumed fractional-volume composition of dry air.....	69
Table.A.A.1	Spectroscopic data for neutral and ion lines of Helium.....	100
Table.A.A.2	Spectroscopic data for neutral and ion lines of Nitrogen.....	101
Table.A.A.3	Spectroscopic data for neutral and ion lines of Oxygen and Carbon.....	102

LIST OF FIGURES

Figure 3.1	Timing of a LIPS process: (a) plasma ignition, (b) broadband emission due to <i>Bremsstrahlung</i> and free-bound transitions, (c) line emission due to bound-bound transitions.....	13
Figure 3.2	(a) Doppler shift of a monochromatic emission line, (b) absorption line.....	23
Figure 3.3	(a) Gaussian profile centered at $\omega' = \omega_0(1 + v_z/c)$ which belong to molecules with a definite velocity component v_z . (b) Voigt profile as a convolution of Gaussian line shapes.....	23
Figure 3.4	Lifetime measurement by direct observation of laser-induced plasma.....	26
Figure 3.5	Schematic arrangement for lifetime measurement by delayed coincidence.....	27
Figure 3.6	Schematic arrangements for lifetime measurement with the beam foil method.....	29
Figure 3.7	Schematic arrangement for the Hanle method.....	31
Figure 4.1	Schematic diagram of experimental set-up for LIBS.....	40
Figure 4.2	The block diagram of the used laser.....	42
Figure 4.3	Timing charts of the used laser.....	43
Figure 4.4	Threshold position of the laser pulse.....	45
Figure 4.5	Efficiency Curve for Grating HC1.....	46
Figure 4.6	External Hardware Triggering – Trigger Timing.....	47
Figure 4.7	Observed spectrum from spectrometer for Hg lamp.....	48
Figure 4.8	Observed spectrum from spectrometer for He lamp.....	48
Figure 4.9	Pulse generation timing diagram.....	50
Figure 4.10	Pulse shape for triggering.....	51
Figure 4.11	Timing period of plasma generation and data acquisition.....	52

Figure 4.12	Differential acquisition of spectrum.....	53
Figure 5.1	Laser Induced He Plasma Lines.....	55
Figure 5.2	Laser Induced Air Plasma Lines.....	55
Figure 5.3	Example of typical spectrum (air) that is divided in to several bands. All interfering lines in one band are fitted in one run.....	57
Figure 5.4	He I-318.72 nm, a) Fitting Observed Data to Gauss Distribution, b) Normalized Gauss Analysis c) Time Evolution	59
Figure 5.5	He I-388.78 nm-396.46nm-402.59, a) Fitting Observed Data to Gauss Distribution, b) Normalized Gauss Analysis c) Time Evolution.....	61
Figure 5.6	He I-447.14 nm, a) Fitting Observed Data to Gauss distribution, b) Normalized Gauss Analysis c) Time Evolution.....	62
Figure 5.7	He II-468.77nm He I-471.41nm, a) Fitting Observed Data to Gauss Distribution, b) Normalized Gauss Analysis c) Time Evolution.....	63
Figure 5.8	He I-492.19, a) Fitting Observed Data to Gauss Distribution, b) Normalized Gauss Analysis c) Time Evolution.....	65
Figure 5.9	He II-656.01 nm, a) Fitting Observed Data to Gauss distribution,b) Normalized Gauss Analysis c) Time Evolution	66
Figure 5.10	He I-706.50 nm, a) Fitting Observed Data to Gauss Distribution, b) Normalized Gauss Analysis c) Time Evolution	67
Figure 5.11	He I-728.14 nm, a) Fitting Observed Data to Gauss Distribution, b) Normalized Gauss Analysis c) Time Evolution	68
Figure 5.12	N II-399.50 nm, a) Fitting Observed Data to Gauss Distribution, b) Normalized Gauss Analysis, c) Time Evolution	71
Figure 5.13	N III-434.57, N II-443.9 nm, a) Fitting Observed Data to Gauss Distribution, b) Normalized Gauss Analysis, c) Time Evolution	72
Figure 5.15	N II-478.8-480.3 nm, a) Fitting Observed Data to Gauss Distribution, b) Normalized Gauss Analysis c) Time Evolution	74

Figure 5.16	N II-500.27 nm, a) Fitting Observed Data to Gauss Distribution, b) Normalized Gauss Analysis c) Time Evolution	75
Figure 5.17	C II-514.5 nm, a) Fitting Observed Data to Gauss Distribution, b) Normalized Gauss Analysis c) Time Evolution.....	76
Figure 5.18	C II-566.2 nm, N II-567.7, a) Fitting Observed Data to Gauss Distribution, b) Normalized Gauss Analysis, c) Time Evolution	77
Figure 5.19	N II-593.2-594.2 nm, a) Fitting Observed Data to Gauss Distribution, b) Normalized Gauss Analysis c) Time Evolution	79
Figure 5.20	O I-715.67 nm, a) Fitting Observed Data to Gauss Distribution, b) Normalized Gauss Analysis c) Time Evolution.....	80
Figure 5.21	N I-742.34--746.8 nm, a) Fitting Observed Data to Gauss Distribution, b) Normalized Gauss Analysis, c) Time Evolution	82
Figure 5.22	O I-777.4 nm, a) Fitting Observed Data to Gauss Distribution, b) Normalized Gauss Analysis c) Time Evolution.....	83
Figure 5.23	O II-794.76 nm, a) Fitting Observed Data to Gauss Distribution, b) Normalized Gauss Analysis c) Time Evolution	84
Figure 5.24	C III-819.6, N I-O I-822.0, N I-824.24 nm, a) Fitting Observed Data to Gauss Distribution, b) Normalized Gauss Analysis, c) Time Evolution.....	86
Figure 5.25	O I-844.6 nm, a) Fitting Observed Data to Gauss Distribution, b) Normalized Gauss Analysis c) Time Evolution.....	87

CHAPTER I

INTRODUCTION

In spectroscopy science, founding of lasers was a technological revolution. Soon after the invention of the pulsed lasers, they were used to produce plasma for material analysis. Detection of pollutants in the environment or in material production processes is a significant application of laser spectroscopy. Therefore, the pulsed lasers are useful for dissociating materials into their elemental composition. Laser Induced Breakdown Spectroscopy (LIBS), has been one of the most important areas for rapid material analysis. LIBS, briefly, is an atomic emission technique in which a powerful laser beam is focused onto the sample. The sample can be in a wide variety of phases, such as solid, liquid, gas, and aerosol. Using a laser pulse as an excitation source to get a breakdown is known as LIBS. The spectral analysis of the light from the breakdown is used to analyze, characterize, and determine the sample composition, concentration, electron density, and plasma temperature. In recent years, LIBS has been applied to many areas having particular applications, including the analysis of metals, glass and its elemental composition, nuclear samples, liquids, gases and aerosols and alloys. Gas composition determination is very important in many areas. Gas composition determination is also used for military applications in order to detect the hazardous gas abundance. Briefly LIBS results from the need for a new spectroscopic technique for quick and on-line elemental analysis.

The goal of this study is to develop a new technique to analyze the time evolution of the laser produced plasma in air. A pulsed laser is focused into air and the emission lines of nitrogen, carbon and oxygen are detected simultaneously. The basis of the technique is to apply a time delay to the acquisition start of the spectrometer.

Chapter 2 gives the definition of LIBS, advantages and disadvantages of LIBS, general application and intent of the thesis. Chapter 3 provides a brief overview of both emission spectroscopy and laser-induced breakdown spectroscopy, general properties of LIBS, atomic processes in LIBS, general LIBS parameter, plasma lifetime measurement technique and overview. It concludes with a thorough review of the recent literature concerning the fundamentals, applications and temporal evolution of LIBS. Chapter 4 describes the experimental setup as well as the details and the properties of apparatus used in the study. Chapter 5 presents the experimental results; the first section includes a general look on spectroscopic observation. In the second section, the data analysis method is discussed. In the third section, investigation of helium emission lines, last section air plasma emission line analyses are discussed. Chapter 6 is dedicated to the conclusion of the study.

CHAPTER 2

LASER INDUCED BREAKDOWN SPECTROSCOPY

2.1. *Laser Induced Breakdown Spectroscopy*

Laser Induced Breakdown Spectroscopy, *LIBS*, is one of the applications of lasers for material analysis, which can also be used for gas composition determination. A high power laser pulse is brought to a sharp focus on a target (solid, liquid or gas). Typically, a 40 mJ/pulsed from a laser with 10 ns pulse width, corresponding to a focused power densities of 10 GW/cm^2 is sufficient for plasma generation. A plasma with high temperature and electron density is created. Spectroscopic analysis of the radiation emitted from the plasma can then be performed to determine the composition, temporal and other properties of the material being analyzed.

This technique is known by several acronyms. Besides LIBS, TRELIBS (Time Resolved Laser Induced Breakdown Spectroscopy) and LSS (Laser Spark Spectroscopy) are also used to refer to the same process in the literature.

LIBS and TRELIBS [1], share many advantages in common; non invasiveness, the absence of electrodes disturbing the plasma and real time detection capability. In addition, TRELIBS possesses the advantage of temporal resolution and hence inherently lower the limits of detection.

2.2. *Advantages of LIBS method*

Atomic spectroscopic techniques, including atomic absorption spectroscopy (AAS), atomic emission spectroscopy (AES), inductively coupled plasma (ICP), and atomic fluorescence spectroscopy (AFS), are widely used for many years in the laboratory in order to determine elemental abundances. Advantages and disadvantages of these methods have been discussed in many articles [2-6], in terms of applicability, detection limit, sensitivity and selectivity, multi-element capability and modest cost per sample.

Atomic emission spectroscopy is a well established technique for the measurement of materials. Excitation of atoms may be performed by raising the temperature of the sample using a flame [7], an inductively coupled plasma [8], a microwave induced plasma [9], an arc or spark between electrodes [10, 11]. Emission measurements are preferred over absorption measurements when high sensitivity is required. An absorption signal is measured as the reduction in transmitted signal, "negative signal", in which small absorptions involves detection of small signal decrease on a large transmitted background. However, emission signal is zero for no signal, then emission measurements can be performed with a better sensitivity than absorption measurements.

Laser produced spark spectroscopy [12-14], is an emission based spectroscopic technique and subject to all the problems associated with emission spectroscopy including self absorption, spatial and temporal non-uniformities of the source, and spectral line interferences. However, there are several significant advantages which make the technique useful in situations when other types of technique fail. Those can be mentioned as follows:

- i)* Since the source brightness is extremely high, the spatial and temporal resolution can be high; all atomic species are accessible depending on the pumped energy. There is no physical intrusion to the sample, and spectra usually are sensitive only to atomic abundances, independent

of molecular composition. Since some of the molecular bonds can be broken easily.

- ii)* Sample preparation is not necessary and only small sample amounts enough to apply the method.
- iii)* No contact with the sample is necessary and the physical state of the sample is not a factor. It can be a solid, liquid, gaseous or aerosol.
- iv)* The plasma generation is simple, because the laser pulse both vaporizes and excites the sample in one step; no auxiliary analysis equipment needed. Thus it is economical.
- v)* Being an emission technique, direct spark analysis provides simultaneous multi-element analysis capabilities without increased instrumental complexity and cost.
- vi)* Because the spark can be generated in remote locations, it is useful in applications requiring non-invasive analysis. Only optical access to the medium of interest is required. Therefore, analysis can be performed in-situ in harsh environment, such as stack gaseous emission.

2.3. General Applications of LIBS

The fact that LIBS generally requires little-to-no sample preparation, is simple instrumentation, and can easily be performed on-the-field in hazardous industrial environments in real-time, it is a very attractive analytical tool. The following are a few examples of real life applications, where LIBS is successfully used [79]:

- Express-analysis of soils and minerals (geology, mining, construction)
- Exploration of planets (such as projects using LIBS for analyzing specific conditions on Mars and Venus to understand their elemental composition)
- Environmental monitoring (Real-time analysis of air and water quality, control of industrial sewage and exhaust gas emissions)
- Biological samples (non-invasive analysis of human hair and teeth for metal poisoning, cancer tissue diagnosis, bacteria type detection, detection of bio-aerosols and bio-hazards, anthrax, airborne infectious disease, viruses, sources of allergy, fungal spores, pollen). Replacing antibody, cultural, and DNA types of analysis
- Army and Defense (detection of biological weapons, explosives, backpack-based detection systems for homeland security)
- Combustion processes (analysis of intermediate combustion agents, combustion products, furnace gases control, control of unburned ashes)
- Metal industry (in-situ metal melting control, control of steel sheets quality, 2D mapping of Al alloys)
- Nuclear industry (detection of cerium in U-matrix, radioactive waste disposal)

2.4. *Aim of this study*

This work was the laboratory based preliminary studies for understanding the physical processes involved in LIBS in order to perform time resolution of He and air plasma produced by laser.

While a large number of studies of laser produced plasmas have been performed, the knowledge on the time history of laser induced plasma in air is very limited. In this study, a new technique is investigated to perform detailed analysis for laser induced air plasma. For this reason, a set-up was suggested, was tested for reliability with single gas He (under 1 atm pressure) flow gas. After, the reliability test, air plasma is generated. The generated plasma is analyzed spectrally. The plasma will be investigated in blackbody characterization, spectral analysis helium and air comparatively, life times and decay rate characterization and Doppler shift parameter. The laser produced plasma is assumed in none locally thermal equilibrium.

CHAPTER 3

THEORY OF PLASMA SPECTROSCOPY AND LASER INDUCED PLASMA SPECTROSCOPY

3.1 *General Properties of Plasma*

Matter can exist in a variety of stable forms which are governed by the physical environment. The conventional classification of stable states is that of the solid, liquid and gas. However, it has been recognized that a fourth state can be distinguished. This is the plasma state. Plasma is characterized by a collection of charged particle (ions and electrons) of low density. These four stable states can pass from one to the other by change in the energy content of the system. Such changes can be brought about by a change in temperature. The plasma state is said to be established when the number of ions and electrons in the gas are sufficiently numerous for their presence to dominate behavior of the system. For example normally gas is an insulator, but plasma is a conductor of electricity.

Atomic spectroscopy is the oldest instrumental elemental analysis principle, the origins of which go back to the work of Bunsen and Kirchoff in the mid-19th century. Their work showed how the optical radiation emitted from flames is characteristic of the elements present in the flame gases or introduced into the burning flame by various means. It had also already been observed that the intensities of the element-specific features in the spectra, namely the atomic spectral lines, changed with the amount of elemental species present. Thus, the basis for both qualitative and quantitative analysis with atomic emission spectrometry was

discovered. These discoveries were made possible by the availability of dispersing media such as prisms, which allowed the radiation to be spectrally resolved and the line spectra of the elements to be produced. Around the same time it was found that radiation of the same wavelength as that of the emitted lines is absorbed by a cold vapor of the particular element. This discovery was along the same lines as the earlier discovery made by Fraunhofer, who found that in the spectra of solar radiation line-shaped dark gaps occurred. They were attributed to the absorption of radiation by species in the cooler regions around the sun. These observations are the basis for atomic absorption spectrometry, as it is used today. Flames proved to be suitable sources for determinations in liquids, and in the work of Bunsen and Kirchhoff estimations were already being made on the smallest of elemental amounts that would still produce an emission or absorption signal when brought into a flame. From this there was already a link appearing between atomic spectroscopy and the determination of very small amounts of elements as being a basis for trace analysis.

Industrial developments arose a large need for the direct chemical analysis of solids. This resulted from expansion of production processes, where raw materials are subjected to large-scale processes for the production of bulk materials, from which products of increased value, complying with very strict specifications, are manufactured. The search for appropriate raw materials became the basis for mining, which was then developed on a large scale. Geological prospecting with the inevitable analyses of large amounts of samples for many elements, often down to low concentration levels as in the case of the noble metals, took place. Accordingly, analytical methodology that allows widely diverse materials to be characterized for many elements became necessary. Because of economic implications this information must frequently be obtained rapidly, which necessitates so-called multi-element methods for the direct analysis of solids. Not only is there a need for the characterization of raw bulk materials but also the requirement for process controlled industrial production introduced new demands. After World War II this task was efficiently dealt with by atomic spectrometry, where the development and knowledge gained about suitable electrical discharges for this task fostered the growth of atomic

spectrometry. Indeed, arcs and sparks were soon shown to be of use for analyte ablation and excitation of solid materials. The arc thus became a standard tool for the semi-quantitative analysis of powdered samples whereas spark emission spectrometry became a decisive technique for the direct analysis of metal samples. Other reduced pressure discharges, as known from atomic physics, had been shown to be powerful radiation sources and the same developments could be observed as reliable laser sources become available. Both were found to offer special advantages particularly for materials characterization.

The need for environmentally friendly production methods introduced new challenges for process control and fostered the development of atomic spectrometric methods with respect to the reliable determination of elements and their species in among solids, liquids and gaseous samples. The limitations stemming from the restrictive temperatures of flames led to the development of high temperature plasma sources for atomic emission spectrometry. Thus, as a result of the successful development of high-frequency inductively coupled plasmas and microwave plasmas these sources are now used for routine work in practically all large analytical laboratories. Accordingly, atomic emission spectrometry has developed into a successful method for multi-element analyses of liquids and solids as well as for determinations in gas flows. This is due to the variety of sources that are available but also to the development of spectrometer design. The way started with the spectroscope, then came the spectrographs with photographic detection and the strongest development since photoelectric multichannel spectrometers and flexible sequential spectrometers, has recently been with array detectors becoming available.

Lasers will be shown to give new impetus to atomic absorption work and also to make atomic fluorescence feasible as an extreme trace analysis method. They will also give rise to new types of optical atomic spectrometry such as laser enhanced ionization spectrometry.

3.2 *Physics of Laser Induced Plasma*

3.2.1 *General Properties*

When the output of a high power laser light is focused on a gas and the intensity in the focal region reaches a critical threshold value, plasma is observed. The gas which is initially electrically neutral and optically transparent suddenly becomes ionized and opaque. The associated plasma is very luminous and appears as a bluish white spark with a very sharp sound.

Plasma is regarded as the fourth state of matter, as distinct from the solid, liquid and gaseous states. Although in our immediate environment its occurrence is rare, on the cosmological scale it is reckoned to constitute about 99 % of all matter in the universe whether as stellar, interstellar or inter-galactic material. Plasmas are therefore an important area of the natural sciences for the research activities of physicists and chemists.

In simplest terms, plasma is a state of matter, exhibiting either partial or complete ionization. Unfortunately, a fully ionized plasma state is difficult to maintain in the laboratory and the partially ionized plasmas obscure the basic physical plasma effects by the presence of additional processes such as elastic and inelastic collisions, and excitation and de-excitation of atoms and molecules. The transition from neutral matter to plasma can occur in a variety of ways but in general it involves the absorption of energy from some appropriate source to generate the assembly of ions and electrons. In this process the system is assumed to retain its overall neutrality, which may be expressed as;

$$n_e = \sum_z n_z z \quad (1)$$

where n_e is the electron density and n_z is the density of ions of charge number z .

3. 2. 2. Atomic processes in plasmas

The emission spectrum of a plasma is determined by the combined effects of many processes. Collisional and radiative excitation, de-excitation, ionization and recombination all occur involving many energy levels and several stages of ionization. According to the principle of detailed balancing every atomic process is as frequent as the inverse process in a thermodynamic system. A knowledge of the rates of all these atomic processes would in principle allow to predict the emission spectrum. Some of the main atomic processes occurring in plasmas are explained briefly below

Collisional Excitation involves a collision between an electron and a neutral particle or ion resulting in the conversion of kinetic energy into the excitation energy in the atomic system. In the inverse process, Collisional de-excitation excitation energy is converted into the kinetic energy by the collision.

Collisional ionization can occur when the kinetic energy of an electron is sufficient to remove another electron from an atom or molecule. Collisional recombination occurs when two electrons encounter an ion and one electron recombines with a gain in the kinetic energy of the system.

Photo excitation corresponds to the absorption of a photon as a result of which the atomic system is raised to a higher state. Photo-de-excitation is simply the converse emission process.

Photoionization can occur when an incident photon has sufficient energy to remove an electron from an atomic system thus leaving it in a higher stage of ionization. In photo-recombination the electron recombines with an ion with the emission of a photon.

Bremsstrahlung involves an encounter between an electron and an ion of charge (ze); so that the two particles may be regarded as being in a continuum state of the system of charge $(z-1)e$. A transition to a lower continuum state of the system may occur with the emission of a photon. The spectrum associated with this process, which is sometimes called a free-free transition, is continuous. In the inverse process,

inverse Bremsstrahlung, a photon is absorbed by the ion electron system and the electron is raised from a lower level in the continuum to a higher one. Essentially the energy of the incoming photon is converted into the kinetic energy of the free electron. Both bremsstrahlung and inverse bremsstrahlung are of major importance in laser produced plasma.

3.2.3. Breakdown Initiation and Growth

The time evolution of the breakdown plasma can be divided into the stages of initiation, growth and decay. For laser pulses of tens of nanoseconds and in the energy range of millijoules to several tens of joules, (unfocused power density of 10^7 - 10^9 W/cm²), initiation takes a few nanoseconds, growth lasts for the duration of the laser pulse and the decay lasts for tens of microseconds.

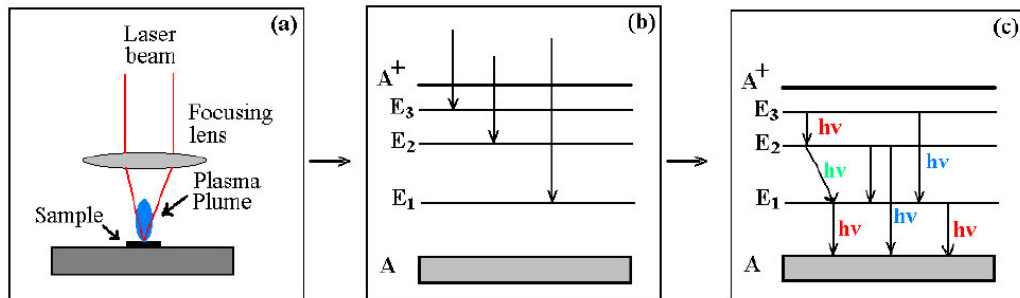
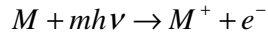


Figure 3.1: Timing of a LIPS process: (a) plasma ignition, (b) broadband emission due to *Bremsstrahlung* and free-bound transitions, (c) line emission due to bound-bound transitions.

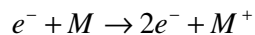
There are two main mechanisms leading to breakdown of a gas by a laser pulse. The first mechanism is the multiphoton ionization (MPI) process, and it is important only at short wavelengths ($< 1 \mu\text{m}$), and at low gas pressures. MPI is described by the reaction



This process involves the simultaneous absorption of a sufficient number of photons by an atom or molecule to cause its ionization. The energy of a single photon from lasers used to generate the spark is usually much less than the energy needed to ionize an atom. For example, the energies of photons from a Ruby and Nd:YAG lasers are 1.79 and 1.17eV respectively, whereas the ionization potentials of most gases are larger than 10 eV. However, because of high power density (MW/cm²) and large photon flux (photons/cm²) of the focused laser pulses, there is a high probability that ionization will occur by the absorption of many laser photons during the laser pulse.

This mechanism may also supply the initial electrons. Any impurity with a low-ionization potential, such as organic vapors or even dust particles, contributes significantly to the generation of initial electrons by MPI.

The second mechanism leading to breakdown is avalanche ionization or cascade ionization, which dominates at long wavelengths and at moderate to high pressures. Cascade ionization involves absorption of laser radiation by electrons when they collide with neutrals (inverse Bremsstrahlung). If the electrons gain sufficient energy they can impact ionize the gas or solid through the reaction below;



In the classical picture, the free electrons are accelerated by the electric fields of the optical pulse in the time period between collisions with neutral atoms. The collisions act to produce an isotropic electron energy distribution. Eventually, if the applied electric field is intense enough and exist long enough, the electron energy becomes sufficiently high to collisionally ionize an atom. This produces other free electrons that gain energy from the electric fields and causes further ionization. This process of electron multiplication continues throughout the laser pulse and results in significant ionization of the gas and breakdown. Since the cascade ionization theory requires the

pre-existence of initial free electrons as a necessary condition, it is assumed that these are provided by multiphoton ionization, as well as other processes.

3.2.4. Equilibrium relations in plasmas

The state of a gas or plasma which is enclosed in cavity with walls having the same constant temperature can be described with a few parameters; the temperature, the electron density and the concentrations of the elements present. When the plasma is in the state of complete thermodynamic equilibrium, these parameters are thermodynamic variables.

If the walls of the cavity are removed, energy dissipation is caused by radiation and heat conduction. In order to get a stationary state, this energy loss has to be compensated by heating of the plasma. For the description of such a real plasma which is not in the state of thermodynamic equilibrium an infinite number of quantities has to be specified. It is apparent that laboratory or astrophysical plasmas are nearly never in complete thermodynamic equilibrium. Nevertheless, the knowledge of equilibrium relationships is extremely important.

Many plasma are in a state which does not differ very much from ideal equilibrium. One denotes this state with the term local thermodynamic equilibrium, LTE, and understands that the energy states of the individual particles in the plasma are populated as in complete thermodynamic equilibrium but that the accompanying blackbody radiation field is entirely or partially missing or reduced.

In plasma of sufficiently high electron densities, the collision processes, especially those involving electrons, become more important than radiative processes in determining excited state populations. The LTE model assumes that the populations of atoms and ions in the various bound states are controlled entirely by electron collisions, and may thus be determined from the principle of equipartition provided plasma conditions do not change too rapidly.

The number density of electrons necessary to obtain complete LTE has been calculated by Griem [65]. This electron density is given by the following equality if one refers all energies to the ionization energy of the corresponding hydrogenic ion or that of hydrogen

$$n_e \geq 9,2 \times 10^{17} \left(\frac{kT}{E_H} \right)^{1/2} \left(\frac{E_2 - E_1}{E_H} \right)^3 [cm^{-3}] \quad (2)$$

where E_2 and E_1 are the upper and the lower level energies and E_H is the ionization energy of hydrogen or hydrogenic ion. The formula means that at least n_e electrons per cm^3 are required in order to reach equilibrium distribution of energy over the levels.

3.3. *Parameters Constituting an Emission Signal*

The absorption of a photon by an atom depends on the population of the lower quantum level whereas the emission of photon from an atom depends on upper quantum level. The intensity of an atomic emission line originating from the transition between the energy levels $k \rightarrow i$, at characteristic frequency of ν_{ki} , can be expressed as

$$I_{ki} \propto N_k \cdot A_{ki} \cdot h\nu_{ki} \quad (3)$$

where A_{ki} is the transition probability (sec^{-1}), N_k is the concentration or density of excited neutral atoms in the level k (number per cm^3), h is the Planck constant (erg.sec) and ν_{ki} is the frequency of the spectral line emitted in the transition $k \rightarrow i$.

The transition probability A_{ki} , also known as the Einstein coefficient of spontaneous emission, is a line constant just like the frequency. It determines the intrinsic intensity of the line. In spectroscopic analysis, where relative intensities are

of concern, the numerical values of transition probabilities are not of special interest. In spectroscopy physics, however, the need for reliable A-values of atom and ion lines is ever increasing.

The basic principles of the most popular methods for the determination of transition probabilities have been summarized, referenced and commented upon by *Wiese et al.*, [66]. In this reference, the data have been presented in separate tables for each element and stage of ionization. The transition probability of each line for spontaneous emission, the absorption oscillator strength, and the line strength have been given along with the spectroscopic designation, the wavelength, the statistical weights, and the energy levels of the upper and lower states. In addition, the estimated accuracy and the source have been indicated.

Transition probabilities or related quantities, such as oscillator strength, which are readily converted into A-values, can be determined either by theoretical calculations or by experimental procedures. Two methods are used for calculating transition probabilities theoretically. The first is a procedure based on the self-consistent field approximation, and the second one is the Coulomb approximation [67]. The transition probabilities or related parameters can be determined experimentally, by the measurement of the intensities of spectral lines that are emitted from the plasmas under known conditions, from the direct measurements of lifetimes of excited atomic states or from anomalous dispersion at the edges of spectral lines [67, 68].

Instead of transition probabilities one often makes use of the oscillator strength, f_{ik} . The numerical conversion of transition probability into oscillator strength is made by applying the equation

$$f_{ik} = 1.4992 \times 10^{-16} \cdot \lambda^2 \left(\frac{g_k}{g_i} \right) A_{ki} \quad (4)$$

where; g_i and g_k are the statistical weights of lower and upper levels respectively. The statistical weight of a particular state is the probability of populating a state

under identical conditions. The statistical weights are calculated from the total angular momentum quantum number, J_i , with the relationship,

$$g_i = 2J_i + 1 \quad (5)$$

3.4. *Evaluation of Plasma Parameters*

The goal of plasma analysis is the quantitative knowledge of the physical constitution of the plasma including the number of free electrons and temperature. These quantities may be uniform throughout the plasma (homogeneous plasma) or different for different parts of the plasma (inhomogeneous plasma). The temperature may be different for the different species present in the plasma (no equilibrium) or the concept of temperature may be meaningless. In non-equilibrium plasmas, one can talk about various temperatures [68], such as electron temperature, gas temperature, excitation temperature and ionization temperature, each describing a distinct aspect of the physical state of the system. When the system reaches a state of thermal equilibrium, however, all the temperatures become numerically equal.

A gaseous system, in complete thermodynamic equilibrium or at least in local thermodynamic equilibrium, is characterized by the following conditions.

- i) The velocity distributions of all kinds of free particles (molecules, ions, atoms and electrons) in all energy levels satisfies Maxwell' s equation;
- ii) For each separate kind of particle the relative population of energy levels conforms to Boltzmann' s distribution law;
- iii) Ionization of atoms, molecules and radicals is described by Saha' s equation .

In order to reach the goal indicated above all available analytical techniques should be used to obtain information as detailed as possible. Spectroscopic line shape

measurements allow the determination of the electron density and the gas temperature. The relations used to calculate the temperature from observed intensities also involve the electron density. Temperature and electron density measurements are therefore not really independent. These plasma parameters will be explained below.

3.4.1. *Temperature measurements*

The oldest method for the determination of temperatures in LTE plasmas is the measurement of relative atomic line intensities from the same element and same ionization stage. This method based on the assumption that the population of atoms, ions and molecules of the thermometric species at different energy levels follow a Boltzmann distribution, in which densities in various excited states are proportional to the products of statistical weights with the exponentials of the negative ratios of excitation energy and the thermal energy kT , given by;

$$N_k = N_i \cdot \left(\frac{g_k}{g_i} \right) \cdot \exp\left(\frac{-E_k}{kT} \right) \quad (6)$$

where N_k and N_i are the number of atoms in states k and i , g_k and g_i are the statistical weights for those states, E_k is the energy of the excited state, k is the Boltzmann constant and T is the absolute temperature. The subscripts k and i refer to excited and ground states, respectively.

The intensity of an atomic emission line originating from the transition between the energy levels $k \rightarrow i$, has been expressed before in equation (3). Inserting equation (6) in to the equation (3) the intensity of an emission line under LTE can be expressed as;

$$I_{ki} = N_i \frac{g_k}{g_i} A_{ki} \frac{1}{\lambda} \cdot \exp(-E_k/kT) \quad (7)$$

Taking the logarithm of the above equation and applying the equation to the relative intensity of the two lines of a given atomic species results in an equation in the form;

$$\ln \frac{I_1}{I_2} = \ln \frac{g_1 A_1 \lambda_2}{g_2 A_2 \lambda_1} - (E_2 - E_1)/kT \quad (8)$$

The Boltzmann temperature can be determined from the measurements of relative intensities of either two lines, or a series of lines, graphically. Since the excited state upper energy levels, E , statistical weights, g , transition probabilities, A , and wavelengths, λ , are known for the levels considered, one needs only to measure line intensities. A Boltzmann plot is constructed by plotting the log term on the left hand side of the Eqn.8, against the excited state energy, for a series of emission measurements. A linear relation is expected, and the temperature is calculated from the slope of the curve.

Although, wavelength, statistical weights, and energy levels may be taken from the well known multiplet tables [66] precisely, this can not be said for oscillator strength or transition probabilities. Except for one electron systems, the oscillator strengths given in the literature are all approximate, with estimated errors ranging from 10 percent in the case of relatively simple spectra to uncertainties of factors of 2 or 3 for more complex spectra [67].

Relative line intensities from the same element and ionization stage usually do not result in accurate temperatures. The main reason for this is the relatively small separation between the upper levels of the two lines; it is normally not too much larger than typical thermal energies and may be smaller. This renders the line intensity ratio rather insensitive to temperature changes. Considerable improvement in the sensitivity is obtained if lines from successive ionization stages of the same

element are compared with each other, because the effective energy difference is enhanced by the ionization energy, which is larger than the thermal energy.

3.4.2. Stark Broadening of Atomic Lines

An atom located in plasma is subjected to the electric microfields of charged particles; electrons and ions. Hence, in addition to the Doppler broadening of the spectral lines, the lines can also be broadened by the Stark effect. The theory of line broadening is described by several authors [69-71].

The Stark effect is seen in the shift of the spectral lines in the presence of an electric field. Stark broadening is caused by the microfields surrounding the ions in plasma. Extensive calculations have been carried out to obtain electron densities from the line shape measurements. The Stark broadening method is limited to dense plasmas, with temperatures in the 1-10 eV range, emitting neutral or singly ionized lines since Doppler broadening becomes competitive for lines from multiple ionized atoms. If the degree of ionization exceeds a few percent, other pressure broadening mechanisms are almost always negligible. Stark profiles depend on the electron density and are only weak functions of the temperature. Thus, measured Stark profiles can be used to determine electron densities also in situations where the temperature is only approximately known, or even when the existence of temperature is questionable.

3.4.3. Doppler Width of Atomic Lines

Generally the Gaussian-line profile with the natural linewidth σ , cannot be observed without special techniques, because it is completely concealed by other broadening effects. One of the major contributions to the spectral linewidth in gases

at low pressures is the Doppler width, which is due to the thermal motion of the absorbing or emitting molecules.

Consider an excited molecule with a velocity $v = \{v_x, v_y, v_z\}$ relative to the rest frame of the observer. The central frequency of a molecular emission line that is ω_0 in the coordinate system of the molecule, is Doppler shifted to

$$\omega_e = \omega_0 + k \cdot v \quad (9)$$

for an observer looking towards the emitting molecule (that is, against the direction of the wave vector k of the emitted radiation; Figure 3.2 (a)). The apparent emission frequency ω_e is increased if the molecule moves towards the observer ($k \cdot v > 0$), and decreased if the molecule moves away ($k \cdot v < 0$).

Similarly, one can see that the absorption frequency ω_0 of a molecule moving with the velocity v across a plane EM wave $E = E_0 \cdot \exp(i\omega t - k \cdot r)$ is shifted. The wave frequency ω in the rest frame appears in the frame of the moving molecule as

$$\omega' = \omega - k \cdot v \quad (10)$$

The molecule can only absorb if ω' coincides with its eigenfrequency ω_0 . The absorption frequency $\omega = \omega_a$ is then

$$\omega_a = \omega_0 + k \cdot v \quad (11)$$

As in the emission case the absorption frequency ω_a is increased for $k \cdot v > 0$ (Figure 3.2 (b)). This happens, for example, if the molecule moves parallel to the wave propagation. It is decreased if $k \cdot v < 0$. If we choose the $+z$ direction to coincide with the light propagation, (Eqn.11) becomes with $k=(0,0,k_z)$ and $|k| = 2\pi / \lambda$

$$\omega_a = \omega_0(1 + v_z / c) \quad (12)$$

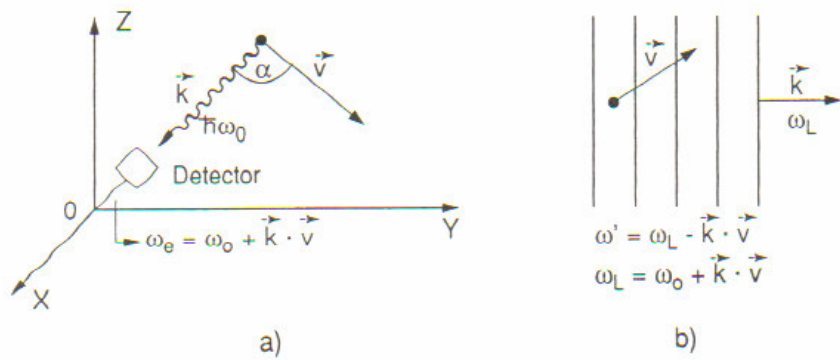


Figure 3.2: (a) Doppler shift of a monochromatic emission line, (b) absorption line.

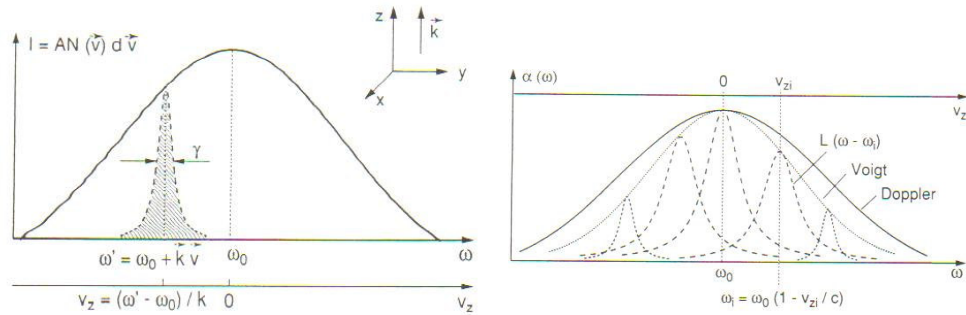


Figure 3.3: (a) Gaussian profile centered at $\omega' = \omega_0(1 + v_z/c)$ which belong to molecules with a definite velocity component v_z . (b) Voigt profile as a convolution of Gaussian line shapes.

This intensity profile, which is a convolution of Gaussian profiles, (Figure 3.3 (b)) is called a *Voigt profile*. Voigt profiles play an important role in the spectroscopy of stellar atmospheres where accurate measurements of line wings allow the contributions of Doppler broadening and natural linewidth. This profile is also important to determination of molecular velocity determination in laser produced

plasma. In order to determine mean velocity in the plasma, the wavelength which is correspond to FWHM value, is used [72].

3.5. Radial Distribution of Spark Parameters

In non-homogeneous optically thin plasmas, the measured line intensities represent radiation from all parts of the source within the line of sight of the spectrometer. Different plasma layers, each having an individual emissivity and individual thickness contribute to the measured intensity in different weights. Then the plasma parameters, such as temperature and electron density, obtained from those measurements correspond to some average values. In plasma analysis, if the source is optically thin and if the symmetry is known, then the radial emission distribution of individual plasma layers can be calculated from the observed integrated intensities by using several reconstruction techniques.

Onion peeling, Abel transformation and filtered back projection methods [74, 75] are some of the mostly used reconstruction techniques. If the projection data are taken at equally spaced radial positions, the deconvolved field is given by weighted sums of the projections divided by the data spacing. The weighting factors are independent of the data spacing and directly determine the relative noise performance. All the methods are remarkably similar and have Abelian behavior. Based on ease of calculation, robustness, and noise, the three point Abel inversion is recommended by Dasch et al., [75].

3.6. *Lifetime Measurements*

There are three rather different ways of determining lifetimes of excited states: delay-time measurements, beam measurements and Hanle effect. None of them is universally applicable. Some work only for states that can be excited directly from the ground state; others are no good if the lifetime is too short (strong line) or the intensity too low (weak line). Amongst them, they cover a very wide range of transitions, both atomic and molecular. Lifetime measurements get away from the uncertainties of population densities and assumptions about LTE, but they do not lead directly to oscillator strengths, unless there is only one transition of any significance from the excited state [73].

3.6.1. *Delay Methods*

If a large number of atoms is excited to the required level with a very short pulse, of either electrons or radiation, the intensity of a line starting from this level should be a decaying exponential,

$$I(t) \propto A_{12}n_2(t) = A_{21}n_2(0) \cdot e^{-t/\tau_2} \quad (13)$$

the time constant of which gives τ_2 . The trouble with this rather simple idea is the noise associated with the low photon flux attainable. Fluctuations due to the random arrival of photons follow Poisson statistics, for which the noise is equal to the square root of the signal. A signal-to-noise ratio of 100 requires at least 104 photons per measurement interval. If the lifetime is itself of order 10 ns, a measurement interval can be only a few ns. Taking into account detection efficiency and restrictions on gas density, this method is not usually feasible with conventional methods of excitation, but it certainly can be used with tunable laser excitation.

Lifetime measurements with pulsed tunable lasers have the advantage that only one level is excited by the laser pulse, and the recorded signal consists of a single exponential decay. Stepwise excitation makes it possible to study the decay of levels that cannot be reached directly from the ground state, but the method is limited to the wavelength range where tunable laser radiation is available.

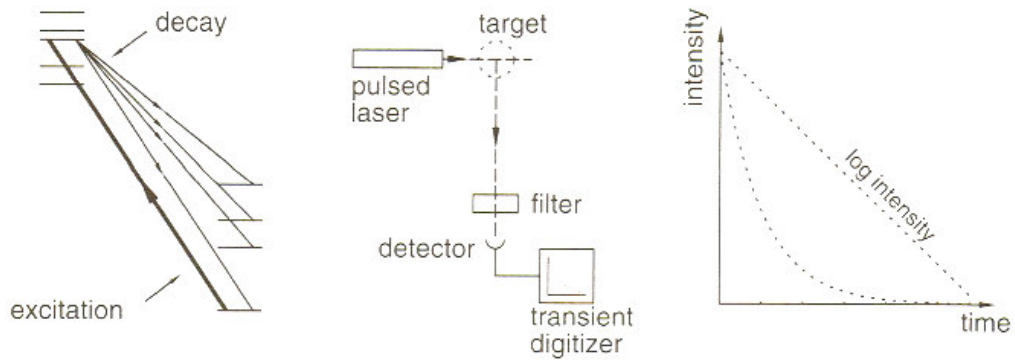


Figure 3.4: Lifetime measurement by direct observation of laser-induced plasma.

The basic principle, known as time-resolved laser-induced breakdown (TRELIBS), has been adapted for different types of problems. In the most straightforward method the decay signal detected by a fast photomultiplier is sampled at constant time intervals by a transient digitizer and stored in a computer. The signal-to-noise ratio can be improved by adding the data from a large number of laser pulses. Due to the selective excitation all the radiation recorded by the detector comes from the decay of one level, and in principle no monochromator is needed. In practice a low resolution monochromator or a filter is used to eliminate background light and scattered light from the laser. Generally the exciting wavelength is excluded from the detection, which is performed at longer wavelengths, as shown in Figure 3.4. With sufficiently short exciting laser pulses and fast electronics, lifetimes down to and even below $1 \mu\text{s}$ can be measured. However, there is a potential difficulty with the short pulses needed for very short lifetimes. This means that more than one level

may be excited in a complex system where the density of levels is high, and a high resolution monochromator is then needed to separate the different decay signals.

One of the difficulties with the direct recording of the whole decay curve is caused by the large number of photons at the start of the pulse, which may cause deviation from the linearity of the spectrometer. Such problems are avoided with the delayed coincidence method, which is based on the detection of single photons. The method was developed for electron or radiative excitation and is now frequently used with pulsed lasers. The principle of the method is shown schematically in Figure 3.5. The short exciting pulse also triggers the 'start' of a time-to-pulse-height converter. This is basically a capacitor charged by a steady current, so that the final charge is proportional to the time the current is allowed to flow. The 'stop' signal is provided from the first photon received by the spectrometer detecting the fluorescence.

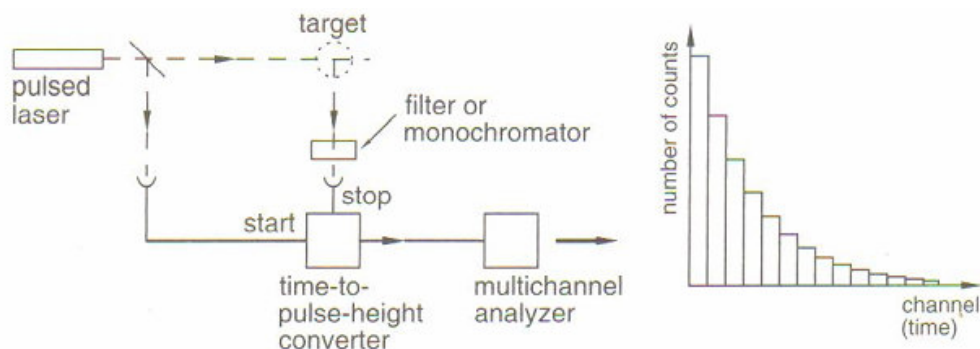


Figure 3.5: Schematic arrangement for lifetime measurement by delayed coincidence.

Apart from difficulties associated with scattered light and sometimes insufficient spectral resolution, the delay methods have three principal potential sources of systematic error. The first, cascading, is relevant only to electron or broadband radiative excitation. If higher levels are excited and subsequently decay to the level under investigation, the lifetime of the latter is apparently prolonged by the

repopulation. This difficulty can evidently be avoided by selective population of one level only, a great bonus provided by tunable lasers. The second problem affects all levels emitting to the ground or a metastable state and is known as imprisonment of resonance radiation. If the gas is not optically thin, some of the photons are absorbed and re-emitted one or more times before they eventually get out, and the effect is, again, to prolong the apparent lifetime of the state. Finally, longer-lived states may be collisionally depopulated, or 'quenched', which of course shortens the apparent lifetime. Both of these last problems can be dealt with in principle by going to sufficiently low pressure, but one may then run into difficulties with low light intensities. Systematic errors of this type have often been underestimated in the experimental data.

The delay methods as described here can be used for lifetimes from a few microseconds to less than a nanosecond. The decay rates of metastable levels by forbidden transitions with lifetimes in the range from microseconds to seconds have also been measured, but special precautions are required. Besides the need for a very low particle density, and thus a very good vacuum, the ions must also be prevented from disappearing from the field of view of the detection system before they decay.

3.6.2. Beam Measurements

A beam of ions of various degrees of ionization emerges from the thin foil in different states of excitation. The excited states decay as the ions travel downstream from the foil, and the rate of decrease of the intensity of any particular line as a function of distance from the foil gives directly the lifetime of the relevant excited state. Historically this method is the successor to the experiments of Wien in the 1920s on canal rays, in which the lifetime was measured from the decay of emitted radiation as the excited ions in a discharge tube travelled beyond the cathode. The beam foil method has intrinsically much greater accuracy because of the much higher ion velocity. In practice the spectrometer is kept fixed and the intensity is measured

as the foil is moved upstream. It is necessary to monitor the constancy of the beam while this is going on, either by measuring the total charge collected at the end or by using a second photomultiplier at a constant distance from the foil. The principle of the method is shown in Figure 3.6.

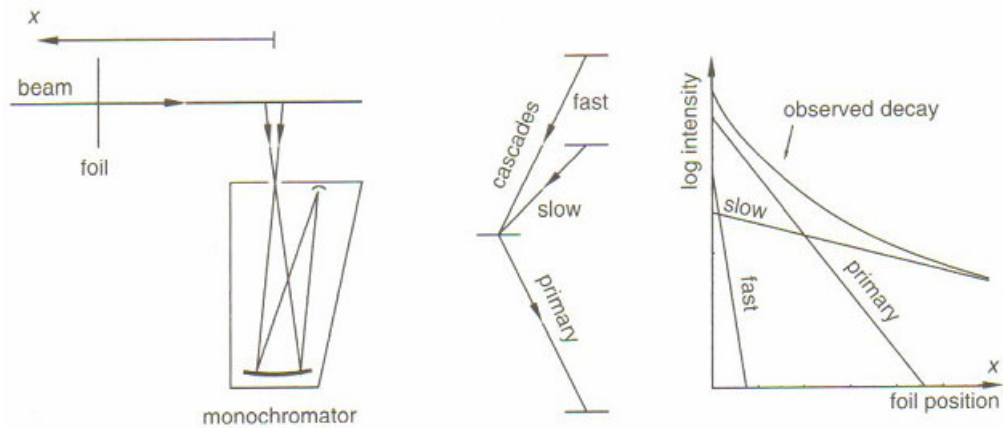


Figure 3.6: Schematic arrangements for lifetime measurement with the beam foil method.

The main difficulties of the method are cascading from higher excited states, low light intensity and large Doppler broadening. If the lifetimes of the repopulating cascades are much shorter than the lifetime to be measured, only the first part of the decay curve is affected, and this part can be omitted in the data analysis. The lifetime of a repopulating transition having a much longer lifetime can be determined from the long tail of the decay curve, and the contribution from this decay can easily be subtracted from the primary decay curve. The real problem appears when the lifetimes are of the same order of magnitude, but even in this case it can be solved with a technique known as ANDC, "Arbitrarily Normalized Decay Curves", where both the primary decay and the separately recorded decays of the most important cascades are included in the analysis.

The second difficulty, low light intensity, is a consequence of the small population of a particular level of a particular stage of ionization in a beam that is in any case of low density ($\sim 10^5$ ions/cm³). Photon-counting methods are used, and fast spectrometers with low resolution are usually necessary. The latter may lead to problems with line blending in complex spectra. The low density in the beam can, however, also be considered as a great advantage of the beam-foil method: there are no difficulties with imprisonment of radiation or collisional quenching.

The reason for the Doppler problem is the high velocity of the beam, typically of order 10^7 m s⁻¹. The Doppler shift is minimized by observing the radiation perpendicularly to the beam direction, but it cannot be eliminated in this way for all rays because of the finite acceptance angle of the monochromator (Figure 3.6). The effect can, however, be completely compensated because the blueshifted "upstream" photons and the redshifted "downstream" photons hit different parts of the grating. By translating the grating slightly from its normal position, the angles of incidence of the "red" and "blue" rays is changed. A new focus can then be found where this difference exactly compensates the Doppler width, and a sharp image is formed.

The beam foil method has been used over the range 10^{-12} - 10^{-7} s. The short lifetimes present problems of spatial resolution because the decay distance is itself so short, whereas longer lifetimes would require observation of the decay over impractically long distances along the beam. The latter problem can be solved by injecting the excited beam into a storage ring where the decay can be observed as the ions circulate and repeatedly pass the detection area. In cases where the photon emission rate is too low for direct optical detection, the decay of the excited state has been measured by observing the decaying yield from a resonant electron-ion reaction involving the excited state. Precision measurements in the millisecond range have been reported

3.6.3. Hanle Effect

This method is again a resurrection from the 1920s, when the effect, investigated by Hanle, was known as magnetic depolarization of resonance radiation. It is now also known as zero-field level-crossing. For a very brief qualitative description of the effect it is simplest to use a semiclassical model, but when there is hyperfine structure or close fine structure in the excited level, a proper quantum-mechanical treatment is required. A typical experimental layout is shown in Figure 3.7. Light from the source of resonance radiation travelling in the y direction is plane-polarized in the x direction before entering the resonance vessel. The emitted radiation is due to electrons oscillating along the x axis and has the same polarization. A detector on the x axis therefore records no signal. If now a magnetic field B is applied in the z direction, the resonance radiation is partly depolarized, and the intensity rises at strong fields to half that in the absence of the polarizer. The depolarization can be ascribed to the precession of the polarization direction about the z axis with angular frequency ω given in terms of the Lande g factor by

$$\omega = g_j \cdot \mu_B \cdot B / h$$

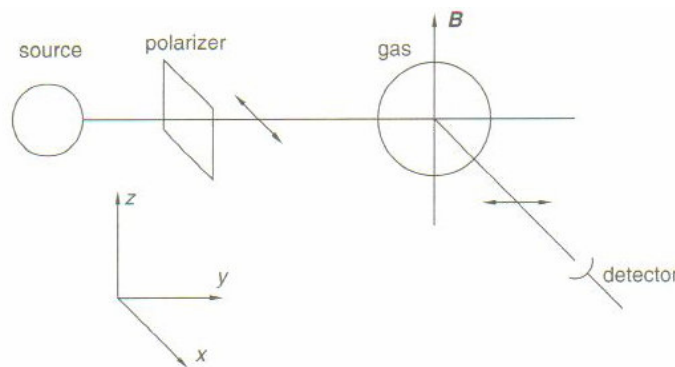


Figure 3.7: Schematic arrangement for the Hanle method.

If ω is sufficiently rapid, the components of the oscillation along the x and y axes are equalized, and the y oscillations, representing half the total intensity, radiate along the x axis. The lifetime enters into the story because for small ω some of the atoms decay before the precessional cycle is completed, so that the depolarization is only partial. The signal thus depends on the relative magnitudes of the precessional and decay times.

3.7. Developments of laser induced plasma spectroscopy

LIBS is a relatively new technique developed after the first operational lasers in 1960 [15]. There are several good reviews of experimental breakdown data on gases [16-20]. Much of the early work on laser plasmas before 1977 is about the determination of the mechanism leading to breakdown, measurements of threshold power densities for spark ignition, and investigation of the influence of various parameters on breakdown threshold intensity. Over the last 30 years, the extensive literature of laser spark spectroscopy covers the development and spectroscopic applications of the technique on different fields.

Since the first report of laser induced breakdown of air [21] in 1963, there has been an enormous growth in understanding the physics of the phenomenon. Influence of various parameters on breakdown threshold intensity, such as pressure [22-25, 28], pulse width [26], spot size [27], and wavelength [29,30], have been studied extensively, both experimentally and theoretically.

The pressure dependence of breakdown threshold has been investigated for the first time by Minck [22], in nitrogen, hydrogen, helium and argon for pressures between 0.3 and 100 atm using a ruby laser producing 25 ns pulses. It is demonstrated that the breakdown threshold intensity decreases with increasing pressures in an approximate inverse two thirds relation for all the gases, but the

pressure dependence of the rare gases are notably different from those for diatomic gases.

The spot size and pulse length dependence of threshold intensities have been investigated by Brueck *et al.*, [27], in ultra pure cryogenic liquids and it was found that the breakdown threshold intensity increases with increasing pulse width and decreases as the spot size increases.

The effect of presence of water droplets on breakdown thresholds of different gases has been investigated in a study made by Chylek *et al.*, [28], It has been found that, in the presence of water droplets the breakdown thresholds decreases up to three orders of magnitude depending on the pressure of the particular gas surrounding the droplet.

Experiments with different laser wavelengths, at constant pressure reveal that the breakdown threshold intensity has a maximum in the 0.3-1 μm wavelength region and becomes lower both for longer and shorter wavelengths. Breakdown threshold intensity of rare gases at wavelengths 1.06, 0.69, 0.53 and 0.35 μm has been studied by Buscher *et al.*, [29]. They found that the threshold intensity increases first and then decreases with increasing wavelength. It is difficult to compare the results of several studies because of the different experimental conditions, but one can make some general comments.

LIBS began to be used as an analytical technique for atomic detection and molecular identification in the 1980's. Applications of LIBS to analysis of gases [32], aerosols [14, 33], liquids [34, 35], and materials collected on filters [36] has been described. In addition, some instruments have been developed based on LIBS [37-39].

A major improvement in the technique was made by Loree and Radziemski [40, 41], at Los Alamos National Laboratory, (LANL), who introduced time resolution. The LANL group has also investigated several applications relating to airborne pollution. The central advantage of the laser spark technique is its remote capability and potential for real time detection. In one experiment [42], they have detected beryllium in air with a limit of detection of 0.5 ng/g, which is one third of

the OSHA limit, and in another experiment [36], they have developed a method, called long spark technique, (LST), to spectroscopic analyze beryllium particles on filters using the laser spark.

LIBS has been used as an alternative impurity detection method for the measurements of trace concentrations of polyatomic molecular impurities in helium by Cheng *et al.*, [47]. For the Group III and V hydrides, such as B₂H₆, PH₃, AsH₃, the detection limits for their apparatus has been determined. The minimum PH₃ level detectable by monitoring the phosphorous orange line (604.3 nm) has been limited to 3 ppm. Two lines of atomic boron 434.5 and 336.0 nm have been observed and the latter has been reproducibly detected down to B₂H₆ concentrations of as low as 1 ppm.

A study [55], for analytical applications of laser spark spectroscopy has been performed by Sandia National Laboratory, which is developing a prototype instrument for monitoring of continuous metal emissions from the stacks. Under the sponsorship of Department of Energy, office of Environmental Restoration and Waste Management, the Sandia research group has been developing a continuous-monitoring instrument to measure toxic metal concentrations coming from thermal treatment units, such as hazardous-waste incinerators. The group has demonstrated that, in the laboratory they can measure eleven toxic metals regulated under the Clean-Air-Act at concentrations below 250 ppb. They can measure important toxic metals such as, Be and Cr at concentrations as low as 1 ppb.

There are extensive studies on arc and spark temperature measurements [14, 56-64]. The mathematical theories applicable to the excitation and ionization of atoms in electrical discharge plasmas have been described in a study by Margoshes [56].

Spatially-resolved radial excitation temperatures and radial electron density distributions experienced by analyte species in the observation zone of 15 to 25 mm above the load coil of a toroidally shaped, inductively-coupled argon plasma have been presented by Kalnicky *et al.*, [58,59]. The addition of a large amount of an

easily ionized element has no effect on the excitation temperature distributions at the respective aerosol carrier flows and observation heights.

Electron temperature and density profiles of excimer laser induced plasmas formed in air, argon, nitrogen and helium, at pressures from 0.5 torr to 760 torr, have been presented by Grant *et al.*, [62], Eleven Fe(I) lines have been used in the Boltzmann plot determination of electron temperature. The temperature ranged from a maximum of 22000 K in 760 torr air at a height of 0.6 mm to about 9000 K in all gases at 0.5 torr at 6.6 mm from the surface. In general, temperature decreases with distance from the surface and with decreasing ambient pressure.

Experiments with flowing liquid samples [35], have shown that liquid velocities up to 90 cm/sec through the spark volume had no effect on the analytical results.

Determination of size, velocity, and elemental composition of particles in combustion flows [48, 49], is another important application of laser spark spectroscopy.

Laser spark spectroscopy for in-situ determination of particle elemental composition in a combustion environment has been developed by Combustion Research Facility group at Sandia National Laboratory [52]. Identification of the three bituminous coals, having different geological origins, with varying amounts of inorganic constituents has been made. Extension of the method to the analysis of several coal types has been reported in a subsequent study [53], made by Sandia group. For a variety of coals the elements of Li, Na, K, Mg, Ca, Ba, Sr, Al, Ti, Si, Mn and Fe in addition to C, H, O, and N have been observed in the spark spectra of single particles.

Time integrated photographic and diode array detection techniques have been used by Schmieder and Kerstein [50], to demonstrate the laser spark as a diagnostic for monitoring the elemental constituents of combustion products using different mixtures of N₂ and O₂. The relative abundances of N and O atoms have been accurately measured by monitoring the spark emission. In another experiment, fuel-to-air ratio in a methane flame has been determined by measuring the C/N ratio.

Spatial information has been obtained by moving the spark within the flame to sample different regions. The relative abundances of H, C, N, O and S from shale oil vapors have also been determined in this study.

Radziemski *et al.*, [14], have determined the electron density and temperature of laser produced air plasma with time resolution. The electron densities have been estimated as $9 \times 10^{17} \text{ cm}^{-3}$ from ion lines at earlier time of plasma evolution and $5 \times 10^{16} \text{ cm}^{-3}$ from neutral lines at late times.

Time Resolved Laser Induced breakdown spectroscopy of aerosol has been studied by Radziemski *et al.*[43]. They predicted that shortly after plasma initiation, the dominant radiation was a continuum mixed with ionic lines. Between 0.1 and 1 μs , both of these contributions decayed, leaving, neutral emission lines which were seen out to 20 μs or longer. At intermediate and late times ($>5 \mu\text{s}$) molecular features also were present. They generally monitored in the quiescent time period between 1 and 20 μs when background emission was reduced and the neutral lines remained intense. They also reported that Stark broadening is the major contributor to spectral line width for many species in the LIB plasma, especially at early times. Pressure broadening by neutral perturbers in LIB plasmas generally yields a detectable contribution only if the neutral particle density is greater than the charged particle density by a factor of 10^3 , which in the LIB plasma occurs after 10 μs . Even though temperatures are higher at early time and pressure broadening due to neutrals is greater, the electron and ion concentrations are also higher. As a result, at all but late times the Stark broadening dominates. Doppler width is also insignificant in most cases. At one extreme, the Doppler width of N I 415 nm at 0.5 μs is 0.01 nm, while the Stark width is 0.76 nm. At later times the Stark width is smaller, but always exceeds the Doppler width for N I 415 nm. At the other extreme, for Be II 313 nm the Stark broadening coefficients are small enough that Doppler width and pressure broadening by neutrals are the main contributors to line width. Usually the lines we observe have widths, corrected for instrumental width, between 0.1 and 0.3 nm.

Kyuseok *et al.* [44], have studied line broadening mechanism for Laser induced copper plasma by TRELIBS. They made experiment in Helium atmosphere,

and predicted the 510.55-nm emission line as the appropriate choice of emission line in LIBS applications for the detection of copper due to its relatively small change in linewidth compared with the 515.32- and 521.82-nm lines. The larger change in linewidth depending on gate delay for 515.32- and 521.82-nm lines were attributed to Stark broadening and characteristics of the Rydberg-like atomic state. As Kyuseok et al., the same method could be applied to other elements so that the emission line with the highest intensity may not be the best choice if this line originated from higher energy levels such as Rydberg states, and line broadening behavior remained similar when the buffer gas was changed.

Giacomo [45], experimentally characterized metallic titanium with laser induced plasma by time and space resolved optical emission spectroscopy. He solved the experimental results with Boltzmann relation, and saw that time of flight of plasma was compatible with theoretical results.

Single and double pulse laser induced plasma spectroscopy of aluminium samples in air was studied by Colao et al.[60]. They used spectroscopic techniques in order to retrieve relevant plasma characteristic during the first few micro seconds after the plasma ignition. When they compared with single laser excitation, saw that dramatic changes in plasma characteristic observed in the double pulse regime at 1.2 GW cm^2 . Above the threshold, the narrowing of both atomic and ionic lines, the increase of the line emission intensity with longer time decay and higher plasma stability were observed.

Temporal analysis of laser induced plasma properties as related to laser breakdown spectroscopy was studied by Hohreiter [57]. They worked the evolution of a laser induced plasma characteristic in terms of its temporally resolved spectral absorptivity, spectral emissivity, and free electron density via Stark broadening during the first few hundreds of nanoseconds.

Santagata et al.[64], have studied space and time resolved emission spectroscopy of $\text{Sr}_2\text{FeMoO}_6$ laser induced plasma. In his work the plasma dynamics induced during pulsed Nd:YAG ($\lambda = 532 \text{ nm}$) laser ablation of $\text{Sr}_2\text{FeMoO}_6$ targets has been studied by time- and space-resolved optical emission spectroscopy

measurements in the range 250–650 nm. The integral intensities of spectral lines were measured as a function of distance from the target surface and laser fluence in the presence of 5×10^{-5} mbar of O₂ partial pressure. The plasma properties as well as ionic and atomic Strontium time-of-flights were measured as a function of laser fluence in the range 0.90–2.40 J cm⁻². The results showed how the different plasma features can influence the film deposition process and the magnetic saturation properties.

Time-resolved plasma properties for double pulsed laser-induced breakdown spectroscopy of silicon was studied by Xianglei et al.[78]. They predicted that the ICCD gate delay time was 600 ns from the second laser pulse. The intensity initially decreases slightly with laser delay time (before 100 ns), but then increased approximately two-fold as the delay time changed from 100 to 200 ns. St-Onge et al. Also observed a dramatic increase of the Mg I line (4 times) at approximately 200 ns delay between laser pulses. Temperature and electron number density also decreased initially and then changed abruptly when the delay time between laser pulses was 100 to 200 ns.

Barthelemy et al. have reported space- and time-resolved measurements of both electron density and temperature of laser-produced plasmas in conditions relevant for the LIPS technique. They observed that the temperature exhibits a slight decrease both at the plasma edge and close to the target surface. They further presented experimental evidence that at least during the first microsecond, the electron density is homogeneous in the ablation plume. Their results were fully consistent with the conclusions previously reported from time-dependent space-integrated measurements concerning the dependence of the plasma characteristics on the pulse duration. From the analysis of the observed plasma characteristics, they also demonstrated that the plasma expansion is in good agreement with the Sedov's model during the first 500 ns and that it becomes subsonic, with respect to the velocity of sound in air, typically 1 μ s after the plasma creation [80].

CHAPTER 4

TIME RESOLVED LASER INDUCED BREAKDOWN SPECTROSCOPY ACQUISITION SYSTEM

4.1 Experimental Setup

Laser-induced breakdown spectroscopy (LIBS) is a technique based on the spectroscopic study of atomic emission of materials from plasma which is formed by focusing a laser of sufficiently high power onto the target gas. Plasma is formed when the laser power density per unit volume reaches the breakdown threshold of the gas. Detection of the resulting atomic emission reveals analytical information about the atomic composition of the gas. LIBS is an established analysis in a variety of applications, including metal and metal alloy analysis, environmental monitoring, content of glass, plastics and gases.

In our study, we establish a new technique to resolve time evolution of air plasma. Resolving the time evolution of a plasma medium is quite difficult, because the plasma medium is unstable. A variety of events occur in the plasma state. In order to resolve the event in time sequence, timing accommodation among apparatus in the setup must be very sensitive. The life time of the laser induced plasma state is affected by the content and the intensity of the gas and environmental conditions. During the experiment, condition must be stable. Therefore experiments are made in a clean room. Our main task for time resolving is described in the data acquisition section.

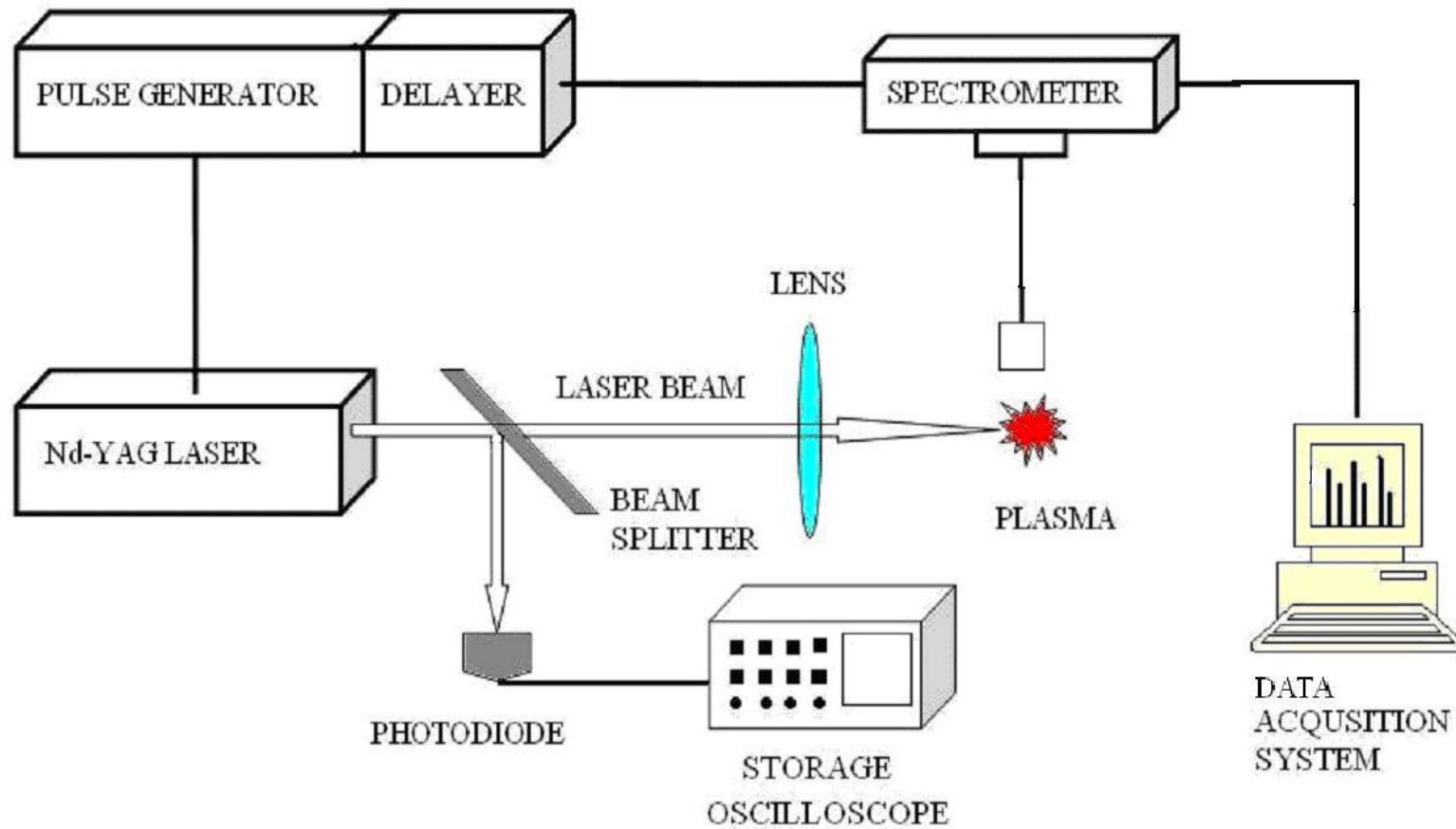


Figure 4.1: Schematic diagram of experimental set-up for LIBS.

A suitable setup for the study must consist of a laser as a light source; a beam splitter in order to excite the gas and to monitor the laser pulse energy, a beam shaper (collimating lens) for focusing laser pulse light, a spectrometer to determine emission line from spark, a function generator to generate pulse for triggering laser and spectrometer, a delayer for synchronization component of setup and lastly data acquisition system to store data from the system. A block diagram of the experimental setup used in the study of LIBS system for the gas analysis is shown in Figure 4.1. The details of the used system are described below.

4.1.1 Light source for plasma generation:

The plasma is generated by pulsed Nd: YAG EKSPLA NL301 model laser. This laser is Q-switched with internally 10 Hz pulse rate (this rate is adjustable with externally triggering case). The standard pulse duration of the laser is 4.7 ns, which releases a pulse energy of 320 mJ at 1064 nm wavelength. Energy stability of the used laser is about 1 percent, this rate is important for us, because the energy which is used in process of spark generation must be stable in every shot. In case of using the externally triggering mode, it is possible to control the released energy by changing the width of triggering pulse. The block diagram of the used laser is presented in the figure 4.2.

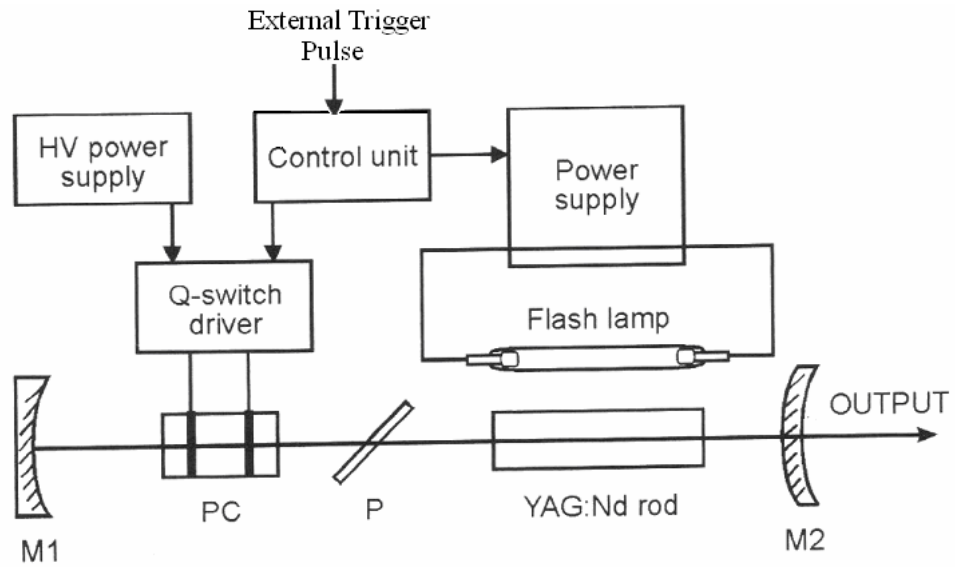


Figure 4.2: The block diagram of the used laser.

The timing diagram of the laser work is presented in Figure 4.3 below

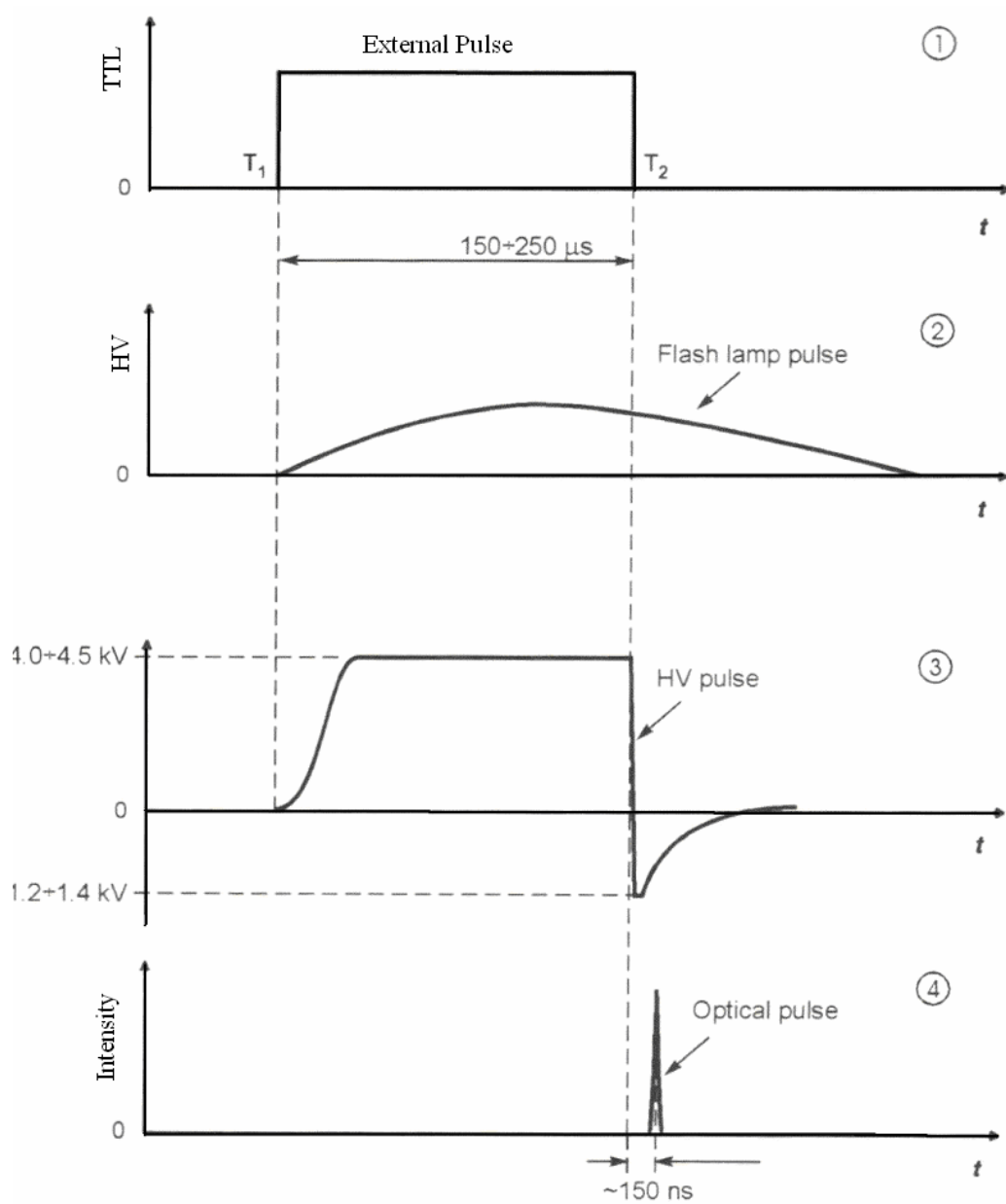


Figure 4.3: Timing charts of the used laser.

For the laser, each external trigger pulse (chart (1)) gives a single laser pulse. The pulse generated by external unit at the moment T_1 (chart (1)) gives the start for the

process resulting in firing of every laser pulse. This pulse initiates the flash lamp and triggering high voltage switch of Q-switch driver providing high-voltage pulse, which closes the resonator by inducing high losses (chart (3)). The laser resonator keeps closed until the adjusted inversion in Nd: YAG rod is achieved. At this moment, the fall of pulse (chart (1)) arrives at the Q-switch driver and enforces it to provide a short pulse of opposite polarity (chart (3)). The losses in resonator become minimum, and very short and powerful optical pulse is generated (chart (4)). In the external triggering mode, the laser initiation pulse in the timing chart (1) is generated by pulse generator. Width of this pulse determines the power of laser accurately and can be adjusted as required. Additionally, the repetition rate of pulses can be adjusted.

4.1.2 Measurement of Laser Pulse Energy

Although the laser is controlled very precisely in the externally-triggered mode, there is a possibility that the energy of the laser pulse can fluctuate in some shots. The energy of the laser pulse must be measured in every shot. The energy of the laser pulse was measured using a high sensitive photodiode and an oscilloscope. A beam splitter is used to split the laser light into two beams. One of them is 5 percent of total power; and is used to measurement the energy of the laser pulse. The other is 95 percent of total laser power; and used to generate plasma in order to increase the energy per unit volume. The laser pulse is focused by a double convex lens which has a 75 mm focal length. The energy per unit volume increases exponentially and reaches the breakdown threshold just before the focal point.

Emission light from the spark is collected with a fiber. The fiber is located perpendicular to laser beam direction in order to avoid the effect the laser light on the spectrometer. The other end of the fiber is connected to a spectrometer.

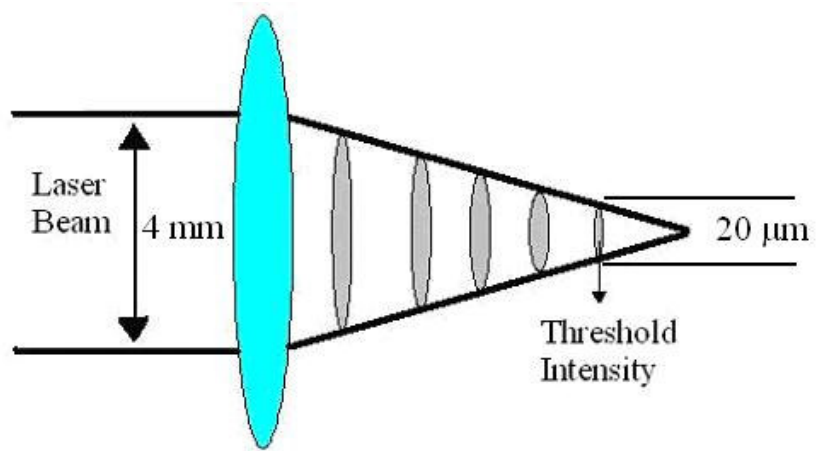


Figure 4.4: Threshold position of laser pulse.

4.1.3. Acquisition of the plasma spectrum:

Determination of wavelength emitted from plasma is very important. All analysis and determination is made by using the emission wavelength and intensity of the emission line. Therefore, we have to use reliable spectrometer. In addition, timing is very important for our work, so spectrometer must be fast and response time must be same in every shot. For this purpose, we used Ocean Optics HR2000 spectrometer in the setup to determine emission wavelengths. This spectrometer can be controlled externally. The spectrometer has a high resolution depending on grating the used in it and responds wavelength between 200 to 1100 nm. This spectrometer has single array 2048 pixel CCD detector, and 300 groove/mm density grating. This grating efficiency depends on the wavelength, efficiency curve for 200 to 1100 nm shown below.

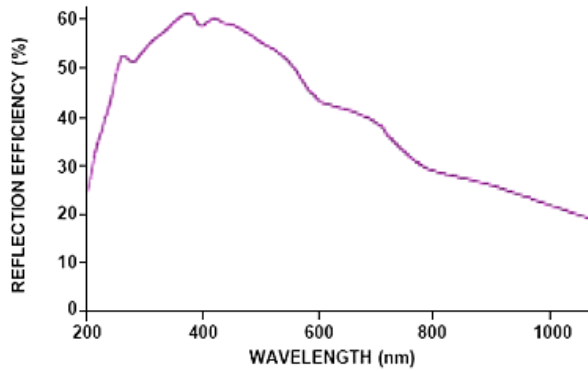


Figure 4.5: Efficiency Curve for Grating HC1

Table 4.1: Specification of used spectrometer

Detector	Sony ILX511 linear silicon CCD array
No. of CCD element	2048
Pixel Size of CCD	14 μ m x 200 μ m
Pixel Well Depth	62,500 electron
Signal to Noise Ratio	250:1
A/D Resolution	12 Bit
Dark Noise	2,5 RMS counts
Corrected linearity	>99,8 %
Spectral Range	200-1100 nm
Resolution	1 nm FWHM
Entrance Aperture	5 μ m slit
Grating	300 line per mm grating

In externally triggering mode, there is no way to synchronize the scanning, acquisition, and transfer of data with an external event. However, trigger pulses for synchronizing an external event with the spectrometer are available. This signal must be applied externally. In External Triggering, an event outside the sampling system

(such as a push button, lever activation, or laser pulse) triggers the voltage level on the spectrometer's trigger pin and instructs the spectrometer to begin spectra acquisition. A TTL (Transistor Transistor Logic) signal can be used as an external triggering for the spectrometer. Triggering signal can start the predetermined integration time ($50 \pm 1 \mu\text{sec}$) and records the spectra. For our system this external signal is created with pulse generator. There is a problem related to integration time for our spectrometer, that is, when applied the triggering signal to our spectrometer, data acquisition starts in pico seconds and continues 50 μsec duration. So in this time period plasma decay is completed.

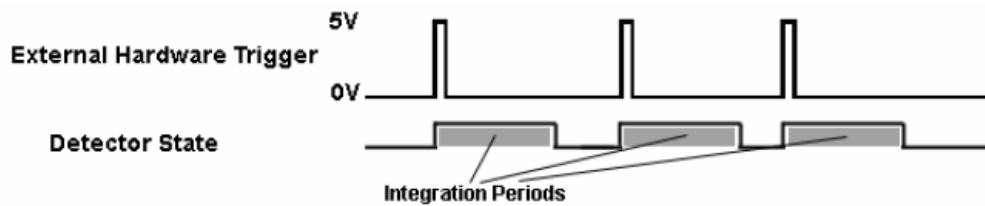


Figure 4.6: External Hardware Triggering – Trigger Timing

4.1.3.1 Spectral Calibration of Spectrometer

For a precise measurement, we calibrate the wavelength scale of the used spectrometer. In this work, the spectral calibration of the spectrometer was done by using standard lamps emitting between 200-1100 nm wavelength ranges. 12 Watt LP-Mercury lamp of spectral irradiance (Model: Philips Lighting - Item No. 93123E), and 60 Watt Spectral Lamp - Noble Gas – Helium lamp of spectral irradiance (Model: Philips Lighting - Item No. 93098E) was used for this purpose. Spectral distribution of this two lamp is shown below.

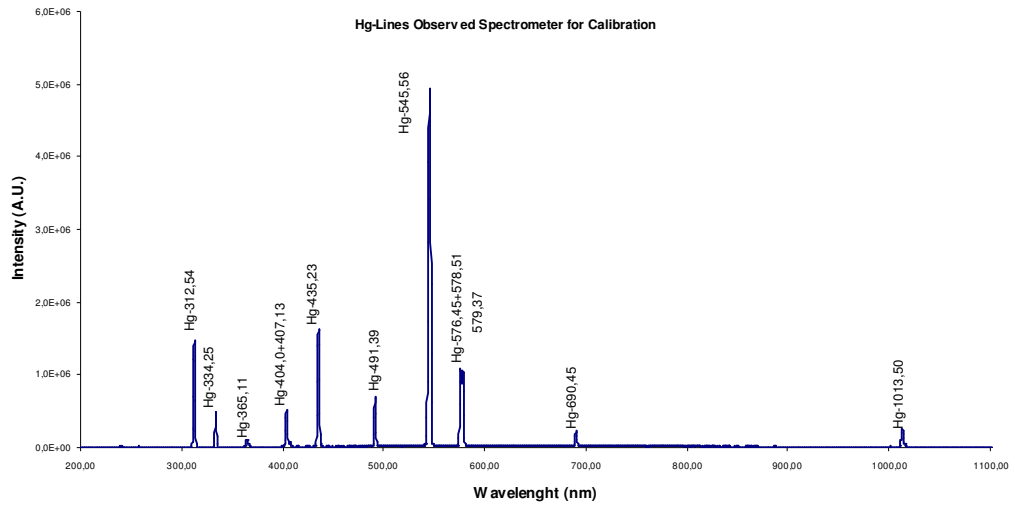


Figure 4.7: Observed spectrum from spectrometer for Hg lamp.

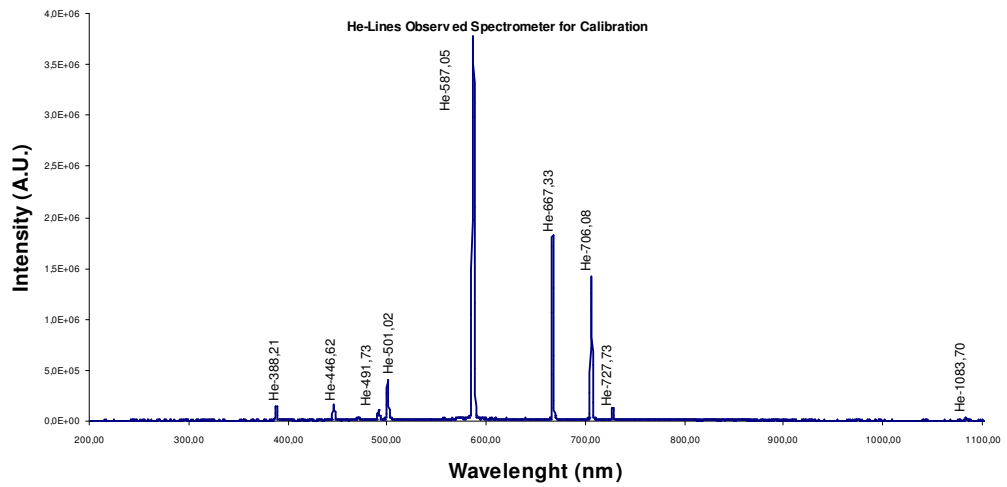


Figure 4.8: Observed spectrum from spectrometer for He lamp.

Table 4.2: He-Hg lines wavelength between 200-1100 nm

Spectrum	Observed Waveleght NIST (nm)	Relative Intensity	Observed Wavelength Spectrometer(nm)	Pixel Number
He I	388,98	500	388,21	428
He I	447,27	200	446,62	555
He I	492,33	20	491,73	653
He I	501,71	100	501,02	674
He I	587,73	500	587,06	863
He I	667,99	100	667,33	1042
He I	706,71	200	706,08	1130
He I	728,34	50	727,73	1179
He I	1083,33	2000	1083,70	2005
Hg I	312,66	400	312,54	265
Hg I	334,24	80	334,25	311
Hg I	365,12	2800	365,11	377
Hg I	404,77	1800	404,0	462
Hg I	407,90	150	407,13	469
Hg I	435,96	4000	435,23	530
Hg I	491,74	80	491,39	653
Hg I	546,23	1100	545,56	772
Hg I	690,94	250	690,45	1095
Hg I	1014,25	2000	1013,50	1838

(NIST: National Institute of Standards and Technology)

Before starting the experiment, the calibration of our spectrometer was done by using these data (Calibration steps and details are in the Appendix B). As mentioned in the appendix, we determine the constants for best calibration coefficient for spectrometer.

4.1.4 Pulse Generation and timing:

For our work, the most important subject is timing accommodation between apparatus. The triggering pulse duration and sequence for laser, spectrometer and computer are very important. For this purpose, we use in the experiment very sensitive pulse generator, this is DG535 Digital Delay/Pulse Generator which provides four precisely-timed logic transitions or two independent pulse outputs. The delay resolution on all channels is 5 ps. Front-panel BNC outputs deliver TTL, ECL, NIM or variable level (-3 to $+4$ V) pulses into 50Ω or high impedance loads. This is important for us, because laser and spectrometer needs TTL voltage for triggering. The high accuracy, low jitter, and wide delay range make the delayer ideal for laser timing systems and precision pulse applications.

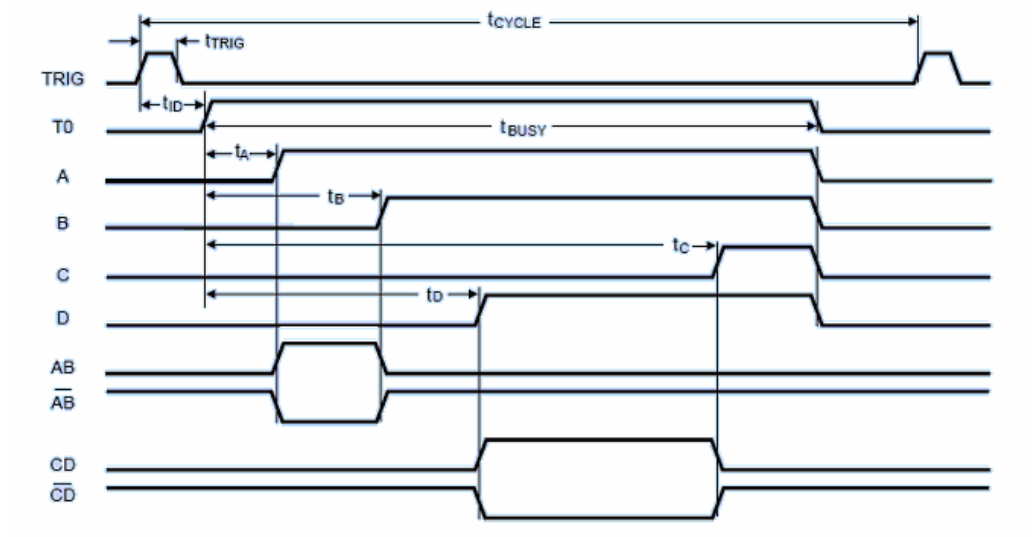


Figure 4.9: Pulse generator timing diagram

The pulse generator has four independent outputs make it ideal for laser timing applications. In our work, the A output of the pulse generator fires the flashlamp of a pulsed laser. Its internal rate generator controls the repetition rate of

the laser and the overall experimental repetition rate. The B delay output controls the firing of the laser Q-switch. The C delay output is used to trigger the spectrometer. Finally, the D delay is used to trigger the gated integrator looking at the spectrometer. Note that both the B and C delays can be specified relative to the A delay. In this way, as the laser pulse is moved by changing the A to T0 delay, the experimental trigger and the gated integrator trigger will stay fixed relative to the laser pulse.

4.2 Data Acquisition

By using this component, we analyze time sequence spectra of Laser Induced Air Breakdown. Our theory is based on triggering the laser and the spectrometer at different time and applying their trigger time by adding the time delay (Δt) between them by using the pulse generator. The pulse shape for triggering the laser and the spectrometer is given in Figure 4.10. Laser power is proportional to triggering pulse width as mentioned above. We can adjust the power of the laser by using this property. Laser trigger pulse duration can be changed from 50 μs to 240 μs . However, the laser gives most stable output at 180 μs pulse duration.

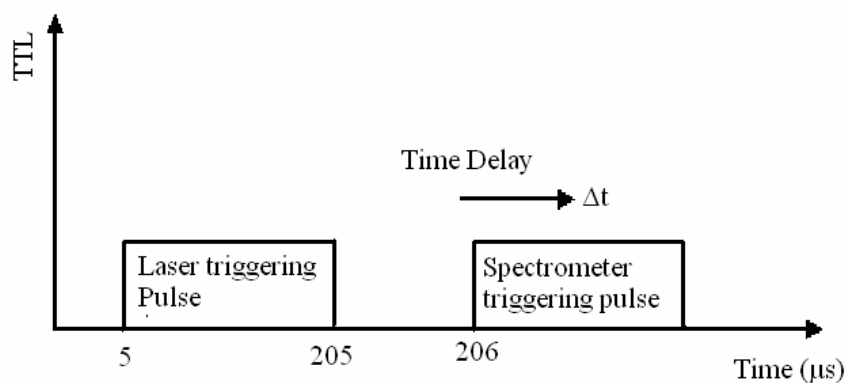


Figure 4.10: Pulse shape for triggering

The plasma was formed under atmospheric pressure, and in a clean room, in order to avoid existing aerosol particles. Plasma emissions were based on the spectral analysis of an ensemble average of 10 spectra. Determining the pulse energy of the each shot, we choose the spectrum which is produced by the same exerted energy. We trigger the system to 20 s time interval (0.05 Hz), thus we avoid the effect of one preceding shot.

There is one serious problem with the spectrometer. The spectrometer has 50 ms integration time at the externally triggered mode. It has an internal clock, and we can't synchronize internal clock with external trigger signal. When triggering pulse come to the spectrometer, the spectrometer starts acquisition independent of the internal clock of spectrometer, but the integration time is determined by the internal clock. Therefore, integration period is not a constant value ($\pm 1 \mu\text{s}$ time deviation). Because of this property, we can't use the tail of the spectrometer integration period. Therefore, we can use only the initiation of the integration period of the spectrometer. When the triggering pulse is activated, the integration of the spectrometer starts at the same time as seen in the Figure 4.6. Laser trigger, plasma life time and spectrometer triggering period are shown in Figure 4.11.

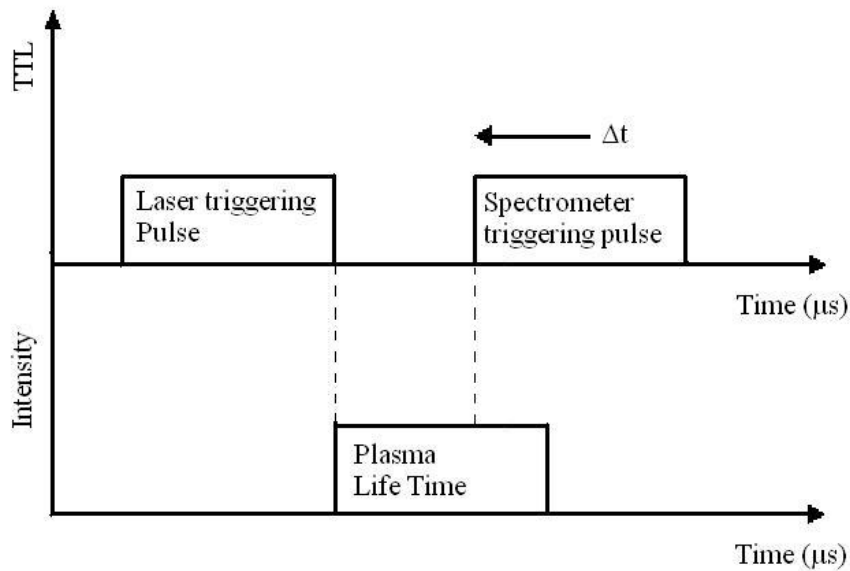


Figure 4.11: Timing period of plasma generation and data acquisition.

As mentioned before, we take 10 data for each time delay which has a step size 1 μs .

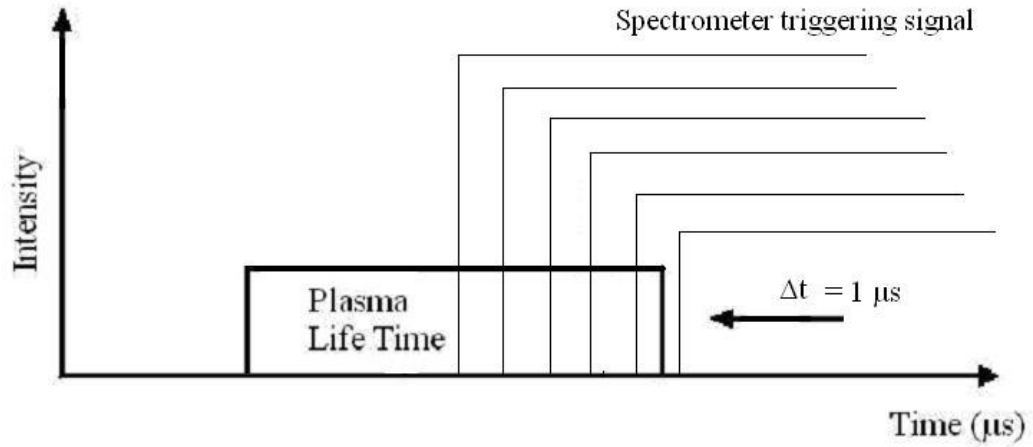


Figure 4.12: Differential acquisition of spectrum.

Figure 4.12 shows the differential acquisition of the plasma emission. As shown in the figure, the initiation of the spectrometer integration period is shifted 1 μs left. Thus, life time of plasma is scanned. While subtracting one emission spectrum from preceding one, the differential decay of the plasma lifetime can be resolved.

CHAPTER 5

OBSERVATIONS and DATA ANALYSES

5.1. Spectral Analysis by LIBS

Spectroscopic information was obtained from the laser produced plasma spectra in helium and air, under atmospheric pressure as shown in Figures 5.1 and Figure 5.2 respectively. Measurements started 20 nanoseconds after the laser pulse with a 50 milliseconds gate width. Each spectrum was obtained over a 200-1100 nm wavelength range. The laser energy during the measurements was kept around 200 mJ. Most of the neutral and ionic lines of helium and air were identified.

The air spectra contain emissions from singly ionized and neutral nitrogen and oxygen lines superimposed on an intense background continuum. Ion lines from higher ionization states were not observed under these conditions. Neutral lines for both oxygen and nitrogen were observed mostly at longer wavelengths, e.g., O (I) at 715.6, 777.4, 748.0 nm and N (I) at 742.4, 744.3, 746.8, 820.03 nm. However, ion lines were observed mostly at shorter wavelengths, between 300 to 500 nm for both oxygen and nitrogen.

The analysis method is described in the next section. The air plasma is really hard to resolve. Because lots of emission lines are presents and some of them interfere each other.

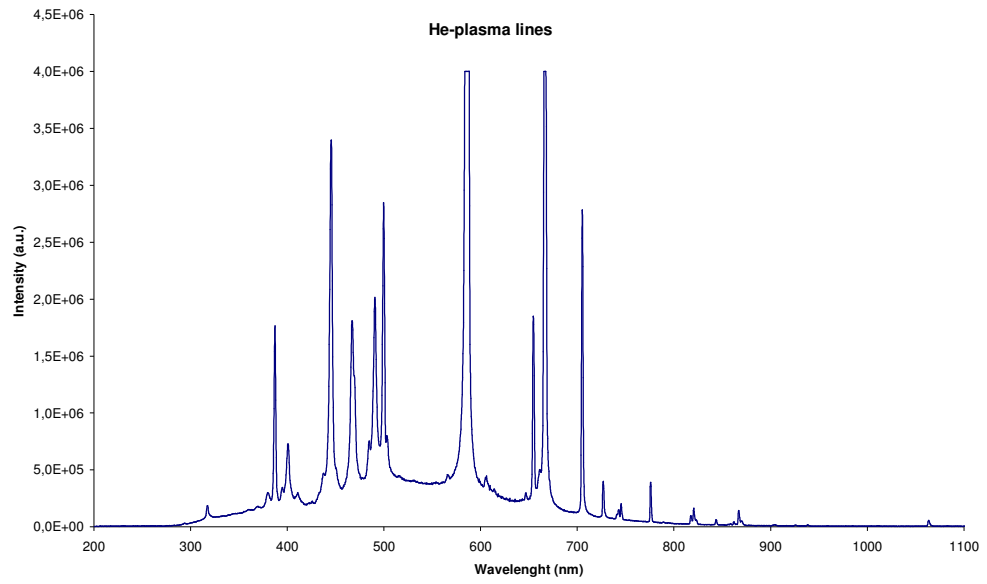


Figure 5.1: Laser Induced He Plasma Lines

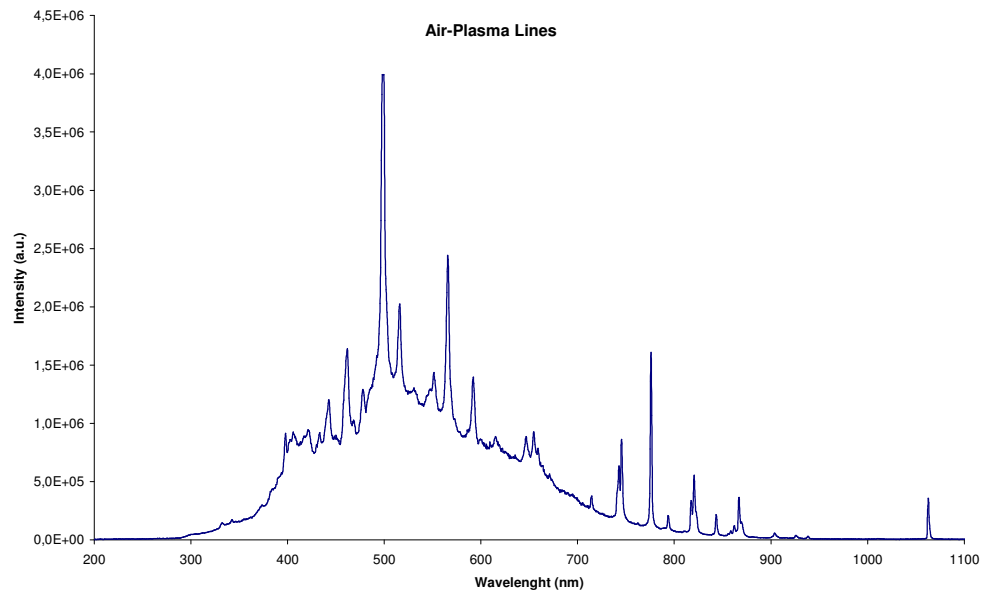


Figure 5.2: Laser Induced Air Plasma Lines

5.2. *Analysis Method of Spectral Lines*

The data analysis computer program is a crucial point in order to extract qualitative analysis even in the presence of spectral interferences. Problems, mostly related to spectral interferences of neighboring lines are taken into account by Curve Fit data reduction software which is presented here. The peak fitting program deals with individual spectra. Due to the low resolution of our system and to the multielement character of LIBS spectra of air, spectral interferences of neighboring lines are a serious problem that is dealt with as follows. The background of LIBS spectra normally consists of: instrumental background; residual plasma continuum; line wing contributions by the constituents of the sample. At a low resolution, the latter make a remarkable contribution to the background and proper subtraction is therefore especially important. Each spectrum has therefore been divided into bands and interfering lines within each band were fitted in one run (see Figure 5.3).

A Gaussian curve has been assumed as the fitting function of the emission broadening. Such Gaussian shaped line emission profiles were found to be much larger than the expected physical line width in LIBS spectra (at atmospheric pressure). Constraints on the peak width have been put in the fit, to avoid an erroneous background simulation by a very broad Gaussian. For each LIBS spectrum, the output of the peak fitting program is a 2D matrix of deconvoluted peak wavelengths, intensities.

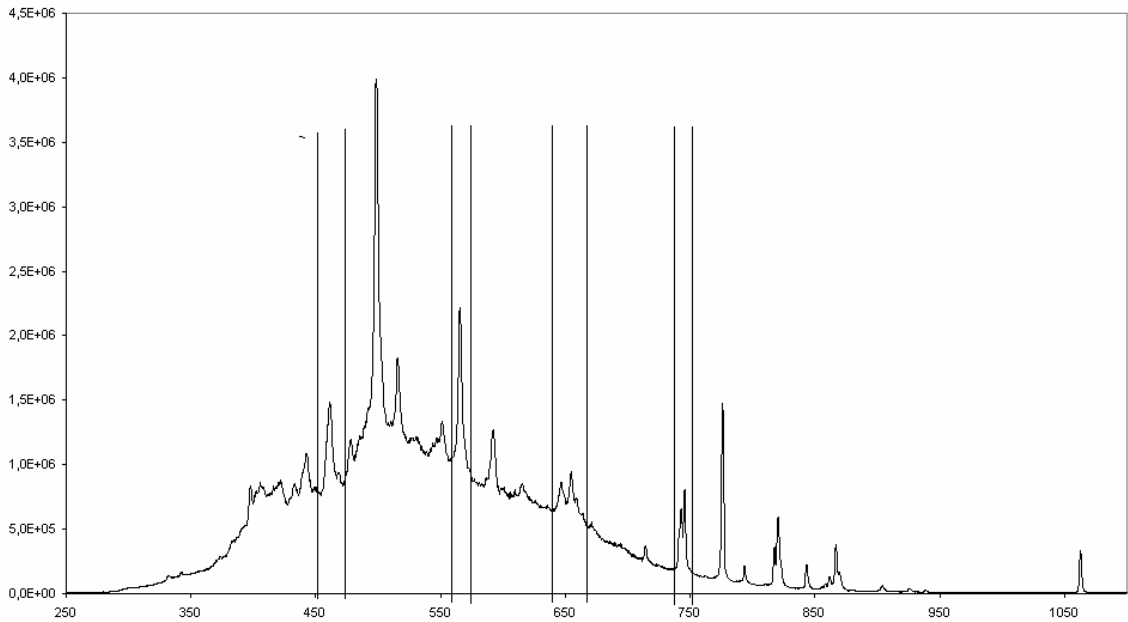


Figure 5.3: Example of typical spectrum (air) that is divided in to several bands. All interfering lines in one band are fitted in one run.

The peak fitting procedure is followed by the assignment, which is the task of the peak identification program. The latter, we compare the measured center wavelengths and intensities to those of each element as listed in a large emission spectra database [NIST]. The matrix with peak information is processed independently for each individual spectrum. Because of the large overlap between two neighboring spectra, the peak identification program first double-checks the results of the peak fitting and corrects for systematic errors in the wavelength calibration, then we search in the database spectral table. The resulting assignment of the main atomic features contributing to all the spectra shown in Figure 5.5 is indicated together with the experimental line origin from the deconvolution.

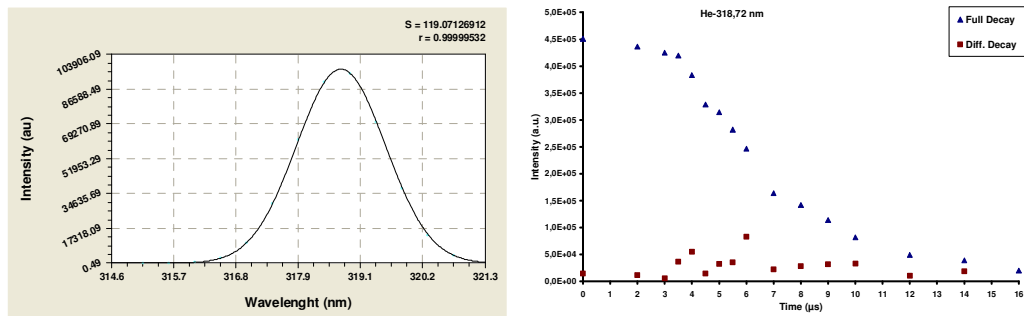
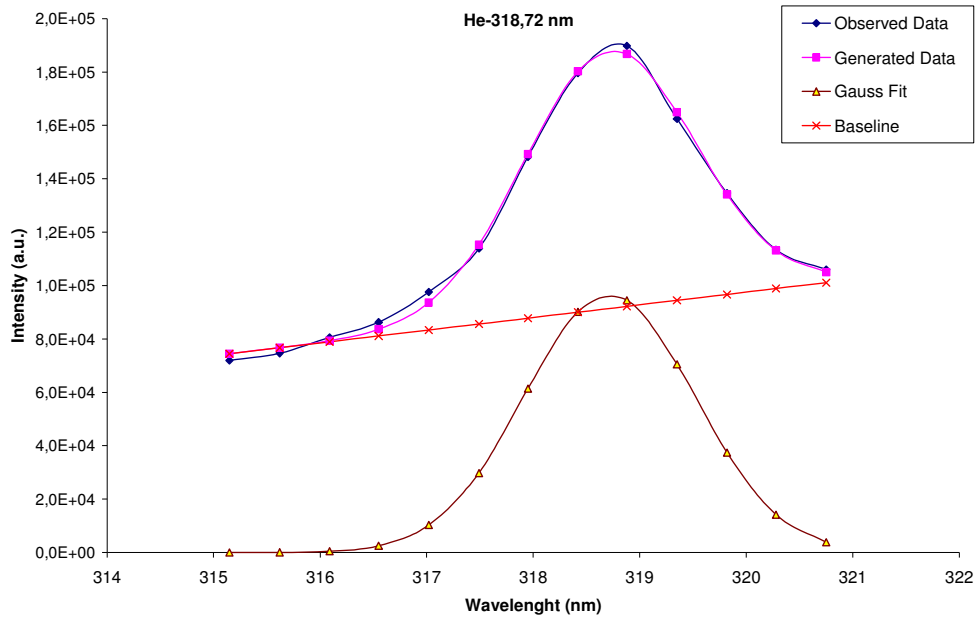
5.3. *Helium Plasma Data Acquisition and Data Analysis*

The reliability of the setup used in the study is tested with single gas helium at the atmospheric pressure. Helium is simplest gas after hydrogen, which has only two electron and definite energy levels. Lots of helium plasma properties have been worked under different condition by scientists.

For the helium plasma data acquisition, the quartz chamber was evacuated to a pressure of 1 Pa and filled with helium up to atmospheric pressure. Breakdown occurred at this pressure by focusing a laser beam. The dimensions of the plasma soon after the breakdown are 5 mm long and 2 mm in diameter.

Some properties of the plasma formed were determined by spectroscopic measurements of singly ionized and neutral helium lines. For this purpose, the time history and emission line shape of the following lines were investigated: He I-318.7 nm, He I-388.8 nm, He I-402.6 nm, He I-446.9 nm, He II-468.7 nm, He I-471.3 nm, He I-492.4 nm, He I-501.3 nm, He I-505.0 nm, He I-656.0 nm, He I-667.9 nm, He I-706.5 nm and He I 728.1 nm. Details of these lines are given below. Data analysis is made by using the technique described in previous section.

As described in data acquisition section in chapter 4, we took lots of spectrum at different time after the plasma initiation. Data analysis is made for all emission spectrum which is taken at different time. The spectrum which is taken at 1st μ s of the plasma life time, however, is shown in that section. Because, some scientist suggest that 1st μ s of the plasma life time can be assumed to supply locally thermal equilibrium conditions.

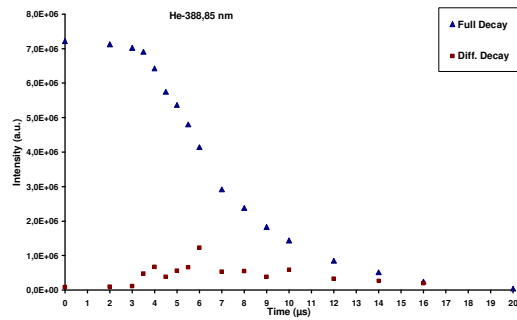
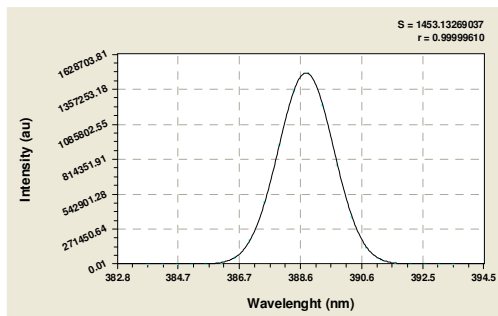
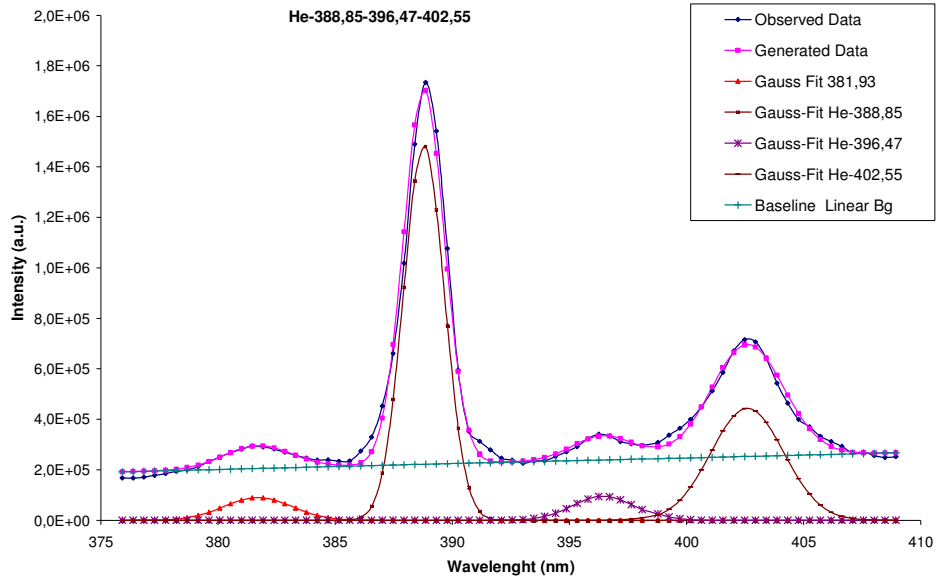


$$\text{Gaussian Model: } I = N \cdot e^{-\frac{(\lambda-b)^2}{2 \cdot \sigma^2}}$$

Coefficient Data: $N = 96560.977$, $b = 318.71491$, $\sigma = 0.80085563$

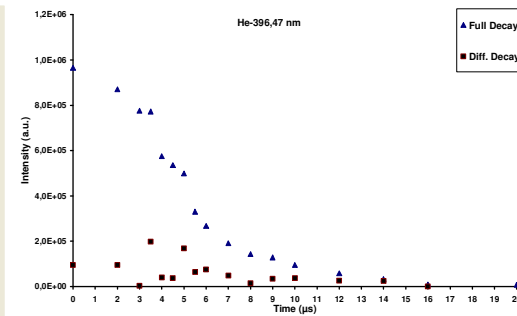
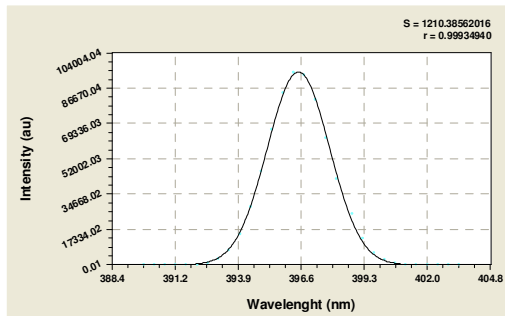
Figure 5.4: He I-318.72 nm, a) Fitting Observed Data to Gauss Distribution, b) Normalized Gauss Analysis c) Time Evolution

The analysis data in the Figure 5.4 belongs to He I-318.71 nm. Its transmission probability (Einstein coefficient) is $5.05 \times 10^{+6}$ and the emission energy is 31631 cm^{-1} . Plasma duration is $16 \mu\text{s}$ and decay start $3 \mu\text{s}$ after the laser shot; total intensity drop 10 percent of initial value at $12 \mu\text{s}$. Calculated Doppler velocities is 246 m/sec .



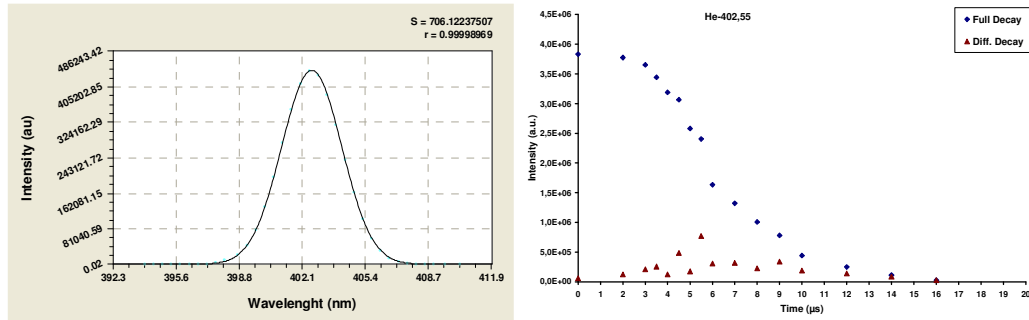
Gaussian Model:

Coefficient Data: N = 1484076.9, b = 388.78814, $\sigma = 0.87345025$



Gaussian Model:

Coefficient Data: N = 94661.032, b = 396.46079, $\sigma = 1.3404455$

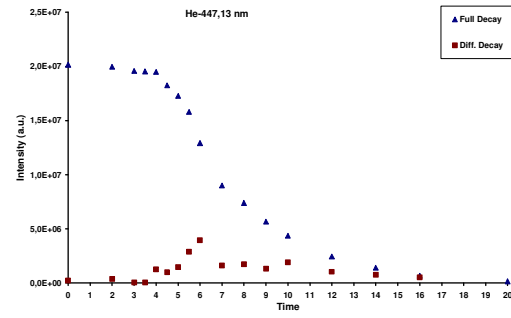
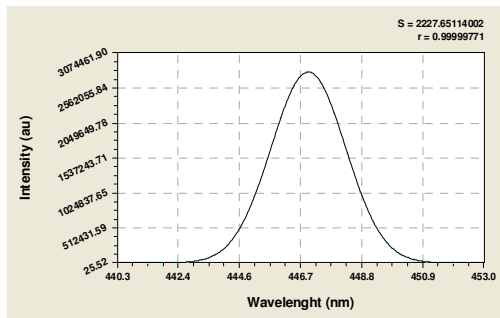
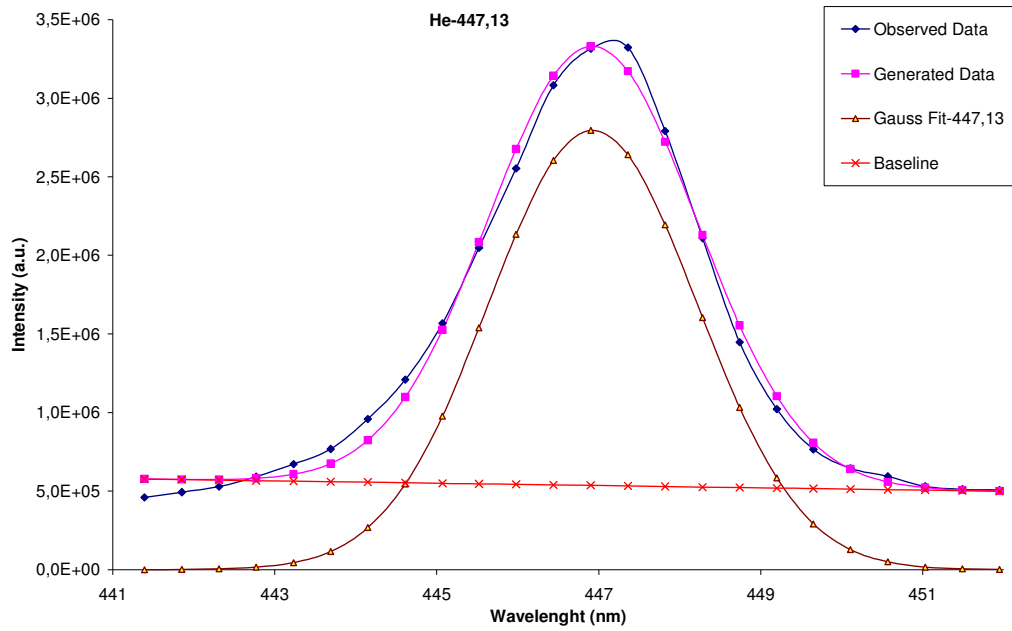


Gaussian Model:

Coefficient Data: $N = 443238.1$, $b = 402.59456$, $\sigma = 1.5568662$

Figure 5.5 : He I-388.78 nm-396.46nm-402.59, a) Fitting Observed Data to Gauss Distribution, b) Normalized Gauss Analysis c) Time Evolution

The analysis data in the Figure 5.5 belongs to He I-388.7 nm, He I-396.5 and He I-402.6 nm. Their transmission probabilities (Einstein coefficient) are $9.48 \times 10^{+6}$, $7.17 \times 10^{+6}$, $2.93 \times 10^{+6}$ and the emission energies are 25706 , 25215 and 24830 cm^{-1} respectively. Plasma durations are $20 \mu\text{s}$ for 388.7 nm, $16 \mu\text{s}$ for 396 nm and 402.6 nm lines, decay start $3 \mu\text{s}$ after the laser shot; total intensity drop 10 percent of initial value at $12 \mu\text{s}$ for all lines. Calculated Doppler velocities are 220 m/sec , 272 m/sec and 365 m/sec respectively.

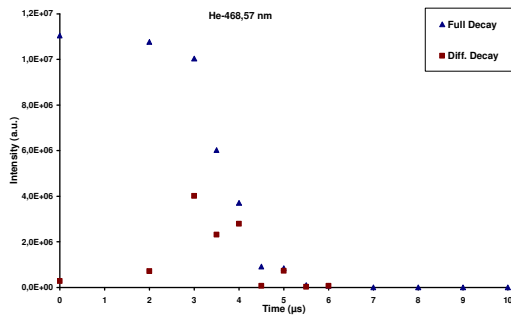
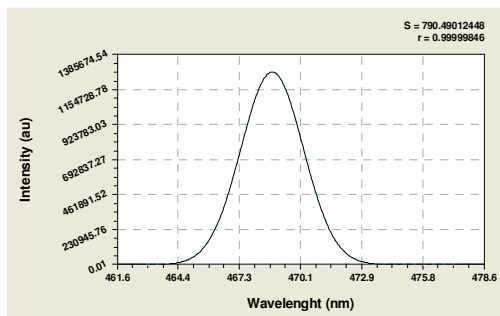
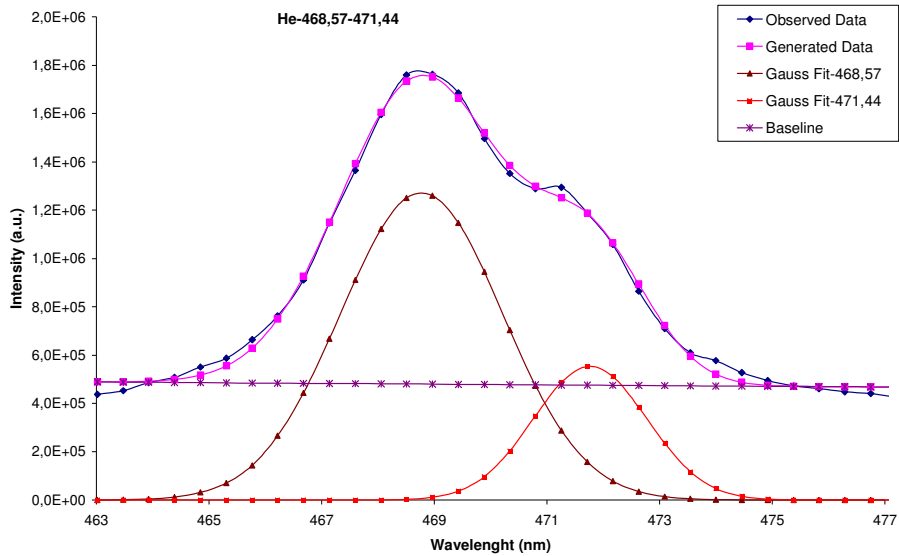


Gaussian Model:

Coefficient Data: $N = 2797351.4$, $b = 447.13639$, $\sigma = 1.2826954$

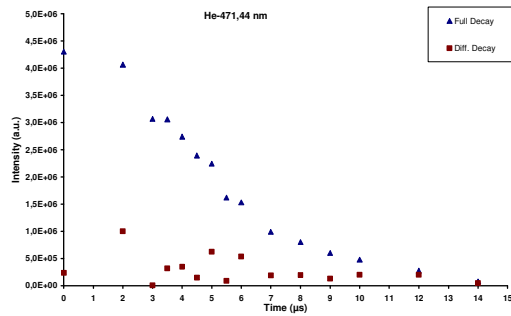
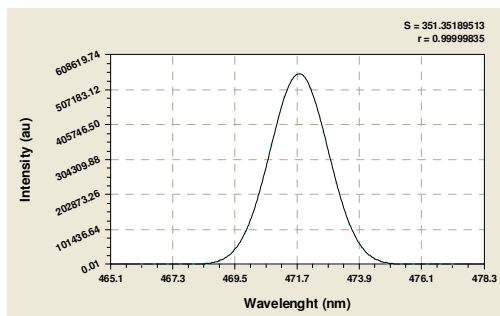
Figure 5.6 : He I-447.14 nm, a) Fitting Observed Data to Gauss Distribution, b) Normalized Gauss Analysis c) Time Evolution

The analysis data in the Figure 5.6 belongs to He I-447.13 nm. Its transmission probability (Einstein coefficient) is $6.28 \times 10^{+6}$ and the emission energy is 22358 cm^{-1} . Plasma duration is $20 \mu\text{s}$ and decay start $5 \mu\text{s}$ after the laser shot; total intensity drop 10 percent of initial value at $12 \mu\text{s}$. Calculated Doppler velocities is 263 m/sec .



Gaussian Model:

Coefficient Data: $N = 1271191.3$, $b = 468.67505$, $\sigma = 1.4416991$

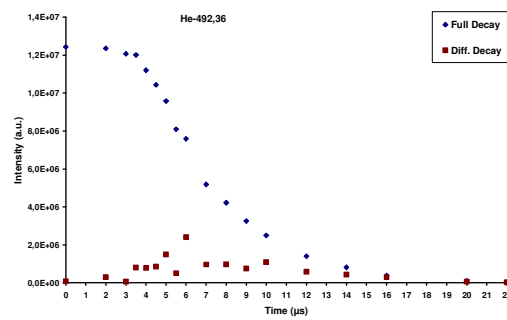
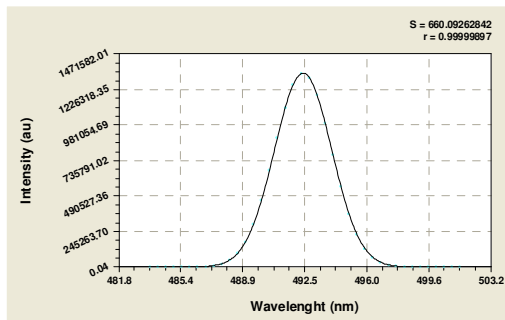
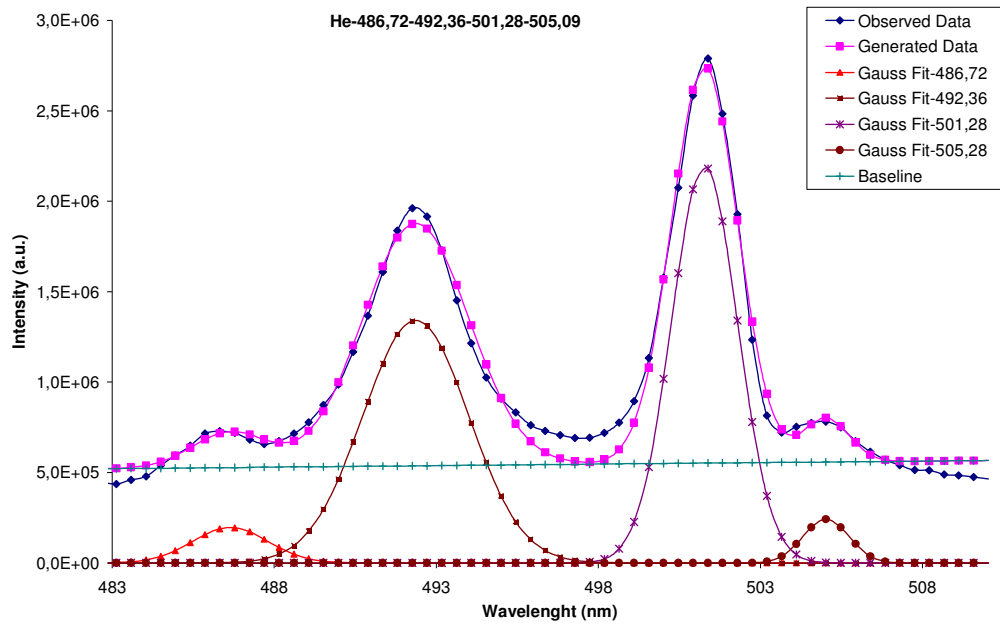


Gaussian Model:

Coefficient Data: $N = 553662.2$, $b = 471.36938$, $\sigma = 1.0089977$

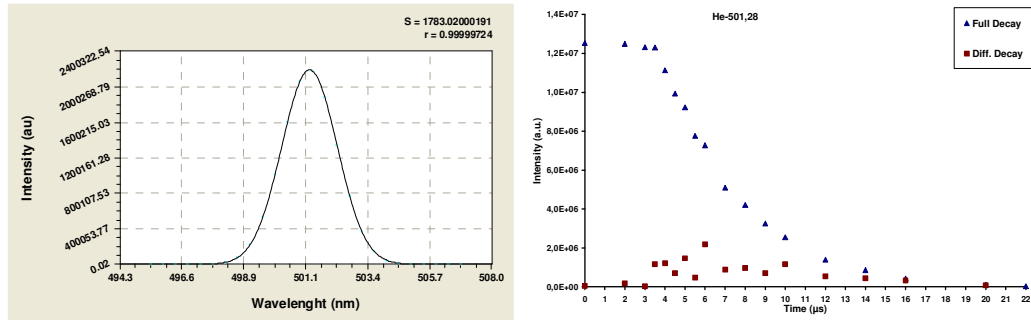
Figure 5.7 : He II-468.77 nm and He I-471.41 nm, a) Fitting Observed Data to Gauss Distribution, b) Normalized Gauss Analysis c) Time Evolution.

The analysis data in the Figure 5.7 belongs to He II-468.77 nm and He I-471.31 nm. Their transmission probabilities (Einstein coefficient) are $5.85 \times 10^{+6}$ and the emission energy is 21211 cm^{-1} for 471.31nm emission line. Plasma duration is 7 μs , 16 μs and decay start 3 μs , 2 μs after the laser shot for He II-468.7 and He I-471.3 nm respectively; total intensity drop 10 percent of initial value at 4 μs for He II level. Calculated Doppler velocities are 301 m/sec and 248 m/sec.



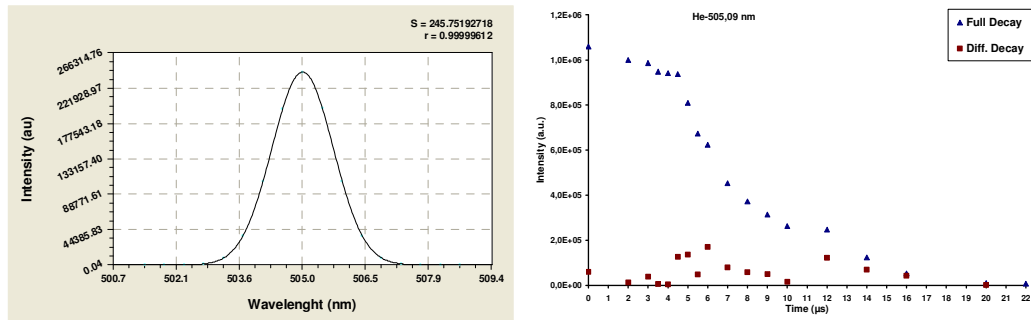
Gaussian Model:

Coefficient Data: $N = 1340398.9$, $b = 492.36748$, $\sigma = 1.6393278$



Gaussian Model:

Coefficient Data: $N = 2192183$, $b = 501.27685$, $\sigma = 1.0215808$

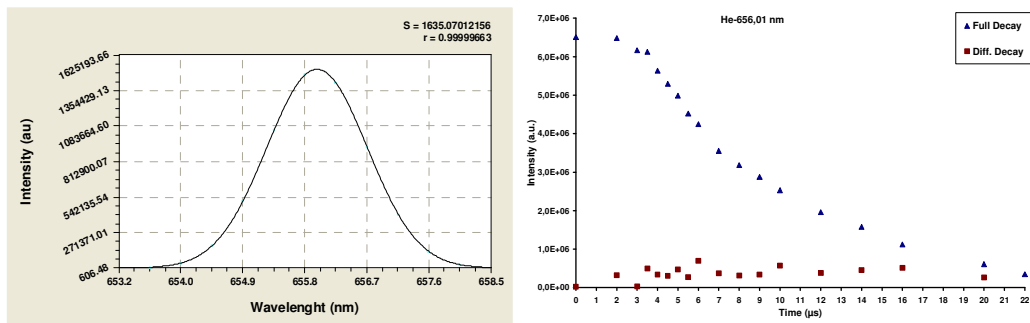
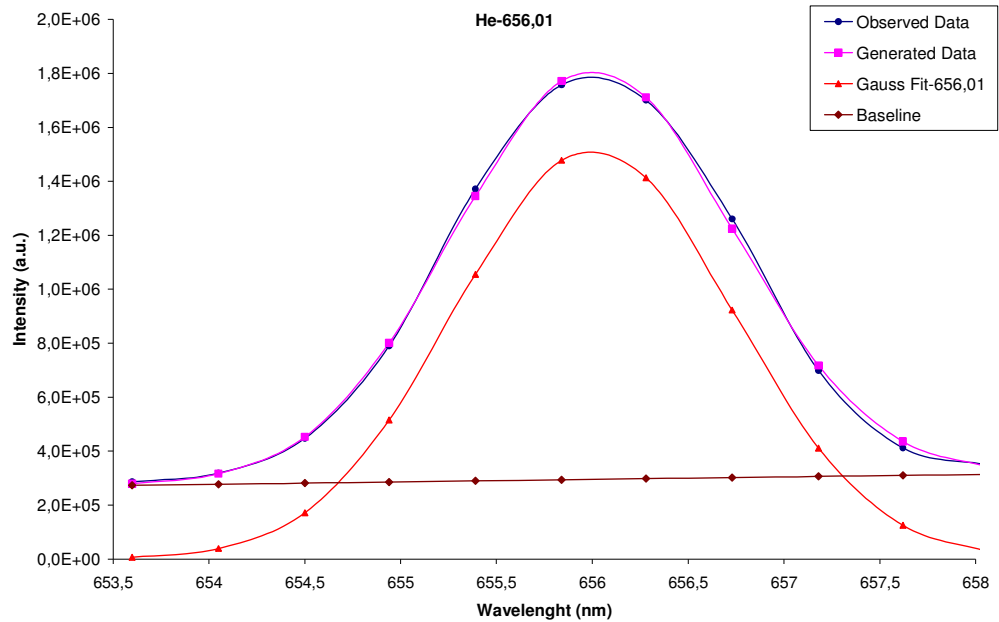


Gaussian Model:

Coefficient Data: $N = 242037.63$, $b = 504.82588$, $\sigma = 0.70804297$

Figure 5.8 : He I-492.19-501.27-504.77 nm, a) Fitting Observed Data to Gauss Distribution, b) Normalized Gauss Analysis c) Time Evolution

The analysis data in the Figure 5.8 belongs to He I-492.19 nm, He I-501.27 nm and He I-504.77 nm emission lines. Their transmission probabilities (Einstein coefficient) are $2.02 \times 10^{+6}$, $1.34 \times 10^{+6}$, $6.55 \times 10^{+6} \text{ sec}^{-1}$ and the emission energies are 20312, 19932 and 19805 cm^{-1} respectively. Plasma durations are 20 μ s for 492.19 nm, 396 nm and 402.6 nm lines, decay start 3 μ s after the laser shot; total intensity drop 10 percent of initial value at 12 μ s for all lines. Calculated Doppler velocities are 277 m/sec, 195 m/sec and 135 m/sec respectively.

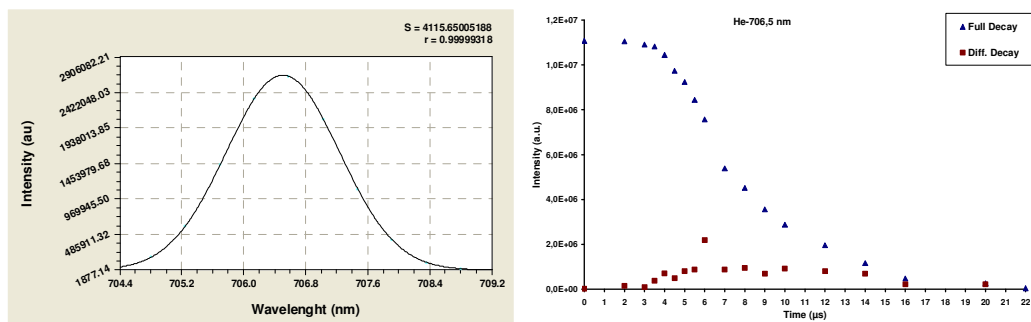
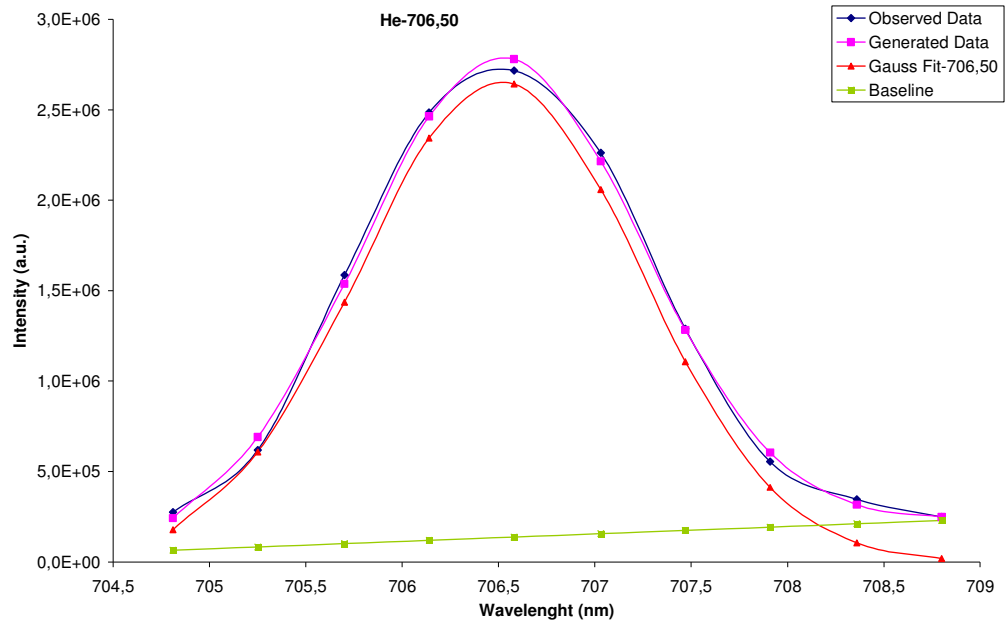


Gaussian Model:

Coefficient Data: $N = 1517663$, $b = 656.00723$, $\sigma = 0.72463751$

Figure 5.9 : He II-656.01 nm, a) Fitting Observed Data to Gauss Distribution, b) Normalized Gauss Analysis c) Time Evolution

The analysis data in the Figure 5.9 belongs to He II-656.01 nm. Plasma duration is 22 μs and decay start 3 μs after the laser shot; total intensity drop 10 percent of initial value at 20 μs . Calculated Doppler velocities is 104 m/sec.

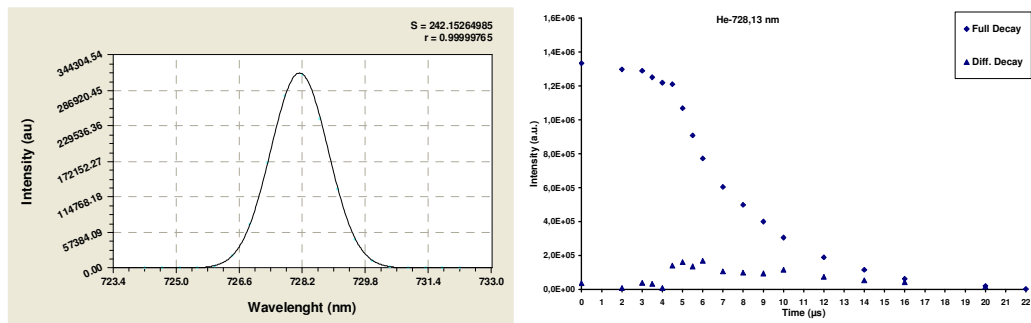
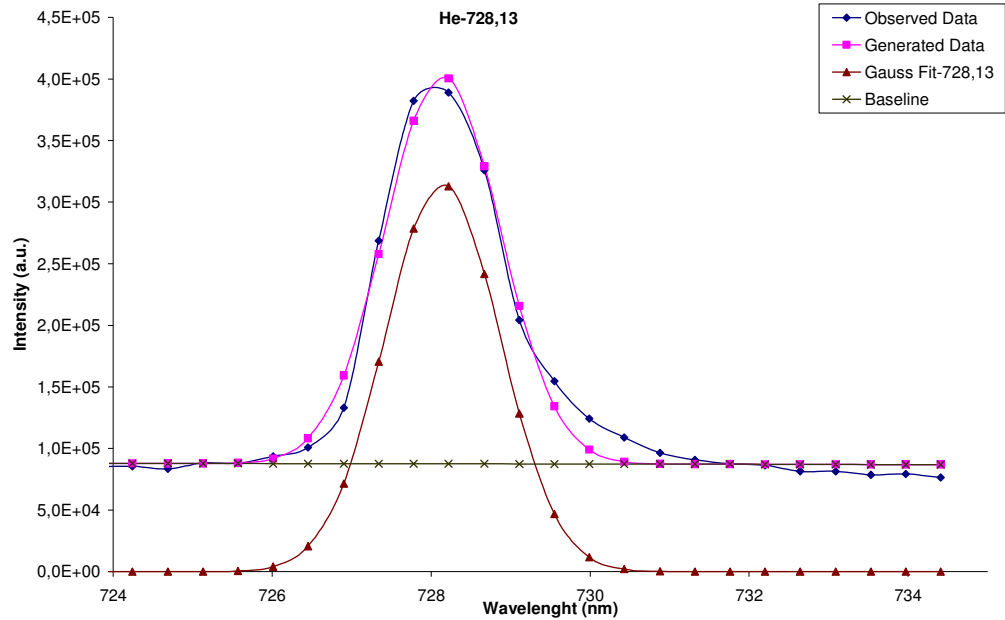


Gaussian Model:

Coefficient Data: $N = 2659285.2$, $b = 706.50646$, $\sigma = 0.72879551$

Figure 5.10 : He I-706.50 nm, a) Fitting Observed Data to Gauss Distribution, b) Normalized Gauss Analysis c) Time Evolution

The analysis data in the Figure 5.10 belongs to He I-706.5 nm, transmission probability (Einstein coefficient) is $1.54 \times 10^{17} \text{ sec}^{-1}$ and the emission energy is 14150 cm^{-1} . Plasma duration is $16 \mu\text{s}$ and decay start $4 \mu\text{s}$ after the laser shot; total intensity drop 10 percent of initial value at $14 \mu\text{s}$. Calculated Doppler velocities is 84 m/sec .



Gaussian Model:

Coefficient Data: $N = 315390.61$, $b = 728.14159$, $\sigma = 0.72220296$

Figure 5.11 : He I-728.14 nm, a) Fitting Observed Data to Gauss Distribution, b) Normalized Gauss Analysis c) Time Evolution

The analysis data in the Figure 5.11 belongs to He I-728.14 nm. Its transmission probability (Einstein coefficient) is $1.81 \times 10^{+7} \text{ sec}^{-1}$ and the emission energy is 13730 cm^{-1} . Plasma duration is $16 \mu\text{s}$ and decay start $5 \mu\text{s}$ after the laser shot; total intensity drop 10 percent of initial value at $14 \mu\text{s}$. Calculated Doppler velocities is 94 m/sec .

5.4. Air Plasma Data Analysis

The main scope of this study is to analyze the air plasma which is produced by the laser. The air plasma characteristics are studied some of scientist in different conditions. In this study, a new technique is established, and it is tested with single gas helium which is discussed previous section. The air plasma is so complex to resolve, because there are lots of the emission lines which is emitted from different components of air. Therefore, the emission lines must be selected carefully. The intensity of the atomic lines depends, among other factors, on the number of atoms present and therefore on the concentration of the gas mixture. Constituent and fraction of air is listed in Table 5.1.

Table 5.1 : Molecular weight and assumed fractional-volume composition of dry air.

Gas species	Molecular Weight (kg/kmol)	Fractional Volume (percent)
N ₂	28.013	0.78084
O ₂	31.998	0.20947
Ar	39.948	0.00934
CO ₂	44.009	0.000314
Ne	20.183	0.00001818
He	4.002	0.00000524
Kr	83.80	0.00000114
Xe	131.30	0.000000087
CH ₄	16.043	0.000002
H ₂	2.015	0.0000005
N ₂ O	44.012	0.0000005

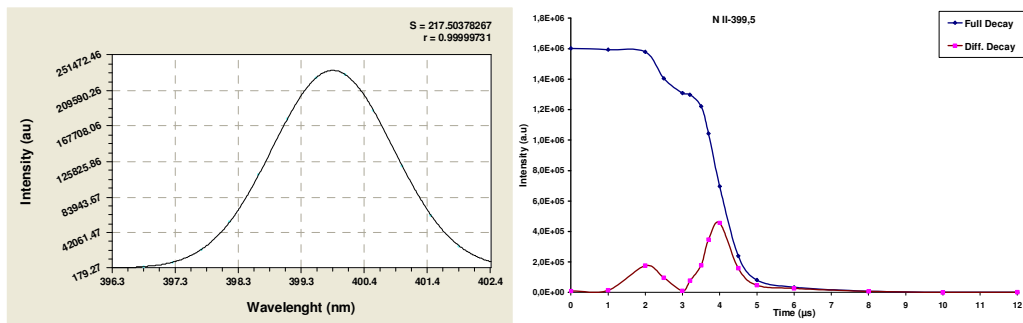
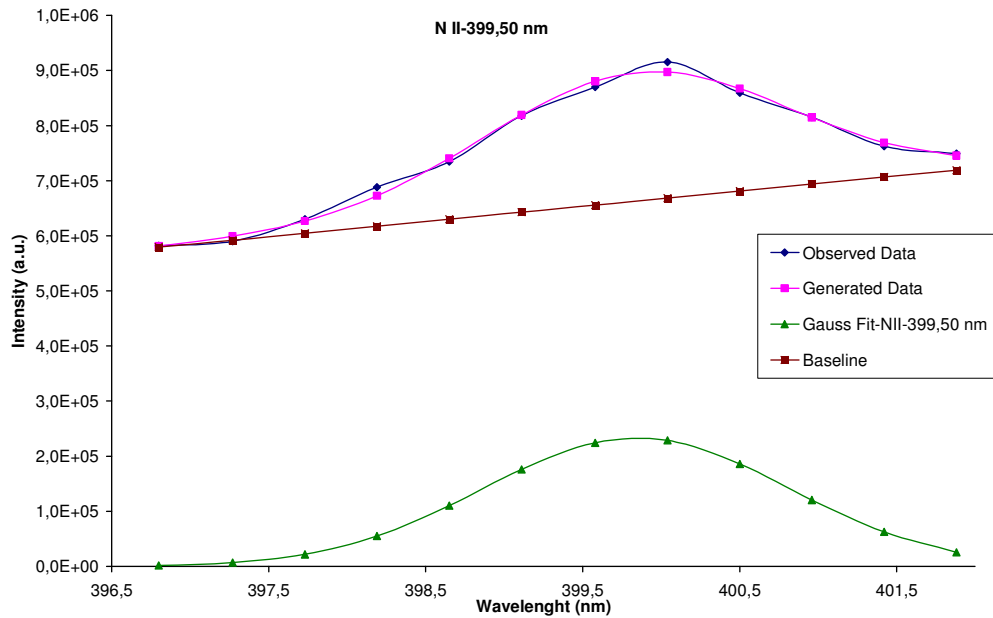
As seen from the table, air mostly consists of nitrogen, oxygen and small fraction of carbon which comes from carbon-di-oxide and methane. It is expected that the spectrum which is observed from air plasma mostly includes nitrogen and oxygen lines. Therefore, choosing lines, we mostly concentrate on nitrogen and oxygen lines.

The air plasma is formed in a clean room in order to avoid aerosol particle and humidity. First observation from the plasma is that the plasma plume shape is more intense and wide than the helium plasma.

The life time of the spark is determined with a fast photodetector and a storage oscilloscope. The photodetector detect the signal during almost 12 μ s, shape of the signal is compatible with our observation which come from the analysis described below.

The observation is started after 50 ns from the laser signal in order to avoid the matrix effects. The emissions are acquired with the 1 μ s steps. The triggering signal is applied per 20 seconds; we avoid one preceding signal effect by this way.

Some properties (line shape, intensity, decay time, differential decay time and Doppler shift) of the formed plasma were determined by spectroscopic measurements of singly ionized and neutral nitrogen, oxygen and carbon lines. For this purpose, the time history and the emission line shape of the following lines were investigated: N II-399.50 nm, N III-434.65 nm, N II-443.99 nm, N II-478.81 nm, N II-480.32 nm, N II-500.27 nm, C II-514.51 nm, C II-566.24 nm, N II-567.65 nm, N II-593.17 nm, N II-594.16 nm, O I-715.67 nm, N I-742.34 nm, N I-744.22 nm, N I-746.86 nm, O I-777.40 nm, O II-794.75 nm, C III-819.64 nm, N I-822.00 nm, N I-824.44 nm, O I-844.51 nm. Details of these lines are given below. Data analysis is made by using the technique described in previous section.

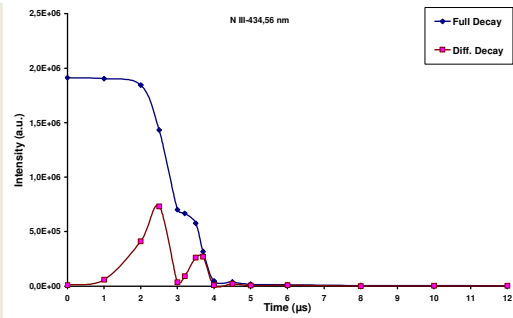
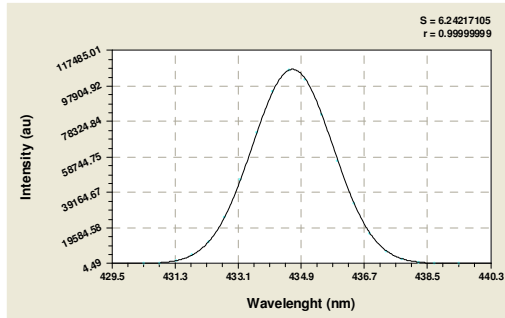
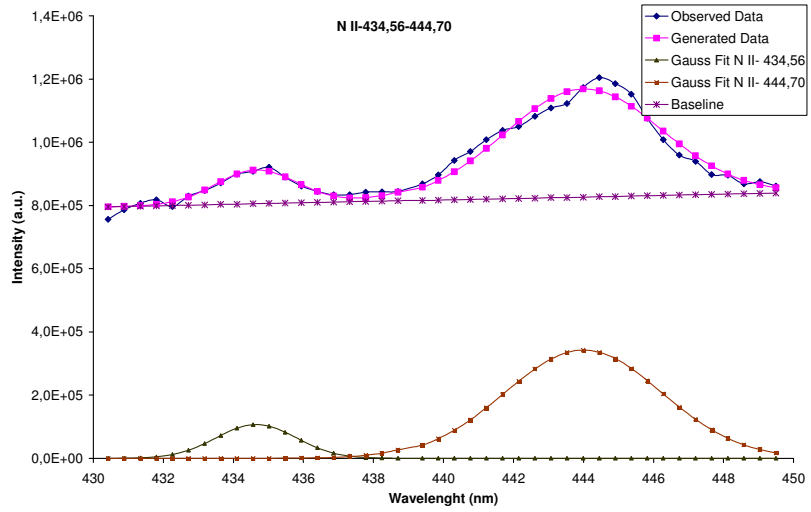


Gaussian Model:

Coefficient Data: $N = 233471.82$, $b = 399.84226$, $\sigma = 0.97340323$

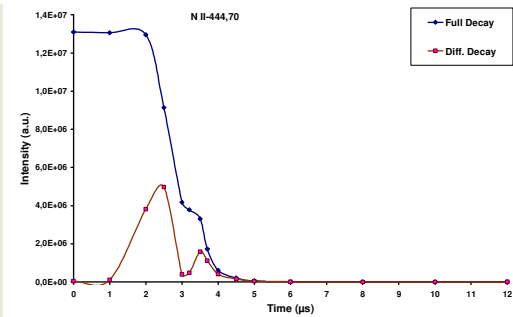
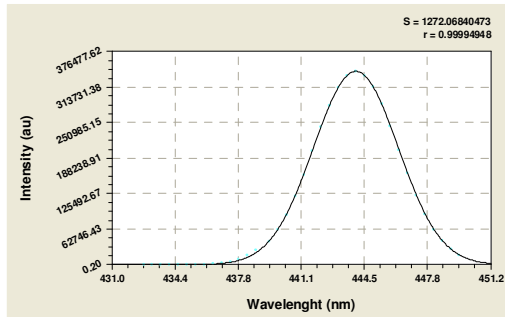
Figure 5.12: N II-399.50 nm, a) Fitting Observed Data to Gauss Distribution, b) Normalized Gauss Analysis, c) Time Evolution

The analyzed data in the Figure 5.12 belongs to N II-399.50 nm. Its transmission probability (Einstein coefficient) is $1.35 \times 10^{+8}$ and the emission energy is 25024 cm^{-1} . Plasma duration is $5 \mu\text{s}$ and decay start $2 \mu\text{s}$ after the laser shot; total intensity drop 10 percent of initial value at $4.5 \mu\text{s}$. Calculated Doppler velocities is 238 m/sec .



Gaussian Model:

Coefficient Data: $N = 107168.58$, $b = 434.65373$, $\sigma = 1.1425949$

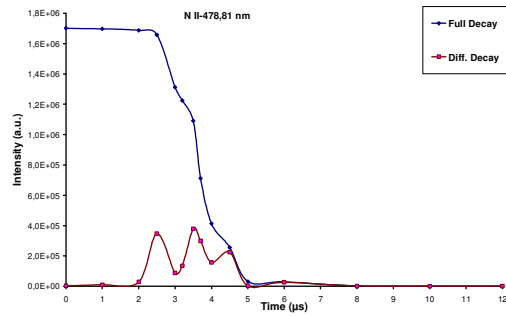
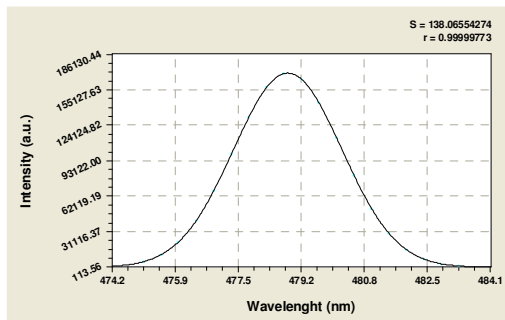
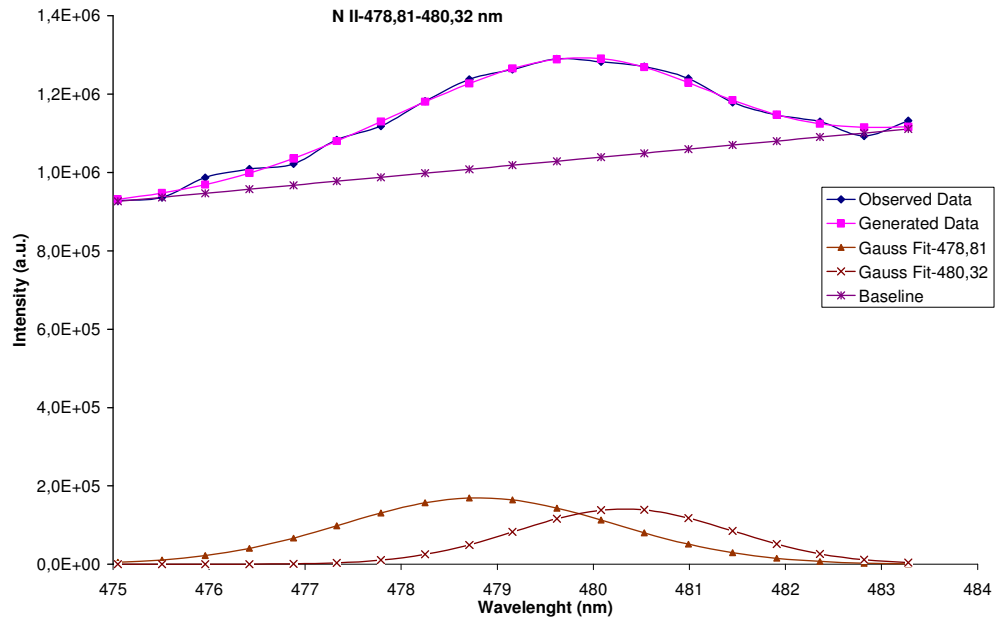


Gaussian Model:

Coefficient Data: $N = 341957.24$, $b = 443.9946$, $\sigma = 2.2502535$

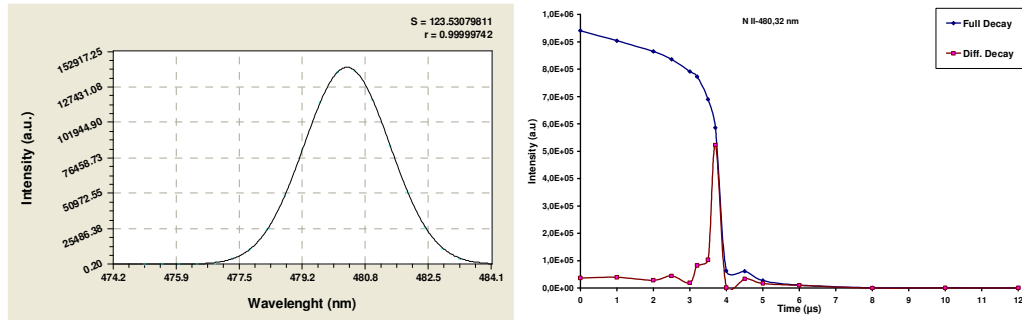
Figure 5.13: N III-434.57, N II-443.9 nm, a) Fitting Observed Data to Gauss Distribution, b) Normalized Gauss Analysis, c) Time Evolution

The analyzed data in the Figure 5.13 belongs to N III-434.5 nm and N II-443.2 nm. Plasma durations are 5 μs for 434.5 nm and 402.6 nm lines, decay start 2 μs after the laser shot; total intensity drop 10 percent of initial value at 3.5 μs for all lines. Calculated Doppler velocities are 257 m/sec and 276 m/sec.



Gaussian Model:

Coefficient Data: $N = 169728.19$, $b = 478.80428$, $\sigma = 1.4132954$

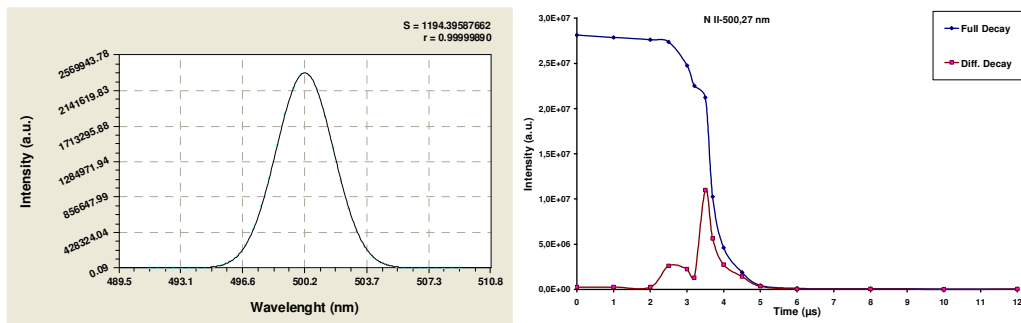
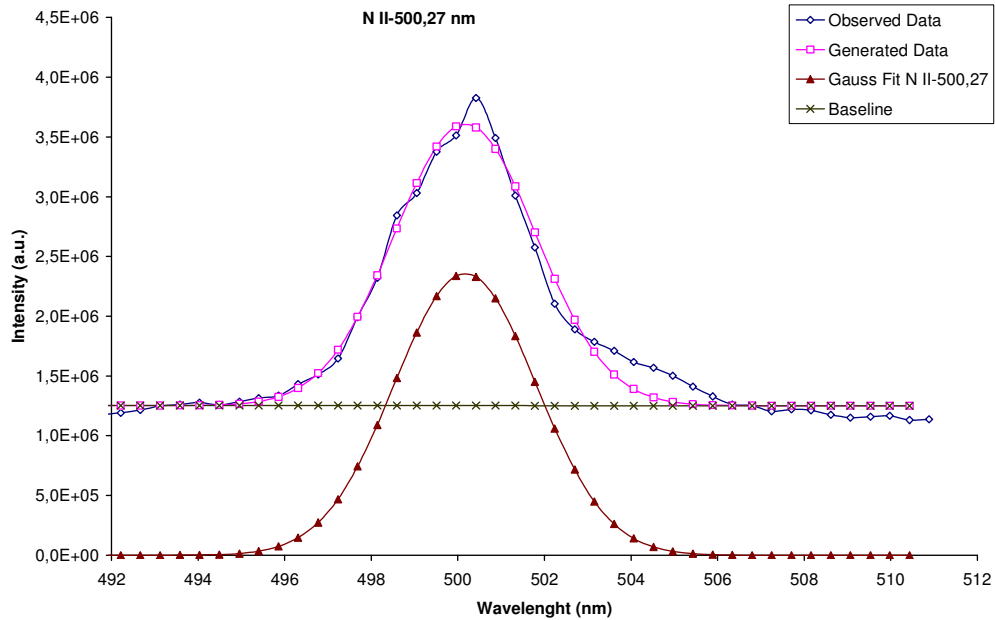


Gaussian Model:

Coefficient Data: $N = 141493.84$, $b = 480.32284$, $\sigma = 1.117474$

Figure 5.15: N II-478.8-480.3 nm, a) Fitting Observed Data to Gauss Distribution, b) Normalized Gauss Analysis c) Time Evolution

The analyzed data in the Figure 5.15 belongs to N II-478.8 nm and N II-480.3 nm. Their transmission probabilities (Einstein coefficient) are $2.52 \times 10^{+7}$, $3.18 \times 10^{+7}$ and the emission energies are 20879 and 20813 cm^{-1} , respectively. Plasma durations are $6 \mu\text{s}$ for the lines, decay start $3 \mu\text{s}$ after the laser shot; total intensity drop 10 percent of initial value at $4 \mu\text{s}$ for all lines. Calculated Doppler velocities are 288 m/sec and 226 m/sec , respectively.

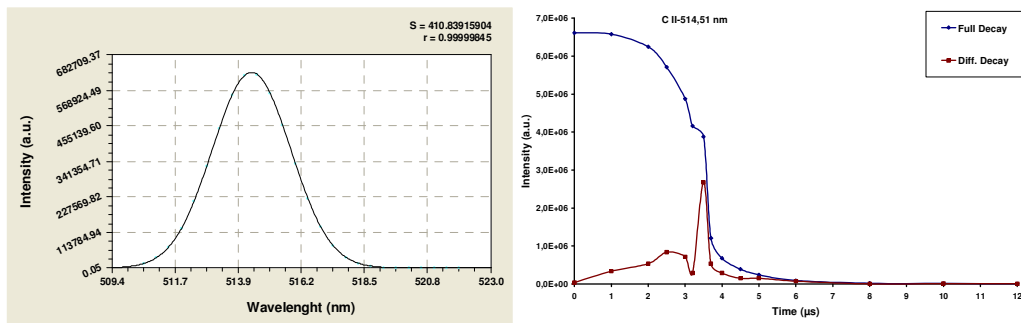
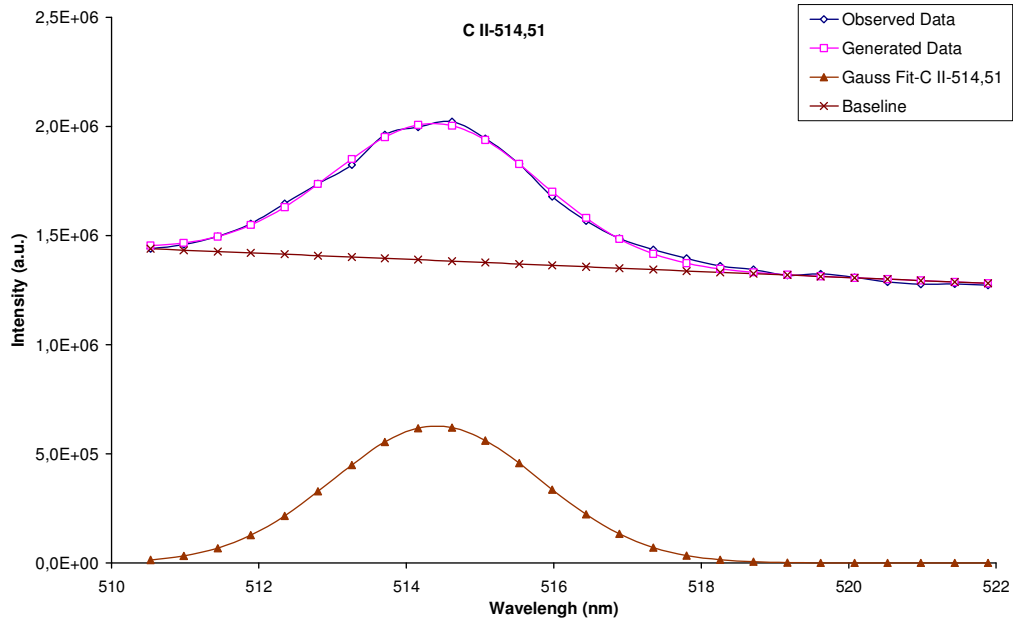


Gaussian Model:

Coefficient Data: $N = 2354975.9$, $b = 500.1707$, $\sigma = 1.63875$

Figure 5.16: N II-500.27 nm, a) Fitting Observed Data to Gauss Distribution, b) Normalized Gauss Analysis c) Time Evolution

The analyzed data in the Figure 5.16 belongs to N II-388.7 nm. Its transmission probability (Einstein coefficient) is $8.45 \times 10^{+6}$ and the emission energy is 19984 cm^{-1} . Plasma duration is $5 \mu\text{s}$, decay start $3 \mu\text{s}$ after the laser shot; total intensity drop 10 percent of initial value at $4 \mu\text{s}$ for the lines. Calculated Doppler velocity is 313 m/sec .

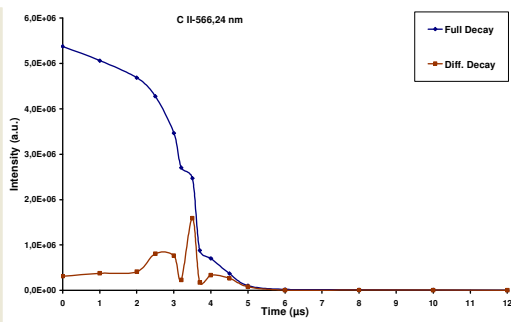
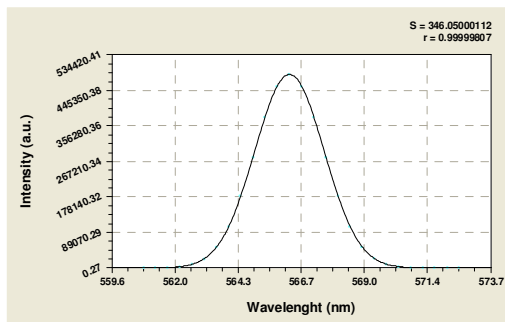
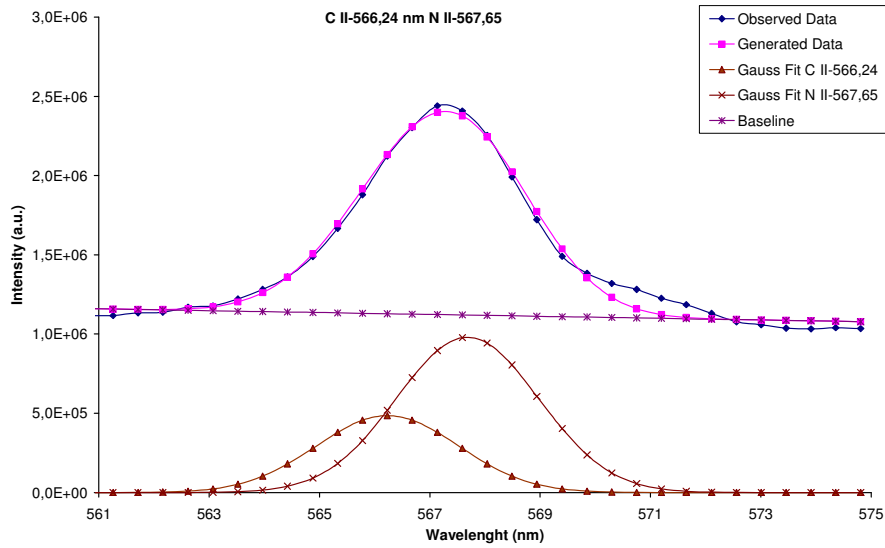


Gaussian Model:

Coefficient Data: $a = 627470.98$, $b = 514.40899$, $c = 1.4111199$

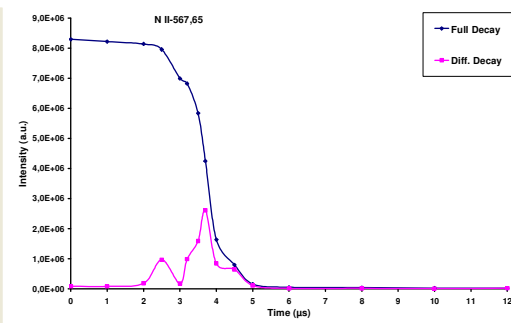
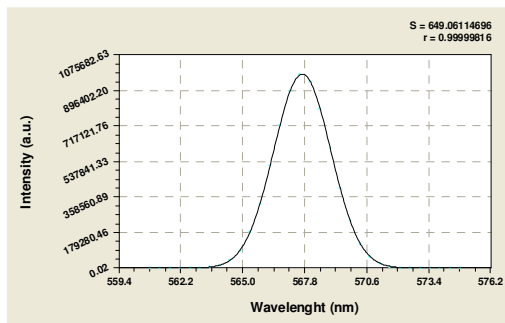
Figure 5.17: C II-514.5 nm, a) Fitting Observed Data to Gauss Distribution, b) Normalized Gauss Analysis c) Time Evolution

The analyzed data in the Figure 5.17 belongs to C II-514.5 nm. Its transmission probability (Einstein coefficient) is $6.49 \times 10^{+7}$ and the emission energy is 19430 cm^{-1} . Plasma duration is $7 \mu\text{s}$, decay start $3 \mu\text{s}$ after the laser shot; total intensity drop 10 percent of initial value at $4 \mu\text{s}$ for the lines. Calculated Doppler velocity is 267 m/sec .



Gaussian Model:

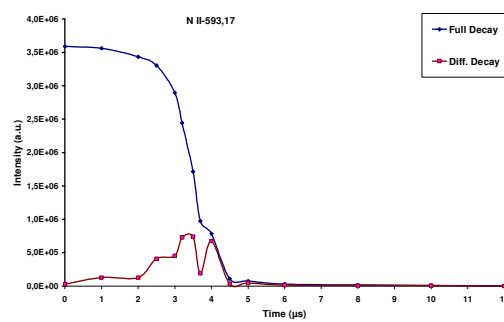
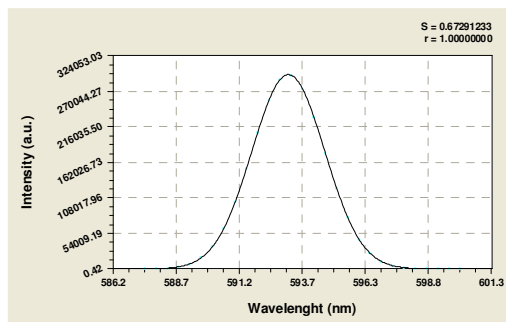
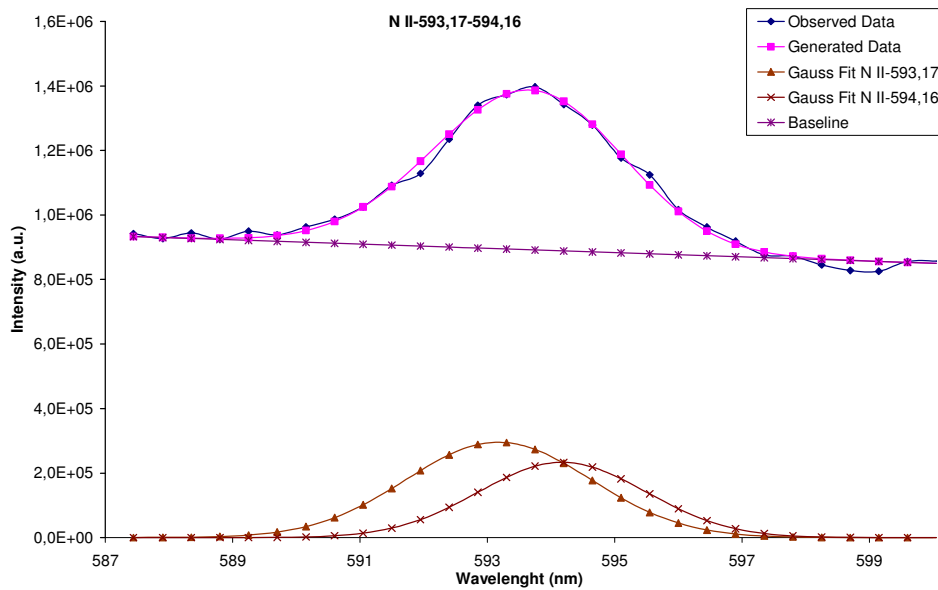
Coefficient Data: $N = 485743.99$, $b = 566.23336$, $\sigma = 1.2868489$



Gaussian Model: Coefficient Data: $N = 980254.12$, $b = 567.68276$, $\sigma = 1.2870787$

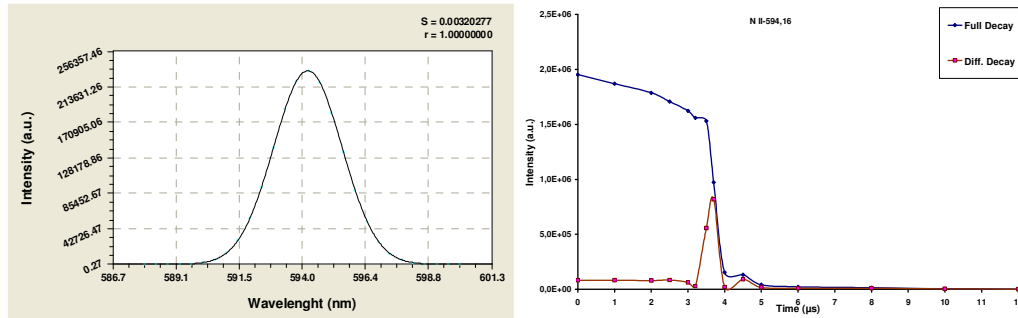
Figure 5.18: C II-566.2 nm, N II-567.7, a) Fitting Observed Data to Gauss Distribution, b) Normalized Gauss Analysis, c) Time Evolution

The analyzed data in the Figure 5.18 belongs to C II-566.2 nm and N II-567.7 nm. Their transmission probabilities (Einstein coefficient) are $2.93 \times 10^{+7}$, $5.25 \times 10^{+7}$ and the emission energies are 17655 and 17602 cm^{-1} respectively. Plasma durations are $5 \mu\text{s}$ for the lines, decay start $2 \mu\text{s}$ and $3 \mu\text{s}$ after the laser shot; total intensity drop 10 percent of initial value at $4 \mu\text{s}$ and $4.5 \mu\text{s}$ for the lines. Calculated Doppler velocities are 221 m/sec and 222 m/sec respectively.



Gaussian Model:

Coefficient Data: $N = 295672.29$, $b = 593.17561$, $\sigma = 1.4551598$

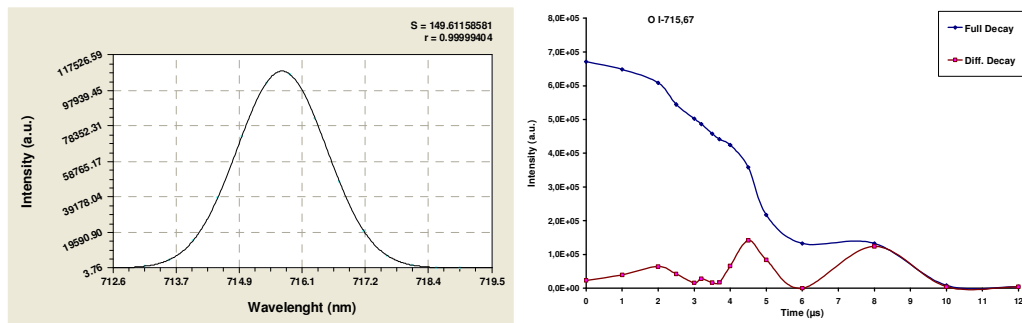
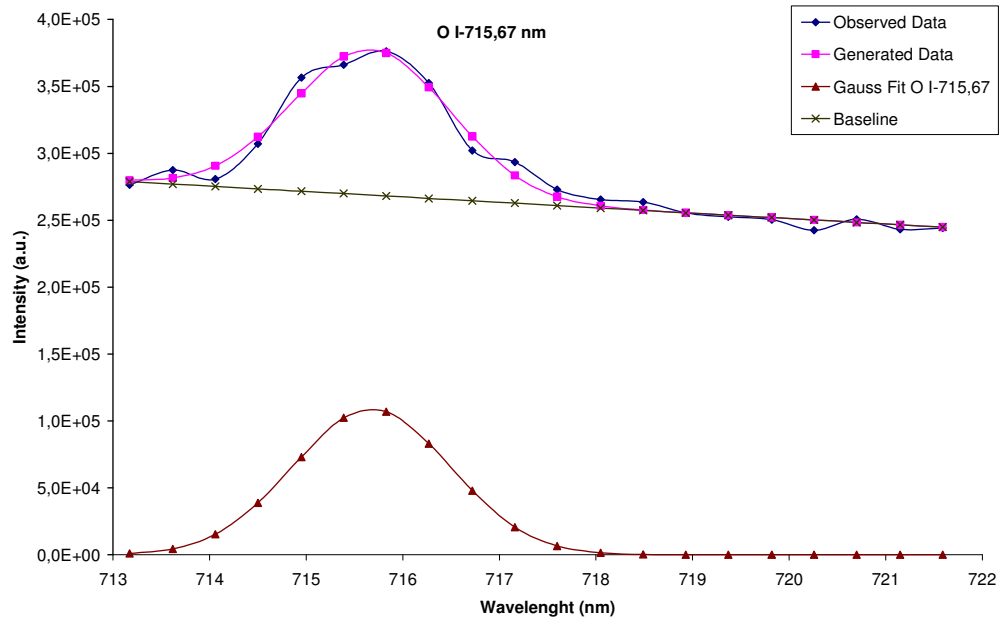


Gaussian Model:

Coefficient Data: $N = 233088.56$, $b = 594.17685$, $\sigma = 1.3158871$

Figure 5.19: N II-593.2-594.2 nm, a) Fitting Observed Data to Gauss Distribution, b) Normalized Gauss Analysis c) Time Evolution

The analyzed data in the Figure 5.19 belongs to N II-593.2 nm and N II-594.2 nm. Their transmission probabilities (Einstein coefficient) are $4.27 \times 10^{+7}$, $5.54 \times 10^{+7}$ and the emission energies are 16854 and 16826 cm^{-1} respectively. Plasma durations are $5 \mu\text{s}$ for the lines, decay start $3 \mu\text{s}$ after the laser shot; total intensity drop 10 percent of initial value at $4 \mu\text{s}$ for all lines. Calculated Doppler velocities are 239 m/sec and 216 m/sec respectively.

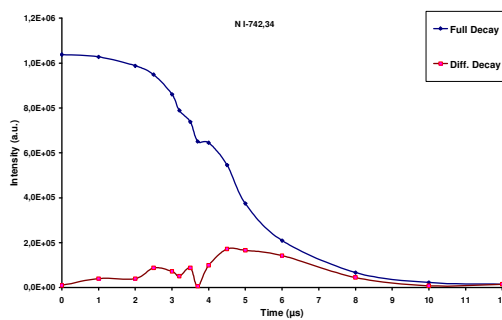
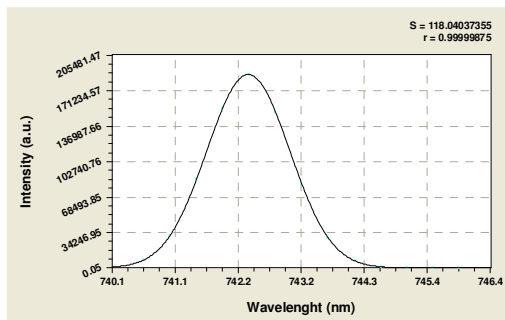
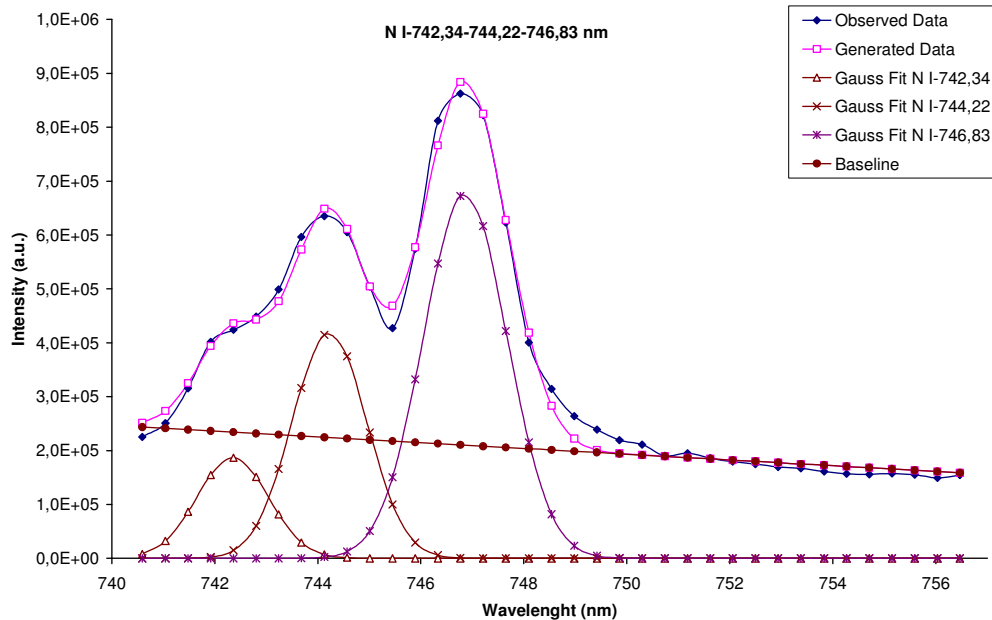


Gaussian Model:

Coefficient Data: $N = 108675.65$, $b = 715.67445$, $\sigma = 0.81655379$

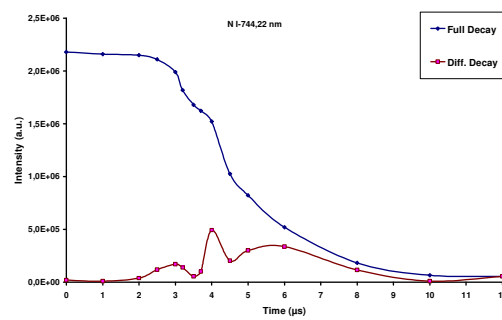
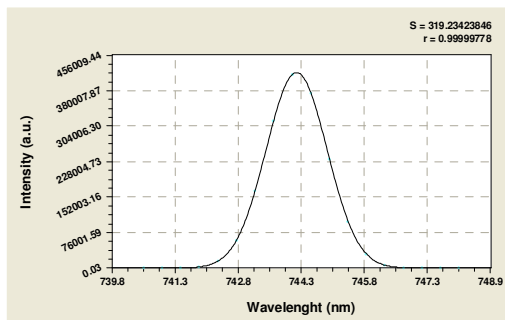
Figure 5.20: O I-715.67 nm, a) Fitting Observed Data to Gauss Distribution, b) Normalized Gauss Analysis c) Time Evolution

The analyzed data in the Figure 5.20 belongs to O I-715.6 nm. Its transmission probability (Einstein coefficient) is $5.05 \times 10^{+7}$ and the emission energy is 13969 cm^{-1} . Plasma duration is $10 \mu\text{s}$, decay start $2 \mu\text{s}$ after the laser shot; total intensity drop 10 percent of initial value at $9 \mu\text{s}$ for the lines. Calculated Doppler velocity is 109 m/sec .



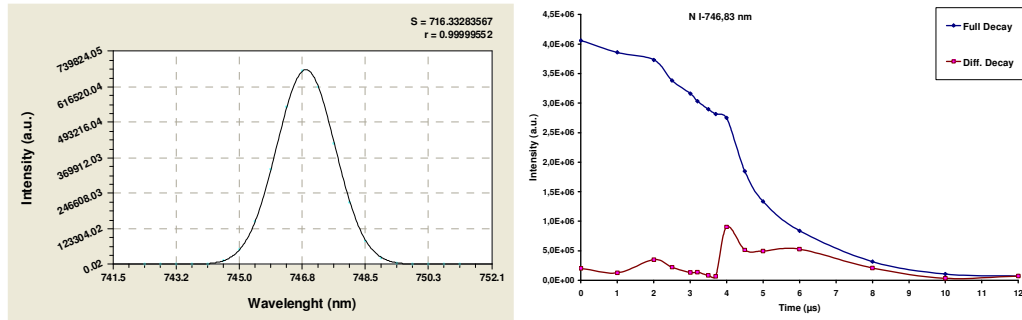
Gaussian Model:

Coefficient Data: $N = 186801.97$, $b = 742.34558$, $\sigma = 0.69597584$



Gaussian Model:

Coefficient Data: $N = 419048.77$, $b = 744.22603$, $\sigma = 0.72472762$

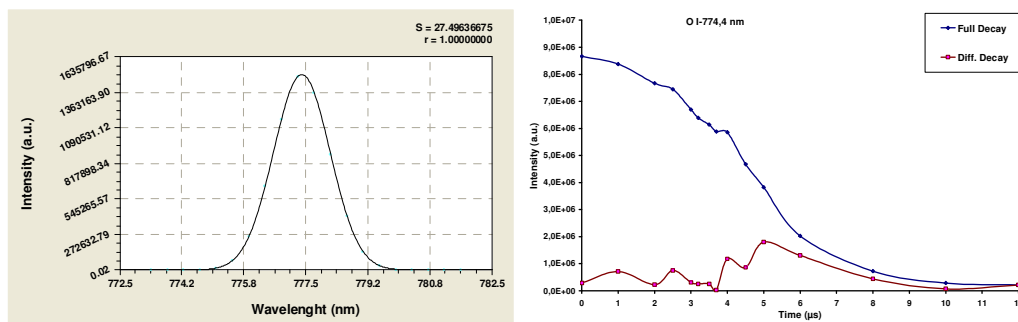
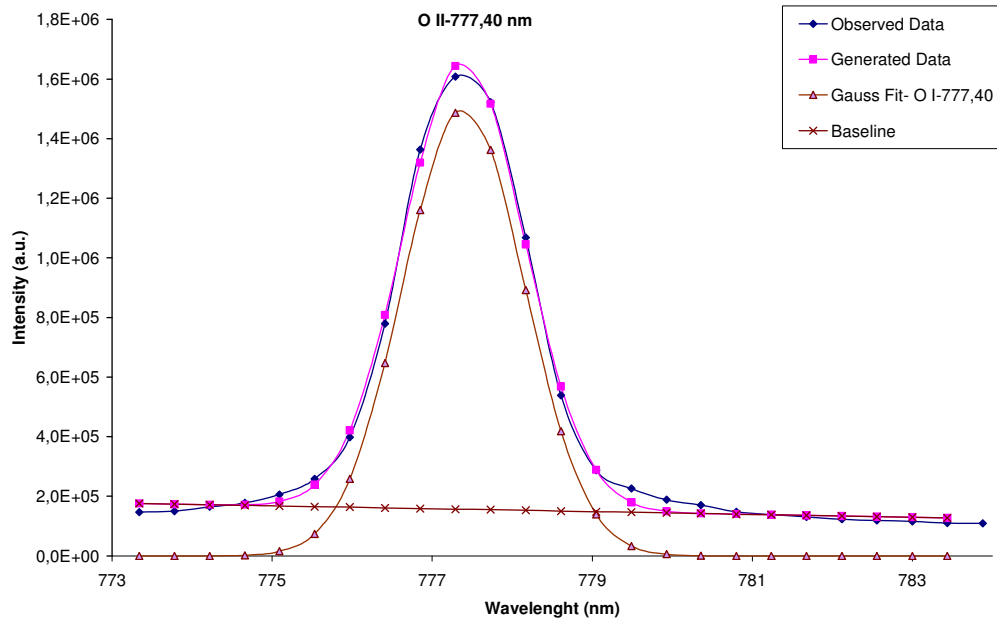


Gaussian Model:

Coefficient Data: $N = 676122.67$, $b = 746.86166$, $\sigma = 0.81533943$

Figure 5.21: N I-742.34-744.22-746.8 nm, a) Fitting Observed Data to Gauss Distribution, b) Normalized Gauss Analysis, c) Time Evolution

The analyzed data in the Figure 5.21 belongs to N I-742.34-744.22-746.8 nm. Their transmission probabilities (Einstein coefficient) are 5.95×10^6 , 1.24×10^7 , 1.93×10^7 and the emission energies are 13467 , 13433 and 13386 cm^{-1} , respectively. Plasma durations are $12 \mu\text{s}$ for the lines, decay start $3 \mu\text{s}$ after the laser shot; total intensity drop 10 percent of initial value at $8 \mu\text{s}$ for all lines. Calculated Doppler velocities are 93 m/sec , 92 m/sec and 97 m/sec , respectively.

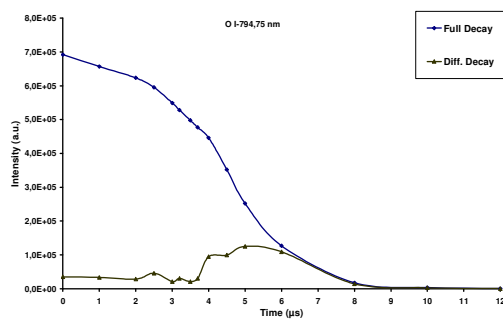
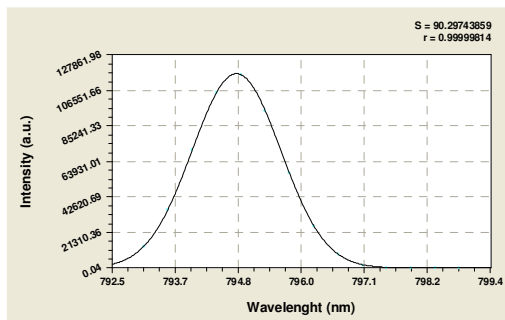
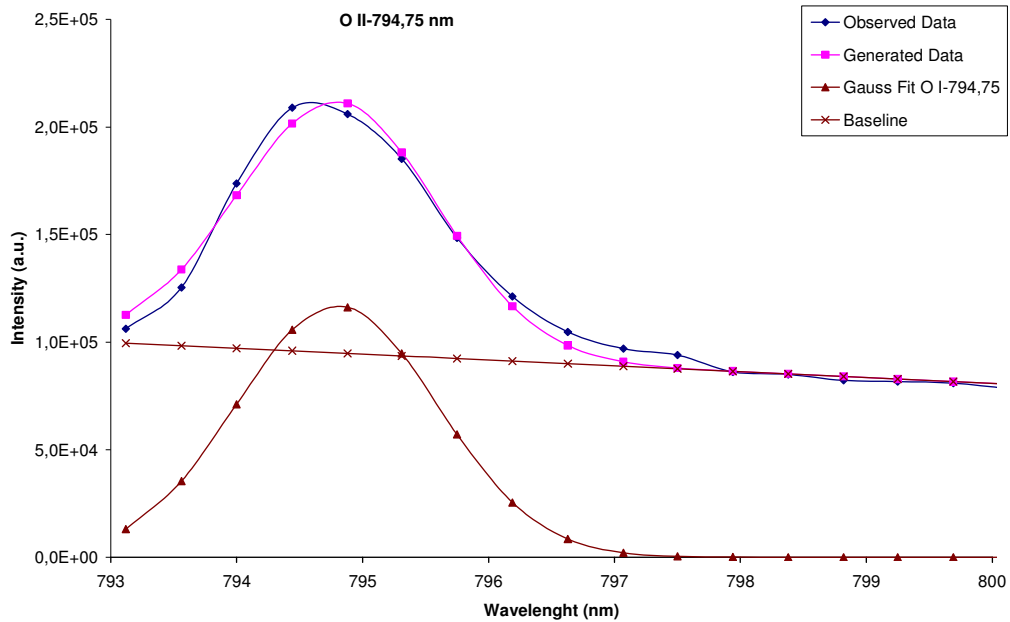


Gaussian Model:

Coefficient Data: $N = 1501423.3$, $b = 777.3952$, $\sigma = 0.75950303$

Figure 5.22: O I-777.4 nm, a) Fitting Observed Data to Gauss Distribution, b) Normalized Gauss Analysis c) Time Evolution

The analyzed data in the Figure 5.22 belongs to O I-777.4 nm. Its transmission probability is $3.69 \times 10^{+7}$ and the emission energy is 12860 cm^{-1} . Plasma duration is $12 \mu\text{s}$, decay start $2 \mu\text{s}$ after the laser shot; total intensity drop 10 percent of initial value at $8 \mu\text{s}$ for the lines. Calculated Doppler velocity is 86 m/sec .

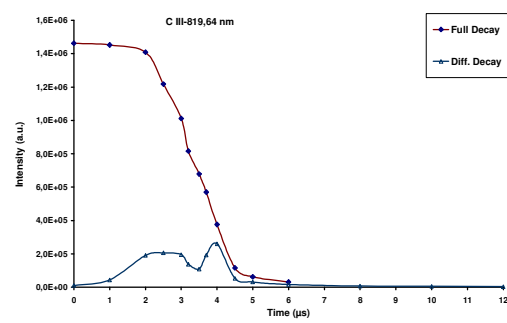
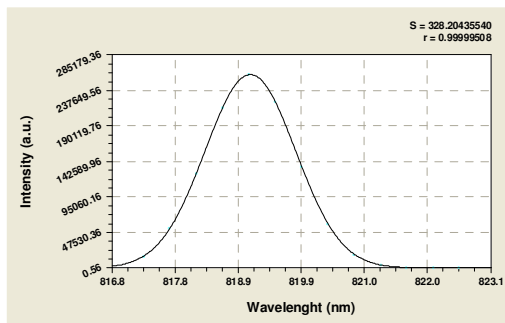
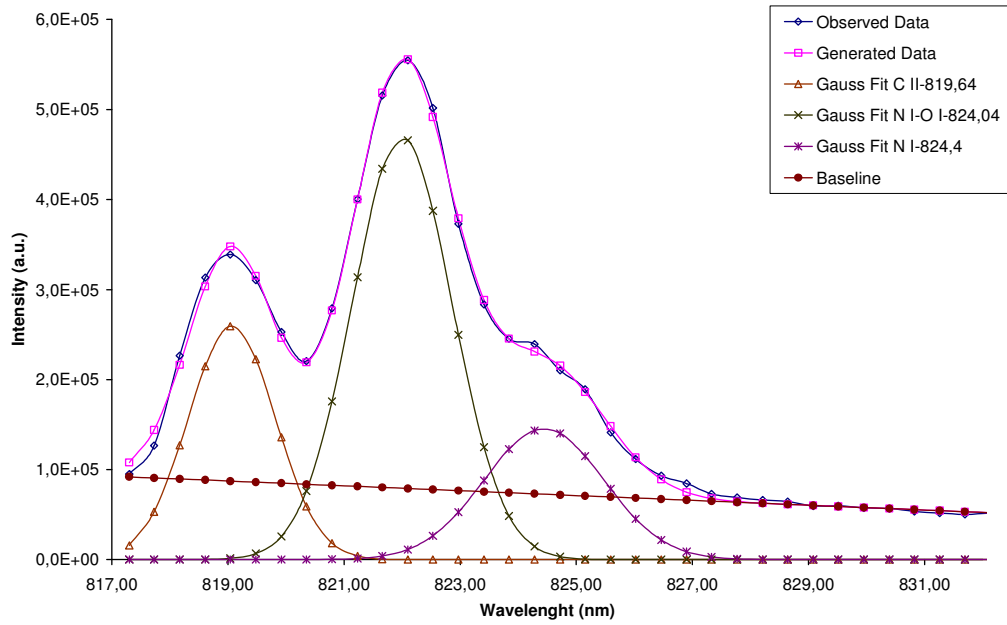


Gaussian Model:

Coefficient Data: $N = 116693.83$, $b = 794.7946$, $\sigma = 0.798857$

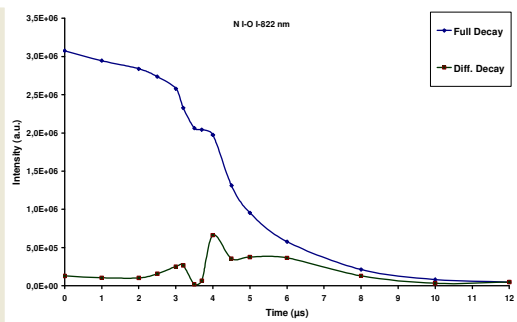
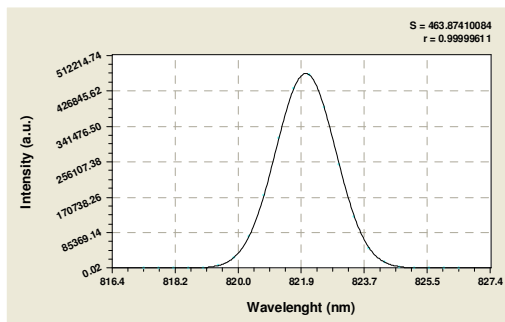
Figure 5.23: O II-794.76 nm, a) Fitting Observed Data to Gauss Distribution, b) Normalized Gauss Analysis c) Time Evolution

The analyzed data in the Figure 5.23 belongs to O II-794.8 nm. Plasma duration is 9 μs , decay start 2 μs after the laser shot; total intensity drop 10 percent of initial value at 7 μs for the lines. Calculated Doppler velocity is 82 m/sec.



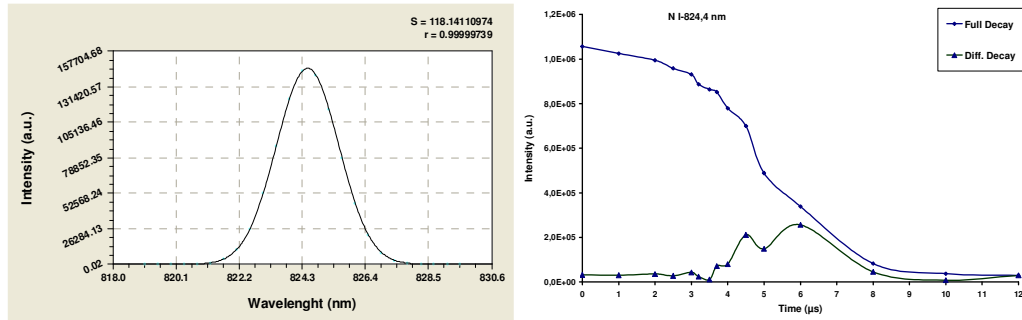
Gaussian Model:

Coefficient Data: $N = 259246.17$, $b = 819.06639$, $\sigma = 0.74899656$



Gaussian Model:

Coefficient Data: $N = 468218.06$, $b = 822.00084$, $\sigma = 0.86468932$

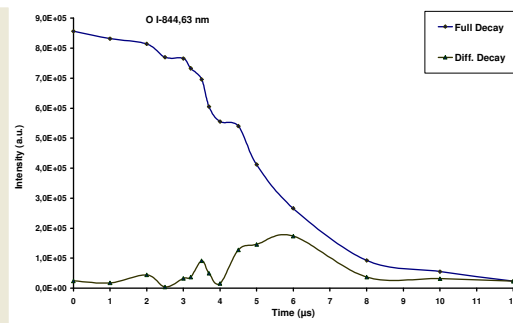
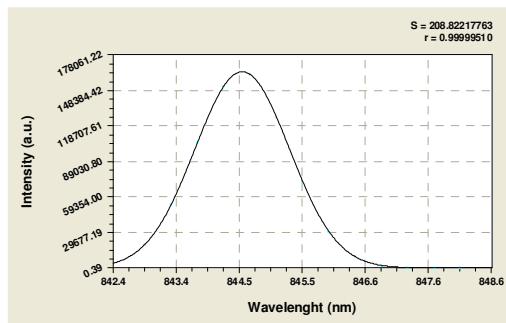
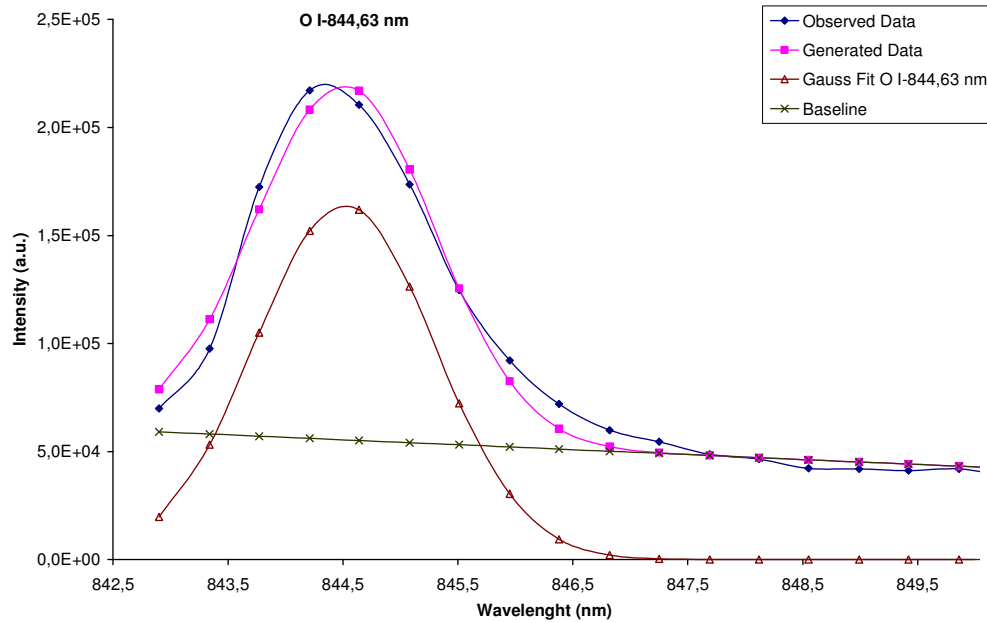


Gaussian Model:

Coefficient Data: $N = 145217.35$, $b = 824.44229$, $\sigma = 1.0350331$

Figure 5.24: C III-819.6, N I-O I-822.0, N I-824.24 nm, a) Fitting Observed Data to Gauss Distribution, b) Normalized Gauss Analysis, c) Time Evolution

The analyzed data in the Figure 5.24 belongs to C III-819.6, N I-O I-822.0, N I-824.24 nm. This analysis is not proper because nitrogen and oxygen lines coincide with each other, it can not be resolved. Plasma durations are 10 μ s for carbon, 9 μ s for N I-824 nm line, and decay start 2 μ s for C III, 3 μ s for N I-824 nm after the laser shot; total intensity drop 10 percent of initial value at 8 μ s for all lines. Calculated Doppler velocities are 84 m/sec and 118 m/sec, respectively.



Gaussian Model:

Coefficient Data: $a = 164137.18$, $b = 844.51193$, $c = 0.78198578$

Figure 5.25: O I-844.6 nm, a) Fitting Observed Data to Gauss Distribution, b) Normalized Gauss Analysis c) Time Evolution

The analyzed data in the Figure 5.25 belongs to O I-844.6 nm. Its transmission probability (Einstein coefficient) is $3.2 \times 10^{+7}$ and the emission energy is 11836 cm^{-1} . Plasma duration is $12 \text{ } \mu\text{s}$, decay start $3.5 \text{ } \mu\text{s}$ after the laser shot; total intensity drop 10 percent of initial value at $10 \text{ } \mu\text{s}$ for the lines. Calculated Doppler velocity is 80 m/sec .

CHAPTER 6

CONCLUSION

The main purpose of this study was to understand the physical processes which are involved Laser Induced Breakdown Spectroscopy for time resolved analysis. This study provides a new method to evaluate the time resolution of the laser induced plasma. System is tested with single gas helium. After that, the laser induced air plasma is investigated in some characteristics.

Conclusions and accomplishments from this study are itemized below.

1) Characteristic and time evolution of the continuum emission:

When looked the continuum for (He) and air plasma, there are some differences between them. The level of continuum for He is lower than the continuum of air. This shows that the temperature of air plasma is higher than the helium plasma. Continuum is related the Blackbody theorem. If we take into consideration this theory, it can be concluded that air plasma has more energy, highly ionized particle, more density and more pressure according to helium plasma. Although air plasma temperature is high, the life time of continuum is very short according to helium plasma. This shows that the particles penetrate quickly and temperature of plasma decrease in a short time. The plasma temperature can be determined by using this continuum. Temperature is calculated by using area of continuum observed from spectrometer just after the laser pulse. For our system, the

temperature can not determine exactly, because of non LTE condition. But, the continuum can give information about the temperature relatively.

In some cases, it is needed to be continuum free measurement for air; for this purpose, data acquisition must be started after 3 μ s to the plasma initiation. Plasma temperature decrease 10 percent of initial value at this time.

2) Spectral line characteristics:

The helium spectral emission contains mostly non ionized states, but only two lines observed from singly ionized helium atoms. This shows that the energy of the laser is not enough to excite the helium atoms the two times ionized level. Analysis of the air plasma spectrum is very difficult, because most lines which come from different component of air interfere with each neighboring line. Because of that, the identification of emission line must be carefully done. The air spectrum contains emissions from singly ionized and neutral nitrogen and oxygen lines superimposed on an intense background continuum. Ion lines from higher ionization states were not observed under these conditions. Neutral lines for both oxygen and nitrogen were observed mostly at longer wavelengths, e.g., O (I) at 715.6, 777.4, 748.0 nm and N (I) at 742.4, 744.3, 746.8, 820.03 nm. However, ion lines were observed mostly at shorter wavelengths, between 300 to 500 nm for both oxygen and nitrogen. Nitrogen lines are more numerous than the other element lines, caused by high concentration in air. We also observed C III lines in the spectrum. This shows that the energy of the laser pulse is enough to break down the molecular bond of CO₂ molecule. Additionally, though air include argon molecule, we can not observe any line from the argon atom. Argon is noble gas so that the energy of laser is not enough to excite this atom.

3) Decay time of the excited atoms:

Determination of the decay time of the laser induced plasma is the most important subject of this work. Firstly, we study single gas helium in order to test the reliability of the system. Although the laser pulse duration is about 4.7 ns, investigation of the time evolution of helium plasma shows that the life times of first excited state is nominally 18-20 μs . But, second excited state life time is about 5 μs . These are expected results and compatible with literature [76]. First excited state start to the decay at 4 - 5 μs after the plasma generation, and it reach 10 percent of initial intensity after 12 – 14 μs after the plasma initiation. So, in order to determine helium concentration in a gas mixture, the measurement must be made before the 14th μs , in order to determine ionized helium atom, the spectrum must be taken before 5th μs .

Air plasma has very complex lines, so we have to be careful in choosing atomic lines. When investigated the decay rates of air plasma lines, mostly we saw N II lines below 500 nm wavelength. Life time of these lines is shorter than over the 500 nm for N II lines. Another observation that the life time of N I lines is longer than N II lines. N II lines in short wavelength region has very sharp decay rate, this is related absorption energy of these state. N I lines in longer wavelength has gradually decay rate. If we want to determine nitrogen concentration in a gas mixture, we take the measurements before 5th μs for the short wavelength region, but we can take measurement up to 7 μs for long wavelength region.

We observe three lines for carbon in the air plasma spectrum, as mentioned above carbon atom comes from CO_2 and CH_4 molecule. Carbon atoms have the same attitude of nitrogen for shorter wavelength. But, while the other component is found first excited state for longer wavelength, C reach 3rd excited state and has longer life time according the other constituents of the air. Like nitrogen, carbon has very sharp decay attitude for short wavelength but gradually for long wavelength. In order to determine CO_2 concentration in the air, C III level emission line could be used. This

line is quite clear, so it can be analyzed easily. Life time of this level longer than the others, and decay decrease gradually. This line reaches 10 percent of initial value at 8 μs after the plasma initiation.

In the case of considering the O lines; three of them come from first excited state, and only one of them comes from firstly ionized atomic excited state. All oxygen lines have long decay time with respect to the other constituent of air. Intensity of all lines reaches 10 percent of initial value after 8 μs the plasma initiation.

4) Differential decay and life time:

The differential decay time of helium shows that transition of electron in the state have different attitude for different energy state. Especially in short wavelength transition become at 4th and 6th μs suddenly, but in longer wavelength this decay tends to decay gradually. By using this behavior, information about helium in gas mixture can be handling for a specific wavelength at a specific time. There is no emission line of helium between plasma initiation and 4th μs .

5) Doppler shift and velocities of component:

Doppler velocities were calculated for all the emission lines. When comparing the velocity of one particle with the other, we have to pay attention the wavelength which is emitted from definite particle. Because, the spectrometer has different efficiency response for the different wavelength. So, when comparing two lines with respect to Doppler velocity, we have to choose the close wavelength, which belongs to different component.

We observe almost the same velocities for the short wavelength (between 300-500 nm) for helium. However, for wavelengths longer than 500 nm, velocities

are seen drop dramatically. In fact, this is completely related with efficiency curve of the spectrometer. Mean velocity of the firstly ionized helium atoms is almost 800 km/h. We can compare 468 nm with 471 nm emissional wavelength in order to find the difference between the first excited state and the second excited state of helium atom with respect to velocities. It is clearly seen that the second ionized state helium atom has greater velocity than the firstly ionized state. Helium atom which is second excited state have more charge, therefore it is effected the electric field, which is formed in the plasma, more than the first excited helium atom.

Air plasma is more complex than the helium, because air consist of atoms whose mass is different from each other. And, more interaction occurs in the air plasma, because of intense medium. Mean velocity of atom in the air plasma is 960 km/h. Mean velocity of the air plasma particle is greater than the helium plasma particle. This shows that the pressure in the air plasma is greater than the helium plasma. The same result is concluded in the continuum section.

In the case of considering the particle in the air plasma, we have to examine the close wavelength for different atoms. In order to compare nitrogen with oxygen, we can examine N I-824 nm and O I-844 nm emissional lines. Nitrogen is faster than oxygen, because nitrogen is lighter than oxygen. In order to compare carbon with oxygen, we can examine O II-794 nm and C II-819 nm emission lines. Carbon is a bit faster than the oxygen. It is expected that there must be large differences in velocity between carbon and oxygen according to their masses, but this is not observed. Carbon comes from CO₂ molecule; therefore it shows different characteristics in plasma.

REFERENCES

- [1] Cadwell, L., Belliveau, J., Huvwell, L., Griffin, H., SPIE Vol. 644, Remote Sensing, 16-18, 1986.
- [2] Browner, R. F., Boom, A. W., Anal. Chem., 56, 7, 787A-798A.
- [3] Sneddon, J., Spectroscopy, Vol. 1, No. 9, 34-41.
- [4] Routh, M. W., Spectroscopy, Vol. 2. No. 2, 45-52.
- [5] Olesik, J. W., Anal. Chem., Vol. 63, No. I, Jan., 1991.
- [6] Radziemski, L. J., Solarz, R. W., Paisner, J.A., Laser Spectroscopy and Its Applications, New York, Marcel Dekker Inc., 1987.
- [7] Vickers, T. J., Winefordner, J.D., in Analytical Spectroscopy Series, Vol. 1, Part 2, Chapter 7, E.L. Grove, Ed., New York, Marcel Dekker, 1972.
- [8] Barnes, R.M., CRC Crit.Rev.Anal.Chem., 9, 203-296, 1978.
- [9] Ishizuka, T., Uwamino, Y., Anal.Chem., 52, 125-129, 1980.
- [10] Boumans, P.W.J.M., in Analytical Spectroscopy Series, Vol. 1, Part 2, Chapter 6, E.L. Grove, Ed., New York, Marcel Dekker, 1972.
- [11] Walters, J.P, Science, 198, 787-797, 1977.
- [12] Cremers, D.A., Appl.Spectros., 41, 572-579, 1987.
- [13] Ottesen, D.K., Wang, J.C.F., Radziemski, L.J., Appl.Spec., 43, 967-976, 1989.
- [14] Radziemski, L.J., Loree, T.R., Cremers, D.A., Hoffman, N.M., Anal.Chem., 55, 1246-1252, 1983

- [15] Moenke, H. and Moenke-Blankenburg, L., Laser Microspectral Analysis, Crane and Russak Company, Inc., 1973.
- [16] Raizer, Y.P., Laser Induced Discharge Phenomena, New York, Consultants Bureau, 1977.
- [17] Hughes, T.P., Plasmas and Laser Light, New York, John Wiley and Sons, 1975.
- [18] Shkarofsky, IP., RCA Review, Vol.35, 48-77, 1974.
- [19] Radziemski, LJ., Cremers, D. A., Laser Induced Plasmas and Applications, New York, Marcel Dekker. Inc., 1989.
- [20] Montgolfier, P., Dumont, P., Mille, M., Villermaux, J., J.Phys.Chem.,Vol. 76, No. 1,31-37,1972.
- [21] Maker, P.D., Terfiune, R.W., Savage, C.W., "Optical Third Harmonic Generation in Various Solids and Liquids ", Proceedings of the Third International Quantum Electronics Conference, 1963.
- [22] Minck, R.W., J.Appl.Phys., 35, 252-254, 1964
- [23] Tambay, R., Sovishesha, M., Kumar, V., Thareja, R.K., Pramana- J.Phys., 37,2, 163-166,1991.
- [24] Strieker, J., Parker, J.G., Appl. Phys., 53(2), 851-855, 1982.
- [25] Rosen, D.I., Wey i, G, J. Phys. D. Appl. Phys., 20: 1264-1276, 1987.
- [26] Tambay, R., Thareja, R.K., J. Appl. Phys., 70(5), 2890-2892, 1991.
- [27] Brueck, S.R.J.,Kildal, H., J.Appl. Phys., 52(2), 1004-1009, 1981.
- [28] Chyiek, P, Jarzembski, MA, Srivastava, V., Pinnick, R.G., Appl., Opt., Vol. 29, No: 15, 2303-2306, 1990.

- [29] Busher, H., Thomlinsen, R., Damon, R., Phys. Rev. Lett., 15, 847, 1965.
- [30] Alcock, A.J., De Michelis, C, Richardson, M.C., Appl. Phys. Lett., Vol. 15, 72, 1969.
- [31] Bettis, J.R., Appl.Optics., Vol.31, No. 18, 3448-3452, 1992.
- [32] Cremers, D.A., Radziemski, L.J., Anal.Chem., Vol. 55, 1252-1256, 1983.
- [33] Belyaev, E.B., Godlevski, A.P., Kopytin, Y.D., Sov.J.Quant.Electron. 8(12), 1459-1463, 1978.
- [34] Cremers, D.A., Radziemski, L.J., Loree, T.R., Appl. Spect., Vol. 38, No. 5 721-729, 1984.
- [35] Wachter, J.R., Cremers, D.A., Appl. Spect, Vol. 41, No. 6, 1042-1047, 1987.
- [36] Cremers, D.A., Radziemski, L.J., Appl. Spect, Vol. 39, No.1, 57-63, 1985.
- [37] Marich, K.W., Treytl, W.J., Hawley, J.G., Peppers, N.A., Myers, R.E., Glick, D., J. Phys. E, Vol. 7., 830-834, 1974.
- [38] Adrain, R.S., " Some Industrial Uses of Laser Induced Plasmas", in Industrial Applications of Lasers, John Wiley, 135-176, 1984.
- [39] Kokko, A.F., Shemanin, V.G., Shugurov, G.S., Measurement Techniques, Vol. 35, No. 7, 819-824. 1992.
- [40] Loree, T.R., Radziemski, L.J., Plasma Chem. Plasma Process. Vol. 1, No. 3, 271-280, 1981.
- [41] Loree, T.R., Radziemski, L.J., SPEE Vol. 288, Los Alamos Conference on Optics, 241-244, 1981.
- [42] Radziemski, L.J., Cremers, D.A., Loree, T.R., Spectrochimica Acta B, Vol. 38, No.1, 349-355, 1983.

- [43] Radziemski, L.J., Loree, T.R., Cramers, Hoffman, M., *Anal. Chem.*, Vol. 55, 1246-1252, 1983
- [44] Kyuseok S., Cha, H., Lee, J., *Microchemical Journal*, Vol. 63, 53-60, 1999.
- [45] Giacomo, A., *Spectrochimica Acta B*, Vol. 58, 71-83, 2003
- [46] Cremers, D.A., Romero, D.J., *SPIE Vol.644, Remote Sensing*, 7-12, 19S6.
- [47] Cheng, E.A.P., Fraser, AD, Eden, J.G., *Appl.Spec.*, V.45, No:6, 949-952,1991.
- [48] Ottesen, O.K., *Gorden Conference Request Reprint*, 9, 15-17, 1987.
- [49] Schmeider, R.W., 13th Ann. *Electro-Opt. Laser Conf. Anaheim, Calif*, 1981.
- [50] Schmeider, R.W., Kerstein, A., *Appl.Opt*, Vol.19., No.24, 4210-4213, 1980.
- [51] Loree, T.R., Radziemski, L.J., *Proc. 1981 Symp.Instr.Control Fossil Energy Prog.*, Argonne National Laboratory Press, ArgonnellL, 768, 1982.
- [52] Ottesen, O.K., Wang, J.F.C., Radziemski, L.J., *Appl.Spec.*,Vol.43, No.6, 967-976, 1989.
- [53] Ottesen, D.K., Baxter, L.L., Radziemski, L.J., Burrows, IF., *Energy & Fuels*, 5,304-312, 1991.
- [54] Singh, J.P., Zhang, H., Yueh, F.Yu, Cook, R.L., *Proceedings of the 28th Intersociety Energy Conversion Engineering Conference*, August 8-13, 1993.
- [55] *Energy and Environment, Sandia Technology Bulletin*, May 1994.
- [56] Margoshes, M., *AppI.Spect*, Vol. 21., No.2, 92-99, 1967.
- [57] Hohreiter V., Carranza J.E., Hahn, D.W., *Spectrochimica Acta B*, Vol. 59, 327-333, 2004.

- [58] Kalnicky, D.J., Kniseley, R.N., Fassel, V.A., *Spectrochimica Acta*, Vol.30B., 511-525, 1975.
- [59] Kalnicky, D.J., Fassel, V.A., Kniseley, R.N., *Appl. Spec.*, Vol.31, No.2, 137-150, 1977.
- [60] Colao, F., Pershin, S., Lazie, V., *Applied Surface Science*, Vol. 197, 207-212, 2002.
- [61] Bye, C.A., Scheeline, A., *Appl.Spect.*, Vol 47, No. 12, 2031-2035, 1993.
- [62] Grant, K.J., Paul, G.L., *Appl.Spec.*, Vol.44, No.8, 1349-1354, 1990.
- [63] Tognomi, E., Palleschi, M., Corsi, M., *Spectrochimica Acta B*, Vol. 57, 1115-1130, 2002.
- [64] Santagata, A., Di Trolio, A., Parisi G.P., Larciprete, R., *Applied Surface Science*, Vol. 248, 19–23, 2005.
- [65] Griem, H.R., *Phys.Rev.*, 131, 3. 1170-1176, 1963.
- [66] Wiese, W.L, Smith, M.W., Glennon, B.M., *Atomic Transition Probabilities*, Vol.1, NSRDS-NBS 4, 1966.
- [67] Griem, H.R., *Plasma Spectroscopy*, Mc-Graw and Hill, 1964.
- [68] Boumans, P.W.J.M, *Theory of Spectrochemical Excitation*, Hilger and Watts, 1966.
- [69] Marr, G.V., *Plasma Spectroscopy*, Elsevier Publishing Comp., 1968.
- [70] Lochte-Holtgreven, W., *Plasma Diagnostics*, North-Holland Publ. Comp., 1968.
- [71] Griem, H.R., *Spectral Line Broadening by the Plasmas*, Academic, New York, 1974.

- [72] Wolfgang Demströder, Laser Spectroscopy, Chapter 3, Springer, 1996.
- [73] Thorne A., Litzen U., Johanson S., Spectrophysics, Chapter 16, Springer, 1999.
- [74] Hughey, B.J., Santavicca, D.A., Combustion Science and Technology, Vol. 29, 167-190, 1982.
- [75] Dasch, C.J., Appl. Opt., 31(8), 1146-1152, 1992.
- [76] Cirkovic L., Vujicic B., Glisic S.M., Applied Physics, Vol. 15, 229-235, 1982.
- [77] Nestor, O.H., Olsen, H.N., SIAM Review, Vol.2., No.3., 200-207, 1960.
- [78] Barr, W.L., J.Opt.Soc.Amer, Vol.52.,No.8., 885-888, 1962.
- [79] Radziemski, L.J., Cremers, D.A., Laser Induced Plasmas and Applications, Chapter.2, New York, Marcel Dekker. Inc., 1989.

APPENDIX A

BASIC ATOMIC SPECTROSCOPIC DATA

The Atomic Spectra Database (ASD) contains data for radiative transition and energy levels in an atoms and atomic ions. The ionization energies in the table are based on a recent survey of the literature. A reference to one or another data compilation is given for a number of elements; the cited compilation gives the references for the original ionization-energy data. For each of the elements a list of the strongest lines in the spectra of the neutral and singly-ionized atoms has been compiled. This list includes the wavelength, the ionization stage, the reference for the wavelength measurement, and an intensity. Wavelengths given to three decimal places in have a stated uncertainty of less than 0.001 Å is rounded off from three-place values in the original literature. Unlike the other tabulated data, the relative intensities are not basic data and must be used with caution. The relative intensities of the spectral lines observed for any element depend upon the light source and excitation conditions. Thus, even if the relative intensities observed in a particular experiment are adjusted to correct for the wavelength dependence of the sensitivity of the spectrometer and detector, the intensities will in general be different from relative intensities given by a previous observer or tabulated in a compilation such as this one. The values are listed as A_{ki} in units of 10^8 s^{-1} . These A_{ki} values can easily be converted to oscillator strengths, f_{ik} , gf_{ik} , or $\log(gf_{ik})$, or line strength, S , by using the following formula:

$$g_i f_{ik} = 1.499 \times 10^{-8} A_{ki} \lambda^2 g_k = 303.8 \lambda^{-1} S ,$$

where i refers to the lower energy level, k refers to the upper level, λ is the wavelength in Ångstroms, and $g = 2J+1$ for a given level.

Table. A. A. 1. Spectroscopic data for neutral and ion lines of Helium

Wavelength(nm)	Energy(cm ⁻¹)	Relative Intensity	A _{ik}
318.77 (I)	31361	20*	5.05x10 ⁺⁶
388.87 (I)	25706	500*	9.48x10 ⁺⁶
396.47 (I)	25215	20	7.17x10 ⁺⁶
402.62 (I)	24830	50*	2.93x10 ⁺⁶
447.15 (I)	22358	200*	6.28x10 ⁺⁶
468.57 (II)		30	
471.31 (I)	21211	30	5.86x10 ⁺⁶
492.19 (I)	20312	20	2.02 x10 ⁺⁶
501.27 (I)	19932	100	1.34 x10 ⁺⁶
504.77 (I)	19805	10	6.55 x10 ⁺⁶
587.56 (I)	17015	500	2.94 x10 ⁺⁷
565.01 (II)		8	
667.82 (I)	14970	100	6.38 x10 ⁺⁷
706.52 (I)	14150	200	1.54 x10 ⁺⁷
728.14 (I)	13730	50	1.81 x10 ⁺⁷
1083.03 (I)	9231	2000	1.02 x10 ⁺⁶

* Average values of several states occupied according to their statistical weights

Table. A. A. 2. Spectroscopic data for neutral and ion lines of Nitrogen

Wavelength(nm)	Energy(cm^{-1})	Relative Intensity	A_{ik}
399,50 (II)	25024	1000	1,35E+08
434,57 (III)	23004	120	1,82E+07
437,91 (III)		300	
443,27 (II)		285	
444,70 (II)	22481	650	1,14E+08
462,14 (II)	21632	450	9,55E+07
463,05 (II)	21590	870	7,72E+07
464,06 (III)	21543	120	7,60E+07
464,31 (II)	21531	550	4,51E+07
478,81 (II)	20879	285	2,52E+07
480,33 (II)	20813	450	3,18E+07
500,15 (II)	19989	650	1,05E+08
500,27 (II)	19984	360	8,45E+06
500,52 (II)	19974	870	1,16E+08
567,60 (II)	17613	550	2,96E+07
567,96 (II)	17602	870	5,25E+07
593,18 (II)	16854	550	4,27E+07
594,17 (II)	16826	650	5,54E+07
742,36 (I)	13467	685	5,95E+06
744,23 (I)	13433	785	1,24E+07
746,83 (I)	13386	900	1,93E+07
824,24 (I)	12129	400	1,36E+07
843,87 (II)	11847	550	2,24E+07
856,77 (I)	11668	500	4,92E+06
859,40 (I)	11633	570	2,09E+07
862,92 (I)	11585	650	2,66E+07
865,59 (I)	11550	500	1,05E+07
868,03 (I)	11517	700	2,46E+07
868,34 (I)	11513	650	1,80E+07
868,62 (I)	11509	500	1,09E+07
871,88 (I)	11466	500	6,75E+06

* Average values of several states occupied according to their statistical weights

Table. A. A. 3. Spectroscopic data for neutral and ion lines of Oxygen and Carbon

Wavelength(nm)	Energy(cm ⁻¹)	Relative Intensity	A _{ik}
615,68 (I)	16238	450	5,08E+06
615,82 (I)	16234	490	7,62E+06
645,44 (I)	15489	360	2,75E+06
715,67 (I)	13969	210	5,05E+07
777,19 (I)	12863	870	3,69E+07
777,42 (I)	12860	810	3,69E+07
794,76 (I)		235	
823,00 (I)	12147	265	3,62E+06
823,30 (I)	12143	325	2,43E+07
844,63 (I)	11836	810	3,22E+07
844,64 (I)	11836	1000	3,22E+07
844,68 (I)	11836	935	3,22E+07
C			
283,67 (II)	35241	1000	3,98E+07
299,26 (II)		800w	
391,90 (II)	25509	570	6,36E+07
426,73 (II)	23427	1000*	1,59E+07
426,73 (II)	23427	1000*	2,38E+08
514,52 (II)	19430	570	6,49E+07
566,25 (II)	17655	350	2,93E+07
657,81 (II)	15197	800	3,63E+07
723,13 (II)	13824	800	3,52E+07
819,65 (III)		300w	

* Average values of several states occupied according to their statistical weights

APPENDIX B

DETAILED TECHNICAL PROPERTIES OF THE USED SPECTROMETER

The HR2000CG-UV-NIR Composite Grating Spectrometer has a new proprietary grating and order-sorting filter to provide a 200-1085 nm wavelength range with 1.0 nm optical resolution in one spectrometer.

The HR2000CG-UV-NIR contains a new OFLV-200-1000 variable order sorting filter to eliminate second and third order effect.

HR2000CG-UV-NIR Specifications:

Dimensions	: 148.6 mm x 104.8 mm x 45.1 mm
Weight	: 570 gr
Power Consumption	: 90 mA @ 5 VDC
Detector	: 2048-element linear silicon CCD array
Wavelength Range	: 200-1085 nm
Grating	: HC-1, 300 lines per mm grating
Entrance aperture	: 5 μ m slit
Optical Resolution	: 1.0 nm FWHM
Fiber Optic Connector	: SMA 905 to single-strand optical fiber (0.22 NA)
Data transfer rate	: Full scans into memory every 13 milliseconds with the USB port
Integration time	: 3 milliseconds to 65 seconds

A. Calibration the Wavelength of the Spectrometer

This Appendix describes how to calibrate the wavelength of the spectrometer.

The following equation must be solved, this equation shows that the relationship between pixel number and wavelength is a third-order polynomial;

$$\lambda_p = I + C_1 \cdot p + C_2 \cdot p^2 + C_3 \cdot p^3$$

where λ is the wavelength of pixel p , I is the wavelength of pixel 0, C_1 is the first coefficient (nm/pixel), C_2 is the second coefficient (nm/pixel²), and C_3 is the third coefficient (nm/pixel³).

Calibrating the Wavelength of the Spectrometer

- The software place into scope mode and take a spectrum of the light source. The integration time is adjusted until there are several peaks on the screen that are not off-scale.
- The cursor is moved to one of the peak and position the cursor so that it is at the point of maximum intensity.
- The pixel number that is displayed in the status bar or legend is recorded. This step is repeated for all of the peaks in the spectrum.
- Using the spreadsheet program, all pixel number and its square and third degree is calculate and recorded from the observed data.
- Using the spreadsheet program or calculator, the wavelength calibration coefficients are calculated for different wavelength.
- Select the true wavelength as the independent variable (Y). Select the pixel number, pixel number squared and the pixel number cubes as the independent variables (X). After executing the regression, the statistical values for coefficients are obtained.
- The intercepts are recorded, as well as the C_1 , C_2 and C_3 .

CURRICULUM VITAE

Personal Information

Surname, Name : Kurt Mustafa
Nationality : Turkish (TC)
Date and Place of Birth : 04 January 1974, Çanakkale
Phone : +90 312 210 76 36
Fax : +90 312 210 50 99
Email : mukurt@metu.edu.tr

Education

Degree	Institution	Year of Graduation
MS	COMU Physics, Çanakkale	2001
BS	METU Physics, Ankara	1999

Work Experience

Year	Place	Enrollment
2002-present	METU Department of Physics	Research Assistant
1999-2002	COMU Department of Physics	Research Assistant

Publications

1. Theory of Fiber Optic Gyroscope and its application in INS (Inertial Navigation System), Mustafa KURT, Ali ALAÇAKIR, 3. Ulusal Elektro-Optik Toplantısı, Aselsan MGEO, 2001.
2. Time Resolved Laser Induced Air Plasma Spectroscopy, Mustafa KURT, Akif ESENDEMİR, 6. Ulusal Elektro-Optik Toplantısı, Koç University, 2006.
3. 600 Watt CO₂ Laser Design and Production, 5. Ulusal Elektro-Optik Toplantısı, Sabancı Üniversitesi, 2004.
4. Theory of Fiber Optic Gyroscope and Application, Optik ve Elektronik Sempozyumu, Çanakkale Onsekiz Mart Üniversitesi, 2003.
5. Time Resolved Laser Induced Air Plasma” 6. Ulusal Elektro-Optik Toplantısı, Koç Üniversitesi, 2006.